JULY 1957 VOLUME 1 (1957) No. 4

GREGG M. SINCLAIR LIBRARY
UNIVERSITY OF HAWAII
8-7-63

NUCLEAR INSTRUMENTS

A JOURNAL ON ACCELERATORS, INSTRUMENTATION AND TECHNIQUES IN NUCLEAR PHYSICS

EDITOR K. SIEGBAHN – UPPSALA

CONTENTS

G. CALAME, P. F. COOPER, JR., S. ENGELSBERG, G. L. GERSTEIN, A. M. KOEHLER, A. KUCKES, J. W. MEADOWS, K. STRAUCH and R. WILSON, Some features of regenerative deflection and their application to the Harvard synchrocyclotron 169
P. R. ORMAN and F. H. WELLS, A millimicrosecond pulse-shaping circuit 183
K. G. MALMFORS, J. KJELLMAN and A. NILSSON, The time-of-flight technique applied to fast neutrons 186
P. A. EGELSTAFF, Glass scintillators for prompt detection of intermediate energy neutrons . 197
S. AKPINAR, The output distorsion of a differential interval analyzer of universal design . . 200
R. L. FAVRE, Demultiplicateurs électroniques d'impulsions 201
H. SLÄTIS, On diffusion cloud chambers (Survey article) 213
E. R. RAE and F. W. K. FIRK, An application of magnetic tape recording to neutron time-of-flight spectroscopy 227
Conferences 232

NORTH-HOLLAND PUBLISHING COMPANY – AMSTERDAM

NUCLEAR INSTRUMENTS

A journal on accelerators, instrumentation and techniques in nuclear physics

EDITOR: K. SIEGBAHN, UPPSALA

EDITORIAL BOARD:

J. B. ADAMS (CERN)
E. AMALDI (Rome)
H. L. ANDERSON (Chicago)
K. T. BAINBRIDGE (Cambridge, Mass.)
C. J. BAKKER (CERN)
P. R. BELL (Oak Ridge)
R. E. BELL (Montreal)
A. BERTHELOT (Saclay)
H. BRINKMAN (Groningen)
S. DE BENEDETTI (Pittsburgh)
M. DE HEMPTINNE (Louvain)
A. DE-SHALIT (Rehovoth)
M. DEUTSCH (Cambridge, Mass.)
S. DU TOIT (Pretoria)
B. S. DŽELEPOV (Leningrad)
W. GENTNER (CERN)
P. C. GUGELOT (Amsterdam)
H. HALBAN (Paris)
O. HAXEL (Heidelberg)
P. HUBER (Basel)
D. J. HUGHES (Brookhaven)
S. KIKUCHI (Tokyo)
J. KOCH (Copenhagen)
M. S. KOZODAEV (Moscow)
S. LIVINGSTON (Cambridge, Mass.)
E. M. MCMILLAN (Berkeley)
M. G. MEŠČERJAKOV (Moscow)
P. B. MOON (Birmingham)
M. L. OLIPHANT (Canberra)
W. PAUL (Bonn)
A. S. RAO (Bombay)
G. SALVINI (Rome)
P. SAVIĆ (Belgrade)
P. SCHERRER (Zürich)
CH. SCHMELZER (CERN)
H. W. B. SKINNER (Liverpool)
R. TANGEN (Blindern)
V. I. VEKSLER (Moscow)
O. WERNHOLM (Stockholm)
D. TAYLOR (Harwell)
G. VON DARDEL (CERN)
R. R. WILSON (Cornell)
S. D. WINTER (Saclay)

Contributions may be sent to the Editor, Professor K. Siegbahn, Institute of Physics, the University of Uppsala, either directly or through the intermediary of one of the members of the Editorial Board of the country or region in which the author is working. Contributions may be written in English, French or German, with an abstract in English.

Books for review should be sent to Professor Siegbahn.

Nuclear Instruments is published in bi-monthly issues. The subscription price of a volume of 360 pages is $ 17.00 (130 s), postage free.

Subscriptions should be sent to the publishers, North-Holland Publishing Company, P.O.Box 103, Amsterdam or to any subscription-agent. Subscriptions for U.S.A. are to be sent exclusively to Interscience Publishers, Inc., 250 Fifth Avenue, New York, 1 N.Y.

No part of this issue may be reproduced in any form, by print, photoprint, microfilm or any other means without written permission from the publisher. Reprints, photoprints or microfilms are obtainable at cost from the publisher.

LELAB METAL-WALLED G-M TUBES
for anti-coincidence applications
where uniformity counts !

Lelab Counter Tubes are individually constructed, filled, and tested. Each is fabricated almost entirely of metal. All components are confined within the diameter of the tube shell to permit close stacking.

Compare our low prices on these superior tubes!

(Makers of Lelab [Robinson-Selverstone Type] Probe Counters for neurosurgery and where a fine needle-like probe for highly localized measurements is useful.)

Write for complete information

H. W. Leighton Laboratories

York & Sunset Lane-Hatboro, Pa. U.S.A.

RADIATION INSTRUMENT CO.
MODEL 412 MERCURY RELAY

Precision Sliding Pulser

for Precise Calibration of Single & Multi-Channel Pulse Height Analyzers

Determines Window Widths Using Principle of *Constant Angular Velocity* } **AUTOMATICALLY** **10 × more accurately** **40 × faster than conventional pulsers**

Incorporates Both Manual Control and Precision Motor Drive

Simulates Pulses from Scintillation, Proportional, or Geiger Counters

RISE TIME—Less than .003 microsec.

DECAY TIME CONSTANT—1, 10, 100, 350, microsec. (selector switch).

PULSE AMPLITUDE—Continuously variable from 0 to maximum. Ranges 2, 3, 10, 30, 100, 1000 mV. Provision for direct connection of external battery for larger pulses.

POLARITY—Polarity switch permits selection of positive or negative pulses.

CALIBRATION—Self contained standard cell and null indicating balance circuit for precision adjustment.

LINEARITY—0.1% 10 turn Helical potentiometer with 5″ dial.

SCAN SPEED—2 RPM standard (1, 3, 5, 6 and 10 rpm also available.)

PRICE $ 450.00 f.o.b. SILVER SPRING, Md., U.S.A.

RADIATION INSTRUMENT CO.

P. O. BOX 733 SILVER SPRING, MARYLAND, U.S.A.

NCA

WORLDWIDE
Film Badge Service

for Beta
Gamma X-rays
and Neutrons

Available in clip-on, wrist, or ring style, for isotope and X-ray laboratories, medical and dental offices, and industrial plants. Write or 'phone for Bulletin N20, containing complete information and prices.

- **Low Cost**
- **Prompt, Reliable Reports**
- **Provides Permanent Records**
- **Covers Wide Range of Energies and Exposures**
- **5 Filters for Highest Accuracy**

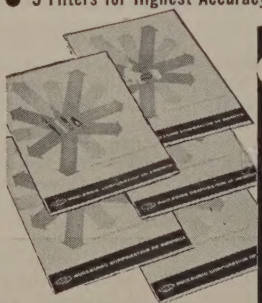

#101. Uranium and Oil Exploration Equipment
#102. Atomic Education Equip't.
#103. Nuclear Laboratory Equip't.
#104. Medical Radioisotope Equipment
#105. Geiger, Proportional, and Scintillation Detectors

NCA

Your One Source of Nucleonic Equipment for Every Field

Send now for above new catalogs

Dept. N17

NUCLEONIC
Corporation of America
196 Degraw St B'klyn 31, N. Y.
MAin 4-7370

NCA

Cary / instrument abstracts

Applied Physics Corporation/Pasadena/California

Radioactivity Measurements Made Faster, Cheaper with Vibrating Reed Electrometer

Measurement of radioactivity in radioisotope determination, reactor control, air contamination studies, oil well logging, and other problems involving precise measurement of small currents, voltages and charges, such as precise pH determination and mass spectrometry, can now be made faster, simpler and cheaper by using the Cary Model 31 Vibrating Reed Electrometer.

Unusually high sensitivity plus high zero stability and ease of installation and operation are responsible for the greater speed and savings. The Model 31 detects as little as 10^{-17} amperes, and measures up to 10^{-6} amperes with a precision of 1%. Zero drift is less than 0.2 mV in 24 hours and less than .02 mV per hour.

C^{14}, H^3 DETERMINATIONS SIMPLIFIED

One widespread application in which the Model 31 has been of particular value is in determining C^{14}, H^3, and S^{35}. Wilzbach and his coworkers at Argonne National Laboratory have developed procedures* which simplify these determinations in a wide variety of organic compounds. Samples are converted directly to a gas suitable for measurement with an ionization chamber and the Model 31. This simple procedure eliminates the necessity for use of a precipitate, with its inaccuracy and time-consuming, tedious preparation.

Since as little as 10^{-12} curies of radioactivity can be detected, use of expensive "tagged" materials can be greatly reduced, often enough to return the cost of the instrument in a relatively short time.

The Model 31 can be used in any laboratory and does not require costly, vibration-free mountings or other special conditions of installation or operation. For additional information on the Model 31, write for bulletin NU-1 today. It gives you details on applications, references, performance, operating principle, specifications, modifications, accessories.

*Wilzbach, Brown, Kaplan, Science, **118**, 522-523 (1953)
Wilzbach, Van Dyken, Kaplan, Anal. Chem., **26**, 880 (1954)
Wilzbach, Sykes, Science **120**, 494-496 (1954).

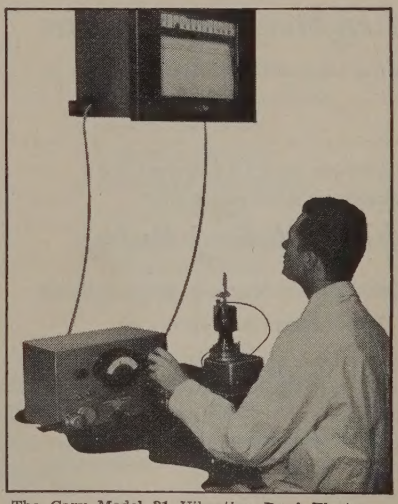

The Cary Model 31 Vibrating Reed Electrometer is capable of detecting a current as small as 1.0 X 10^{-17} amperes originating in a high impedance source. Charges as small as 5 X 10^{-16} coulombs and voltages as small as .02 mV can be measured.

CARY MODEL 36 VIBRATING REED AMPLIFIER IMPROVES MASS SPECTROMETER PERFORMANCE

The Cary Vibrating Reed Amplifier, Model 36, is being used in an increasing number of mass spectrometer installations where high molecular weight analyses make rapid scanning of mass numbers desirable. The Model 36 combines rapid response with high sensitivity. Response is critically damped, with an 0.1 sec. natural period (98.6 percent response in 0.1 second). Thus a range of 100 mass numbers can be accurately scanned in as little as one minute. Sensitivity and range are such that as little as 10^{-15} amperes and up to 10^{-11} amperes can be measured to a reproducibility of 0.2 percent without change of range. The stability of the Model 36 is superior too–zero drift is less than 10^{-15} amperes.

The Model 31 is preferred for mass spectrometer applications where extreme response speed is not required, such as isotope determinations. Sensitivity of the Model 31 is 10^{-17} amperes, and like the 36 it has high stability–less than 5 x 10^{-17} amperes zero drift.

NUCLEAR INSTRUMENTS 1 (1957) 169–182; NORTH-HOLLAND PUBLISHING CO. – AMSTERDAM

SOME FEATURES OF REGENERATIVE DEFLECTION AND THEIR APPLICATION TO THE HARVARD SYNCHROCYCLOTRON

G. CALAME, P. F. COOPER, JR., S. ENGELSBERG, G. L. GERSTEIN, A. M. KOEHLER, A. KUCKES, J. W. MEADOWS, K. STRAUCH, and R. WILSON

Cyclotron Laboratory, Harvard University

Received 22 March 1957

The regenerative deflector system applied to the Harvard synchrocyclotron is described. The theory of LeCouteur has been extended to include the initial radial oscillations, and it is shown, both theoretically and experimentally, that only partial monochromatization of the beam occurs during regeneration. However, it is possible to internally limit the energy width of the regenerated beam at the expense of intensity. The theory is in good accord with experiment. The application of these results to the production of an intense external proton beam and more monoenergetic neutron and polarized proton beams is described.

1. Introduction

The energy of the beam of the Harvard synchrocyclotron has been raised to 159 MeV by increasing the magnet current, reshiming the magnetic field and increasing the frequency range of the oscillator. At the same time the method of regenerative deflection has been used to produce an intense external proton beam and more monoenergetic neutron and polarized proton beam. This method was first suggested by Tuck and Teng[1]), and extensive computations on its use have been performed by LeCouteur[2,3]) and LeCouteur and Lipton[4]). This method has by now been applied to machines at Liverpool[5]), Chicago[6]), Rochester[7]), Upsala[7]) and here. Some features of the Harvard installation are of sufficient interest to warrant a separate description.

The method of regenerative deflection as originally conceived uses two magnetic disturbances, a "peeler" and a "regenerator", suitably superimposed on the cyclotron magnetic field.

These disturbances induce radial oscillations with exponentially increasing amplitudes and a minimum of vertical expansion. The radial oscillations have common nodes, that is they do not precess. Once the increase of the radial amplitude per turn is larger than a minimum value set by the width of a channel bar, the "regenerated" beam is extracted rapidly using a magnetic channel.

Two methods are available for the production of such a regenerated beam. First, a regenerator and peeler can be placed about 3 inches inside the $n = 0.2$ point as in the Liverpool machine[5]). Second, a single regenerator can be located just inside the $n = 0.2$ point and the fall off of the cyclotron field can be used as the peeler as in the Chicago machine[6]). Two considerations led to our choice of the latter system; it gives an additional 15 percent in the maximum available energy, and the total amount of iron placed inside the cyclotron is less. Since we are using two retractable regenerator systems in order to make more effective use of the experimental area, this is not a negligible simplification.

[1]) Tuck and Teng, Institute of Nuclear Studies, 170 in. Synchrocyclotron Progress Report III, University of Chicago (1950) Chap. VIII; Phys. Rev. **81** (1951) 305.

[2]) K. J. LeCouteur, Proc. Phys. Soc. B **64** (1951) 1073 (Hereafter referred to as L1).

[3]) K. J. LeCouteur, Proc. Phys. Soc. B **66** (1953) 25 (Hereafter referred to as L2).

[4]) LeCouteur and Lipton, Phil. Mag. **46** (1955) 1265 (Hereafter referred to as L3).

[5]) K. J. LeCouteur, Proc. Roy. Soc. A **232** (1955) 236. Crewe and Gregory, Proc. Roy. Soc. A **232** (1955) 242.

[6]) Crewe and Kruse, Rev. Sci. Inst. **27** (1956) 5.

[7]) Private communications.

However, as will be shown, the regenerator plus peeler would probably yield a beam of better energy definition.

The theoretical considerations of L1, L2, and L3 and the results at Liverpool[5]) and Chicago[6]) gave rise to the hope that essentially all of the internal beam could be regenerated without vertical blowup and that this beam would have very good energy definition. It is clear that these features are desirable in order to obtain as intense and as monochromatic an external beam as possible. In addition, by placing an internal target into such a regenerated beam, one would expect to produce a neutron beam whose energy width is effectively determined by the nuclear properties of the target and not by the energy distribution of the incident beam. Similarly, polarized protons obtained by elastic scattering of such a regenerated beam from an internal target would be monochromatic and no intensity reduction due to subsequent energy selection would be necessary.

These considerations led us (1) to study the orbits of the regenerated particles and to compare them with theory; (2) to calculate and to measure the energy distribution of the regenerated beam; and (3) to consider the effect of the presence of initial radial oscillations.

As will be discussed below in some detail, we are able at present to regenerate only 25 percent of the internal beam and we have found only partial monochromatization occuring during the process of regeneration. However, it is found both experimentally and theoretically, that it is possible to select a small group of energies internally, and thus to improve the energy definition although at a sacrifice of intensity. One regenerated beam is extracted through a focusing channel. Another regenerated beam is directed upon an internal target to produce neutron and polarized proton beams.

Some of the considerations that led to the design of the Harvard regenerative system will be discussed first. Then the methods of beam extraction and the performance tests will be described.

2. Design Considerations of the Regenerator System

2.1. REGENERATOR DESIGN[8])

The basic problem of beam extraction from a large synchrocyclotron is that the beam will not travel out beyond a radius at which $n = 0.2$, because of the coupling of radial and vertical oscillations at this point. Radial oscillations are in practice always large, and if the energy in them is allowed to go into the vertical motion, the beam will blow up vertically. One can however extract the beam by forcing radial oscillations of large amplitude and simultaneously maintaining vertical stability. Large radial oscillations can easily be produced in a cyclotron by making $\langle n \rangle = 0$, thus giving a coupling between the radial oscillations and azimuthal inhomogeneities; this, however, would lead to no vertical focusing. Fortunately it transpires when an azimuthally inhomogeneous field is used such that $\langle n \rangle = 0$ along a particle orbit higher spherical harmonics give adequate vertical stability. Here $\langle n \rangle$ refers to the average value of n over the particle orbit.

If $\langle n \rangle$ is appreciably less than zero, it becomes impossible to obtain vertical focusing; if $\langle n \rangle$ approaches 0.2, vertical blowup will result. The purpose of the theory of regenerators, as it has been extensively studied by LeCouteur in the three papers L1, L2 ,and L3, is to specify a suitable, easily obtainable field. The simple picture has, of course, to be modified for the inhomogeneous fields actually present, where the radial and vertical focusing are not given solely in terms of n. The solution is obtained by solving the equations of motion.

For a single regenerator, it is necessary to balance the regenerator strength against the radial fall off of the magnetic field, which, in Tuck's[4]) terminology, acts as a peeler. It can easily be seen that for radial motions the regenerator strength cannot be too large; the oscillations will just build up in such a way that the particles spend more of their time in the

[8]) The notation here and throughout this paper is that of LeCouteur in L1, L2, and L3.

fringing field. Figure 3 of L3 shows that there is no reduction in radial gain. For vertical focusing, however, the problem is more difficult, since there are close limits on the average value of n.

In order to follow a step by step procedure for orbit calculation, L3 assumes a regenerator field given by $\frac{r_0}{H_0}\int H_g d\theta = 0.2\rho + 0.2\rho^2$, where ρ is the displacement from the equilibrium orbit[8]). It is found that radial gain and vertical focusing can be combined for values of ρ up to that at which the particles spiral out on their own. For small ρ the regenerator field is quite small and the problem is to achieve adequate radial gain. For large values of ρ, the compensation the regenerator must make for the field fall off is large and becomes critical; vertical focusing is then difficult to maintain.

The calculations of LeCouteur are approximate in that the nonlinear equations are replaced by two linear equations. He justifies his choice of the regenerator strength, however, by an exact computer calculation which bears out his approximate analysis. Still, the exact calculation suggests that vertical stability is more critical than otherwise indicated and that the radial gain is larger.

For our cyclotron, moreover, further errors enter. The regenerator is 15″ long and therefore occupies 1/3 radians azimuthally, whereas the computations were made on the assumption of a point regenerator. Equations (23) and (24) of L1 however give appropriate corrections for the radial and vertical strengths. Secondly, in several places in his calculation, LeCouteur, while retaining terms of order ρ/r_0, which give the desired oscillation, neglects terms of order $(\rho/r_0)^2$. For our cyclotron this omission is an error of the order of 10%. Accordingly we can only use LeCouteur's calculations as a guide and to interpret experimental data.

Since the field in our cyclotron falls off in a similar way to that assumed in L3, a regenerator with a defect given by LeCouteur's prescription was constructed as a first trial. On testing, this gave a low radial gain and a large vertical expansion for $\rho \geq 3''$. The first fact suggests too small a regenerator strength. On examination of the graphs of figure 5 in L3, we indeed see that the prescription $0.2\rho + 0.2\rho^2$ for regenerator strength is a little too small for good vertical focusing at large An additional reason for increasing the regenerator strength for $\rho \geq 3''$ arises when the magnetic channel is considered. In order for the channel to have the desired focusing properties it is necessary to leave a large field defect near the channel in the region through which the particle orbits must pass on the last revolution before entering the channel. This acts like a peeler and, by the crude argument above, must be compensated for by an equivalent increase in the regenerator strength in order to maintain $\langle n \rangle = 0$. This increase must be at a slightly greater radius than that at which the particle passes the channel to correspond to the same orbit. We have not calculated the effect of this in detail, but have contented ourselves with limiting the channel defect close to the inside wall of the channel to 15% of the regenerator strength at the appropriate radius.

The strength of our second regenerator is shown in fig. 1 compared with the recipe of L3. Its performance is discussed below. The second regenerator was designed to have 10–20% greater strength for $4'' \rangle \rho \rangle 3''$. All the later tests described in a later section 4.2. were performed with this regenerator. The regenerator and shims used to achieve this are illustrated in fig. 2. The first regenerator has been retained for internal bombardments.

2.2. EFFECT OF INITIAL RADIAL OSCILLATIONS

LeCouteur has applied his theory only to particles with no initial radial oscillations and has but sketchily treated the start of the regenerative oscillation. In fact, of course, almost all particles have appreciable (and different) amplitudes of radial oscillation. This is fortunate, for, if it were not so, the impossibility of achieving LeCouteur's recipe $0.2\rho + 0.2\rho^2$ for infinitesimal ρ would take on great importance. Furthermore, as we shall see, the radial oscillations affect the energy spectrum, and may affect the efficiency of regeneration. Also, it is important to see that particles do not blow up.

Fortunately, LeCouteur has performed enough calculations so that in our case, where a regenerator alone is used, the effect of these radial oscillations may be quickly calculated. As illustration we present in this section the results for our cyclotron and our regenerator.

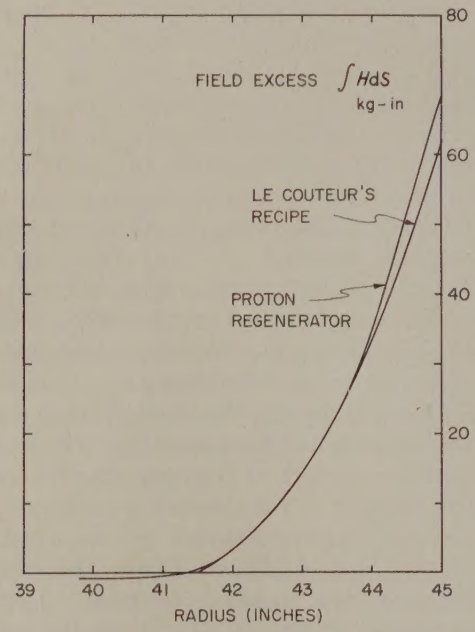

Fig. 1. The regenerator strength as defined in the text, versus cyclotron radius. The experimental curve is compared with LeCouteur's recipe.

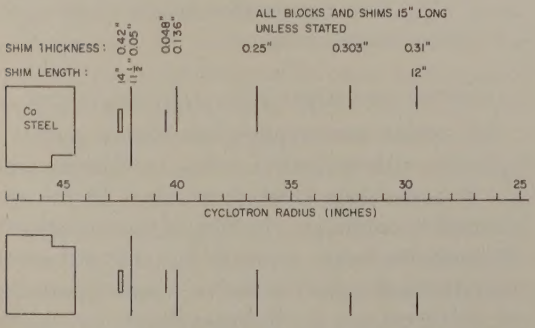

Fig. 2. Schematic arrangement of regenerator blocks and shims to produce the field of fig. 1.

The radial and vertical motions are coupled in this nonlinear case. Fortunately, to our approximation the radial motion is independent of the vertical motion although the vertical motion is dependent upon the radial motion. We therefore follow LeCouteur and calculate the radial motion first.

The regenerator is designed to operate on those particles which have an equilibrium orbit radius of 41.5 inches in our cyclotron where

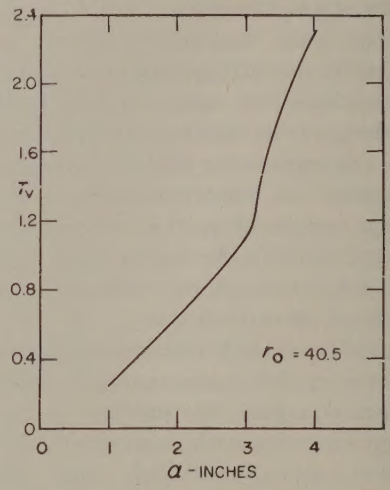

Fig. 3. Plots of T_v (fig. 3a) and T_r (fig. 3b) for an equilibrium orbit of 40.5″ using the regenerator strength of fig. 1.

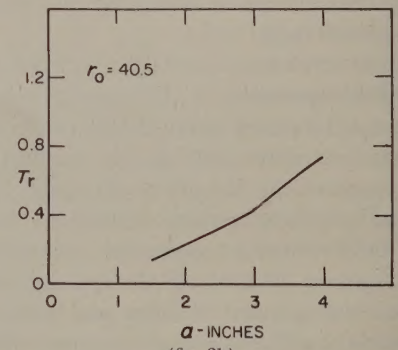

(fig. 3b)

the $n = 0.2$ radius is 42 inches. From the graph of excess field we can plot the radial and vertical regenerator strengths (T_r and T_v) as a function of ρ. Also we must recompute for our machine fig. 6 of L3, which gives the average radial and vertical oscillation frequencies (Ω' and ω') as a function of ρ. With these we can compute the radial gain e^A and the vertical defocusing parameter $\cos\varepsilon$ from figs. 3 to 5 of L3, obtaining results similar to LeCouteur's prescription.

Now, suppose that without moving the regenerator we consider a particle with an equilibrium orbit radius of 40.5 inches and recalculate curves of T_v, T_r, Ω', and ω'. We obtain our figs. 3 and 4.

These may be understood, when we realize that T_v depends on $\frac{d}{d\rho}[\int H d\theta]$ whereas T_r depends upon $[\int H d\theta]/\rho$. These are not simple dunctions of n as in the constant regenerator case of L1. Thus T_r for 40.5 inches at $\rho = 3$ inches is 2/3 T_r for 41.5 inches at $\rho = 2$ inches. We may now use figs. 3 to 5 of L3 as before. Thus for $\rho < 3.3$ inches (considering $r_0 = 40.5$ inches the initial r_0 and using the appropriate values of Ω') fig. 3 of L3 shows that there is no solution with e^A real. If $\rho = 3.3$ inches $e^A = 1$ and regeneration can begin. At this point we observe from fig. 4 of L3 that the phase g is 90° and from fig. 5 that $\cos \varepsilon = 0.2$ so that the vertical focusing is good and remains so as the particles spiral out. The fact that the phase g remains constant validates our analysis. We now have to consider how a particle reaches an equilibrium orbit of 40.5 inches with such a large oscillation amplitude. To answer this question involves finding a solution of the orbit equations which is not increasing in amplitude. The solutions of this type have been discussed numerically in appendix 1 of L1 and graphically in fig. 2 of L2 (though there it is in connection with the vertical oscillations). It is clear that the radial oscillation will not be of constant phase but will precess around the cyclotron. The regenerator will increase the amplitude of oscillation if the particle enters the regenerator with $\rho < 0$ and decrease it if $\rho > 0$. The two are equally likely and each will occur several times before there has been appreciable particle acceleration, so that it is safe to say that, on the average, particles maintain their oscillation amplitude until the moment they start regeneration[9]). Thus particles with initial oscillation amplitude 3.3 inches will accelerate to an equilibrium orbit of 40.5 inches and then regenerate. Similarly those of oscillation amplitude 2.5 inches will regenerate at 41 inches and those of oscillation amplitude 0.5 inches will regenerate at 41.4 inches. Thus if the initial spread of radial oscillation amplitudes extends to 3.3 inches the spread in energy of the regenerated beam is that corresponding to a difference in equilibrium orbit radius of only 0.9 inches. This corresponds in a reduction of the spread in energy from 21 MeV to 6 MeV. Some measure of monochromatization has thus been achieved.

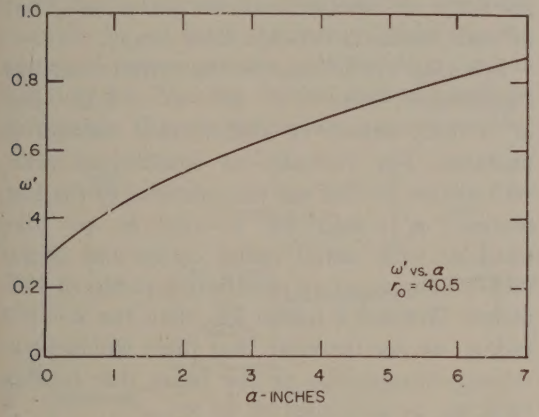

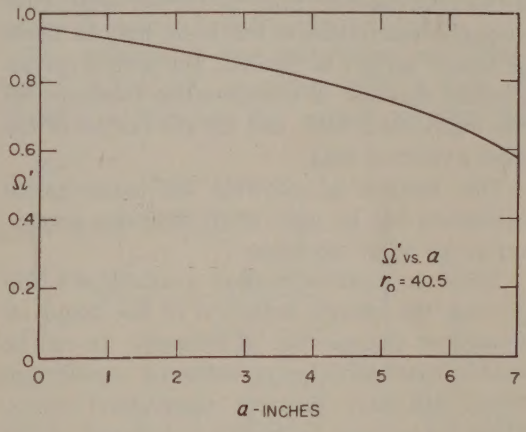

Fig. 4. Plots of ω' (fig. 4a) and Ω' (fig. 4b) for an equilibrium orbit of 40.5" using the measured magnetic field of the Harvard cyclotron.

(fig. 4b)

In future designs this might be improved. Thus if T_r is only just large enough to allow regeneration from the equilibrium orbit (say $T_r = 1.05$ times the minimum value for $\rho < 3$

[9]) This neglects the adiabatic damping of the oscillations as n changes. This is small until n becomes large.

and becoming larger for $\rho > 3$ then a particle near the equilibrium orbit will indeed regenerate but only have a large radial gain for 3.3 inches. For a particle with an equilibrium orbit smaller by x inches. T_r will be reduced by $\rho/(\rho + x)$ whereas Ω' will not be much altered. For $(\rho + x)/\rho < 1.05$ there will be, therefore, no regeneration. Thus all particles with all initial oscillation amplitudes less than 3 inches will regenerate with equilibrium orbits less than 0.15 inches different from the correct orbit. Thus monochromatization of the beam may be made as nearly perfect as desired, but with a corresponding decrease in the allowable tolerance for the regenerator field, and for the fall off of the main cyclotron field.

This method of allowing for initial radial oscillation can be used when designing regenerators for other machines.

There is another method available for improving the energy definition of the beam although at the sacrifice of intensity. It can be shown that particles of different equilibrium orbits will have different regenerated orbits. These orbits may be readily calculated. Again from fig. 4 of L3 determine g for the appropriate values of Ω' and T_r. From this the position of the radial node ψ may be determined. The radial motion between the node and the regenerator has the form $\sin(\Omega'\theta + \psi)$. Since both Ω' and ψ are different for particles of different equilibrium orbits their regenerated orbits may well be different. Computation of these orbits shows that there is a region where the orbit of the lower energy particle will be outside the orbit of the higher energy one. By inserting a probe or slit a narrow group of energies may be selected. The application of this method will be illustrated in section 4.5.

2.3. VERTICAL STABILITY

The only difficulty of successful regeneration is to maintain vertical stability of the motion of the particles. Some features of this are discussed in this section.

First, as an interesting aside, the ordinary blow up of the beam at the radius of $n = 0.2$ may be discussed adequately for what we believe is the first time. As mentioned in the introduction, particles of small radial oscillation pass this point successfully; those with large radial oscillation see a varying n value over the particle orbit.

Blow up of the beam will occur when the vertical oscillation period equals twice the radial oscillation period. This will not occur when the extreme of the orbit touches the $n = 0.2$ circle, nor when the equilibrium orbit is at $n = 0.2$ but at some radius in between these limits.

From fig. 5 of L3 we note that with no vertical regenerator $\cos\varepsilon < 1$ for $\omega' < 0.55$. For $\omega' > 0.55$, $\cos\varepsilon > 1$ and vertical motion is unstable. For particles of equilibrium orbit 40.5 inches, we can use the solutions of the last section; $\omega' = 0.55$ for $\rho = 2.0$ in so that particles with initial radial oscillations of 2.0 inches blow up at an equilibrium radius of 40.5 inches. This is 1.5 inches less than the $n = 0.2$ radius; we see therefore that there will be little monochromatization of the beam due to this blow up, as confirmed by fig. 8.

We are now in a position to discuss the vertical stability of those particles entering the regenerator with large radial oscillations. After the start of regeneration they are stable as discussed in the previous section. Before the start of regeneration the radial oscillations precess around the cyclotron and particles will not, therefore, enter the regenerator on every turn. LeCouteur's solutions for the vertical motion of the particles will not apply. Without a regenerator, we have just seen that the motion is unstable; with one acting on only a few turns the problem is complex.

We have not carried through a consistent solution of the problem but the essential features may be seen as follows. The vertical blowup occurs when $\langle n \rangle = 0.2$, where $\langle n \rangle$ is the average over the orbit. We wish to maintain $\langle n \rangle < 0.2$ over several radial oscillation cycles. In this region the radial oscillation precession period is about six times the cyclotron period, so that the particles pass through the regenerator about once in 6 ro-

tations. The vertical strength must, therefore, be strong enough to maintain $\langle n \rangle < 0.2$ over 6 cycles. A more precise way of formulating this question would be to write down the regenerator matrix (T) for each of several transitions through the regenerator and to find the eigen-values of the matrix

$$A = PT_1\,PT_2\,PT_3\,PT_4\,PT_5\,PT_6$$

where P is a matrix for the motion of a particle around the cyclotron.

We have not set up this matrix. We have calculated $\langle n \rangle$ for 6 revolutions including the action of the regenerator and find that $\langle n \rangle$ is less than 0.2. Thus the vertical motion should be just stable. The vertical motion is very complex, and the expansion is different at different parts of the motion. The maximum value of the expansion can be large, and to this we attribute a loss of intensity as discussed in the next section.

A peeler plus regenerator system, located at a smaller radius, would avoid this trouble of vertical expansion.

3. Magnetic Filed Measurements and Calculations

Extensive magnetic measurements had to be made. In order to simplify these, and electronic fluxmeter was used, followed by an electronic integrator. A search coil was rotated around the cyclotron centre at constant angular velocity so that $\int H d\theta$ may be directly measured. The time saving for the channel and regenerator measurements was considerable.

The diagram of the circuit employed is shown in fig. 5. The galvanometer and photocell unit form part of a General Electric Co. recording fluxmeter (which was not directly suitable for our purpose). This was connected with a feedback system, so that the output was proportional to the search coil voltage. The gain of the DC amplifier was such that the overall gain is equal to $(R_3+R_4)/R_4$ which was variable. The condenser across R_3 assured high frequency stability.

The subsequent two integrators use "Philbrick" K2-W DC amplifiers with a gain of 20 000; in this use the output is equal to

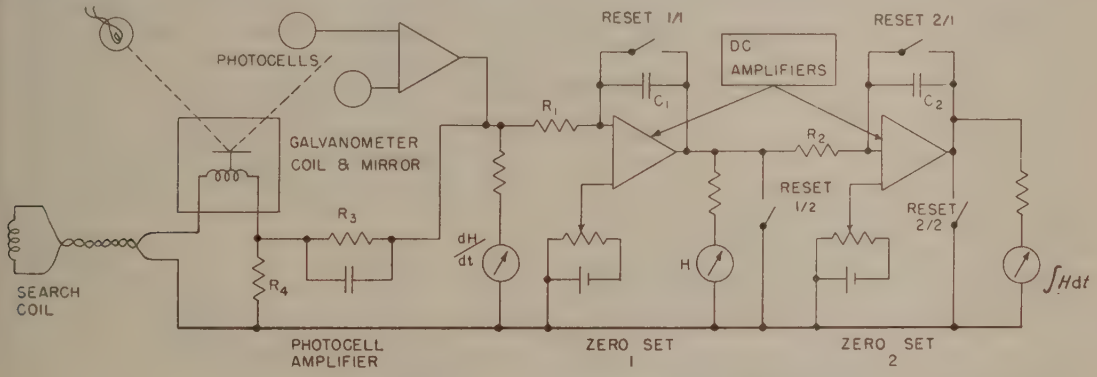

Fig. 5. The magnetic field measuring circuit.

$\frac{1}{RC}\int v_i dt$. This drifts with a time constant ARC where A is 20 000 which is negligible. RC was usually 0.2 secs. Provision is made to reset each integrator, and to adjust the zero of the integration.

To measure field gradients inside the channel a vibrating search coil was used, calibrated in the known field gradients of the cyclotron fringe field.

The field defect due to a regenerator block or a shim may be calculated assuming that the shim is saturated, and considering the effect of the poles induced at the top and bottom of the shims. This neglects the poles induced on the magnet pole pieces[10]). We have found that this

[10]) K. J. LeCouteur privately circulated notes on regenerator and channel design.

procedure, while adequate for initial design, is inadequate for the large quantity of iron used. We have, for example, found that the total defect due to two adjacent shims of different dimensions is *not* accurately given by the sum of the defects of each shim individually. This particularly applies to the *field gradient* near a shim, which is very important for channel design. This difference may well be caused by the poles induced on the magnet pole pieces or on other adjacent steel.

4. Regenerator Performance and Beam Extraction

4.1. ARRANGEMENT OF BEAMS

Fig. 6 shows the present arrangement of regenerators, channel and beams around the cyclotron. Two regenerators are used: one produces, in conjunction with the magnetic channel, an intense unpolarized proton beam, the other produces the regenerated beam which hits an internal target to produce neutrons and polarized protons. The regenerators mount on tracks and are retractable. A further shim, not shown in fig. 2, is used to compensate for the effect of the retracted regenerator assembly. The channel is in a fixed position. This general arrangement makes good use of the available experimental area by separating the three main beams.

4.2. REGENERATOR PERFORMANCE

The final shimming of each regenerator was such that the integrated field defect was less than 0.2 kg-in. from a radius of 37 inches to a radius of 41.5 inches and varied less than this. At smaller radii a defect was left rising to a maximum of 1 kg-in. at 25 inches. The regenerator itself was measured to an accuracy of 2 percent.

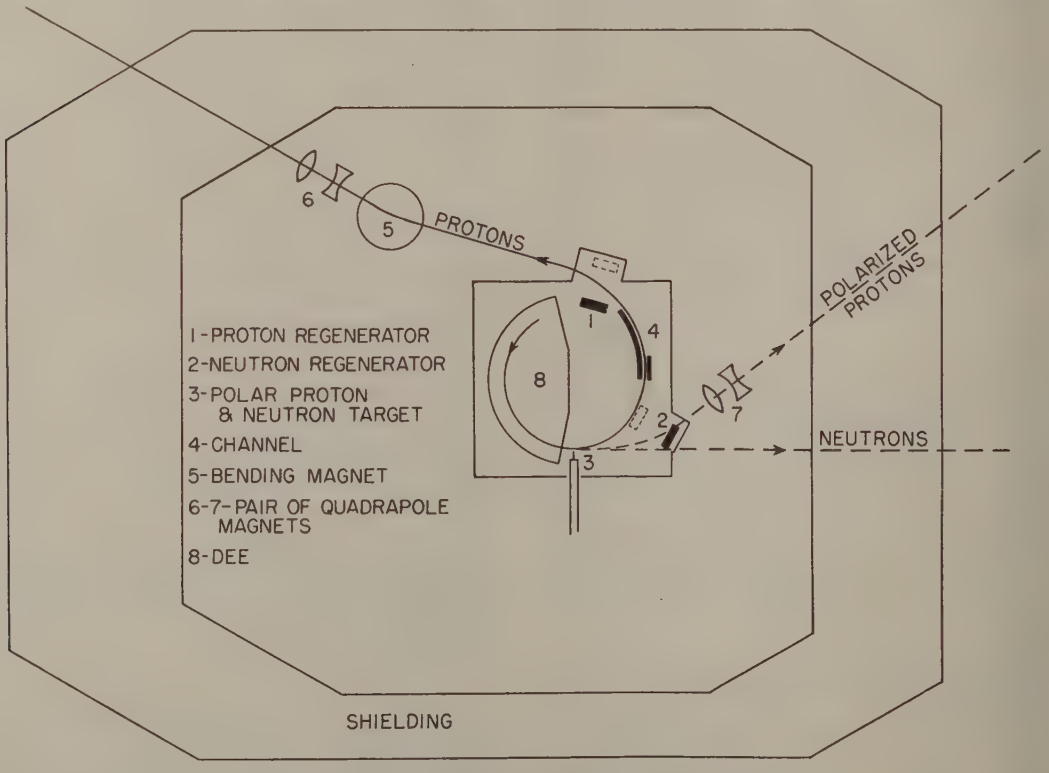

Fig. 6. The final arrangement of beams around the cyclotron.

Our initial regenerator tests were similar to those of Crewe and Kruse[6]). An ionization chamber was mounted on an adjustable probe, with a block of brass between it and the cyclotron centre; the ionization chamber will then only read the current of those protons which are scattered into the ionization chamber or those which regenerate and "jump" the brass block.

Fig. 7 shows such readings for different thicknesses of brass block and different probe positions, using the regenerator at its optimum position, but without the channel in place. For these measurements the probe moved radially at an azimuth 20° before the regenerator. The radial gain for $\rho > 2$ is slightly larger than LeCouteur's approximate theory predicts. This is in line with the exact calculations which, although they do not apply to our regenerator, predict a slightly larger radial gain. To obtain the energy distribution of the beam the time distribution of the beam was measured[11]). Fast neutrons from the nuclear interaction of the

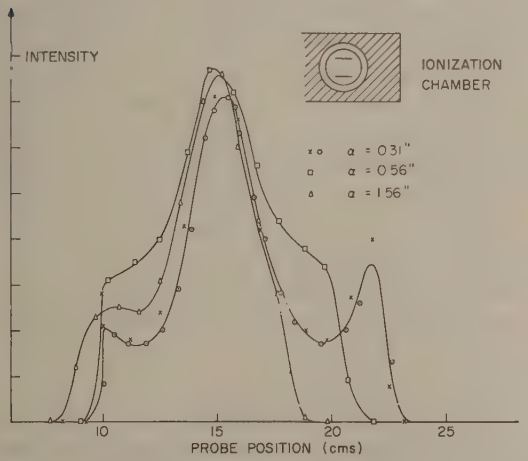

Fig. 7. Readings taken on an ion chamber mounted on a probe; the distance d is the minimum gain per turn for reading in the ionization chamber. Equal abscissae correspond to equal positions of the ion chamber in the cyclotron.

beam with some obstacle enter a scintillator and produce counts; these are displayed on an oscilloscope. The oscilloscope is triggered when the cyclotron radio frequency reaches a certain value near the end of the cycle. Apart from phase oscillations, the time distribution of the

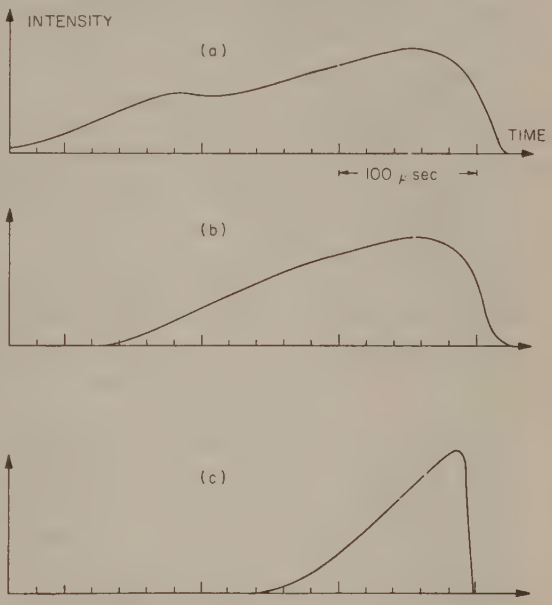

Fig. 8. Time distributions of the beam. 100 microseconds corresponds to about 7 MeV. (a) On an internal target at 41.5". (b) Due to blow up without a regenerator. (c) After regeneration and striking an internal target.

protons should give the energy distribution of the protons immediately *before* they strike a target. While multiple traversals may broaden the effective energy distribution, their effect on the time distribution is negligible. It has been suggested that some protons could fall out of synchronism at some point in the RF cycle, and thenceforward be incoherently affected by the RF; any such protons are not expected to, and do not, enter the channel or strike targets at the maximum radius.

Accompanying regenerative action is monochromatization; this is seen at once by a reduction in the time spread of the beam. This is illustrated by the oscillograms of fig. 8.

(a) Shows that the unregenerated beam striking an internal target in 300 μsec in duration corresponding to a 15 to 20 MeV energy spread.

(b) Shows that without a regenerator, the beam blow up time is about 200 μsec, showing

[11]) Henrich, Sewell and Vale, Rev. Sci. Inst. **20** (1949) 887.

that this produces a little monochromatization as already discussed in section 2.3.

(c) Shows the regenerated beam striking a probe outside the equilibrium orbit. The time spread is about 100 μsec, corresponding to 7 MeV energy spread.

This method is used for tests of energy selection as discussed in section 4.5.

The intensity of the regenerated beam has been checked by bombarding polystyrene foils at various radii. The foils were wider than the radial gain of the regenerated beam so that all particles should pass through them, and were sandwiched between $\frac{1}{4}''$ brass blocks to reduce multiple traversals.

The intensity drops suddenly between 41.5″ and 42″ radius the start of regeneration, and only 25% of the beam persisted beyond this point. In order to study the dependence of this loss upon the initial conditions, a beam clipper was inserted at a 35″ radius which only allowed protons with a $\frac{1}{8}''$ amplitude of vertical oscillation to be accelerated further. The measurement was then repeated. Almost all the beam passing the clipper was regenerated, showing that the loss of beam was due to vertical expansion. Since at large radius our dee aperture is about $1\frac{1}{2}$, and the peak to peak amplitude of vertical oscillations is initially about $\frac{1}{2}''$, an expansion of a factor of 3 can lose the beam. A larger aperature dee would probably allow an increase in intensity of the regenerated beam.

The radial gain at any radius can be measured with the foil, by measuring the radius of entry. For no radial gain all particles will only enter the tip; for a large radial gain they will enter an inch or more from the tip. These measurements agreed with the ionization chamber measurements in showing a radial gain slightly greater than theory predicts.

4.3. THE MAGNETIC CHANNEL AND THE UNPOLARIZED PROTON BEAM

The size and physical layout of the Harvard cyclotron requires that the beam be brought out rapidly with a short channel. This means that the beam must enter the channel at a large radius and it also sets some minimum value on the field reduction in the channel. The center of the channel entrance is placed 55° in front of the regenerator and $\approx$ 3.5 inches from the last equilibrium orbit. The next-to-last oscillation amplitude must then be 3.5 inches which requires that the regenerator action be carried out to larger radii than heretofore required[6]).

Although the construction of the magnetic channel follows the design principles set forth by LeCouteur[9]) the channel has no detailed resemblence to his design. The vertical motion of the regenerated particles have no definite phase relationship as do the radial motions but there is some correlation in the vertical motion. The vertical amplitude is at a maximum near the radial node 115° in front of the regenerator and goes through zero near the regenerator. Since the channel entrance is 55° in front of the regenerator the particles are converging as they enter the channel. The first sections of the channel must have a negative radial gradient which causes further vertical focusing and radial defocusing. LeCouteur suggests that at some point down the channel before the vertical crossover point where thicker channel bars may be used and less shiming is required the channel should have a positive radial gradient to cause vertical defocusing and radial focusing. By a suitable choice of the gradients and lengths of the positive and negative sections it should be possible to produce a nearly parallel beam at the channel exit.

There are limitations on the possible adjustments. Gradients in the channel may come from three sources: (1) The gradient of the cyclotron magnetic field. (2) Unequal thicknesses of the inner and outer channel bars. (3) The channel shims. Only (2) and (3) are variable and these only within fairly narrow limits. The maximum thickness of the inner bar of the first channel section should be as small as possible so as to intercept the least amount of beam. Thus the outer bar cannot be reduced much or the field reduction in the channel will be too small for

rapid extraction. Shims close to the channel also decrease the field reduction in the channel. Conversely, a certain amount of shimming is necessary in order to reduce the field defect produced by the channel bars.

Attempts were made to calculate the configuration of a focusing channel. However, when sample channel sections were tested in the cyclotron magnetic field, the measured gradients were found to be larger than those calculated using the simple assumption of saturated iron by as much a factor of two. The final channel design was obtained empirically using the measured gradients and final adjustments were made by minimizing the angular spread of the extracted beam.

TABLE I

FINAL CHANNEL

Section	Thickness		Length
	Inside Bar	Outside Bar	
1	3/8″	3/8″	5.5″
2	3/8″	1/4″	5.5″
3	1/2″	none	6″
4	1/2″	none	6″
5	1″	none	8″
6	1″	none	8″

All bars were of Cobalt Steel (Hiperco), two inches high and the spacing between the inside and the outside bars was one inch.

One particular difficulty in designing a focusing channel was obtaining a sufficiently small negative gradient in the first sections. This was made even more critical when it was discovered that the vertical convergence of the particles at the channel entrance was more rapid than LeCouteur had estimated in his example. It was not possible to shim the channel in such a way as to have only a small field defect near the channel and still retain the correct negative gradients in the first sections. A limit of 10 kg-in. was arbitrarily set for the integrated field defect due to the channel along the next to last orbit. Shims a few inches removed from the channel have little effect on the gradient, so near the equilibrium orbit the field defect after shimming is about 300 gauss inches and does not vary with radius.

The final channel dimensions are listed in table 1. Section 1 is strongly vertically focusing. Section 2 is also vertically focusing but much less so than section 1 due to the thin outer bar. Sections 3 and 4 are made nearly neutral by removing the outer bar entirely and using shims at the outer edge of the channel. Sections 5 and 6 are vertically defocusing. The positive gradient is obtained by using a single thick bar and having very little shimming at the inner edge of the channel. Since these two sections are already at a much larger radius no particles pass through the rather large field defect here. There is a 4 inch gap between sections 5 and 6 to permit the passage of a probe. The channel was initially positioned with a floating wire. The final position was obtained by optimizing the external beam intensity.

The motion of the particles down the channel has been found by inserting photographic film between the channel sections. The vertical motion is such that a crossover occurs about 5 inches after the end of the channel. At this point the beam is less than 0.25 inches high. The focusing action of the cyclotron fringe field reduces the vertical angular spread to less than 1° at the entrance to the bending magnet 175 inches from the end of the channel. Radially the situation is more complex. The spread in energies introduces a spread in particle orbits. However, the angular divergence of most of the beam is not more than 1°. As a result 90 percent of the beam is accepted by the 2.5 inch by 3.5 inch aperture of the bending magnet.

The spatical structure of the external beam is rather complicated but the major part is contained in two distinct groups, one above and one below the median plane. This is good evidence of the correlation of the vertical motions at the channel entrance.

Range measurements on the total unpolarized proton beam give an energy spread of 5 MeV full width at half maximum. This spread can be reduced by a slit at the channel entrance as

discussed in section 2.2. and 4.5. When this is done, range measurements give the full width at half maximum as $\leqslant 1$ MeV.

The maximum external beam observed at the tank exit is 7 percent of the internal beam. A more usual value is 4 percent. After passing through the bending magnet the beam is focused by two quadrupole magnets into the experimental area. The full beam can be focused into a line 3 inches wide by 0.25 inches high. The high energy part of the beam selected by the channel slit can be focused into a square spot about $\frac{3}{8}$ inches on a side. In a current experimental set-up the intensity of this spot is about 1×10^9 protons per second with an internal beam of about 1×10^{12} protons per second. No effort toward maximization has been made.

4.4. THE POLARIZED PROTON BEAM

A polarized proton beam is obtained by scattering the 159 MeV regenerated beam from an 11 MeV thick carbon target placed at a radius of 43.5 inches and 60° in front of the regenerator. The scattering angle is 17° where 80 percent polarization is expected[12]). Preliminary measurements of the degree of polarization give 75 percent. This may mean that we are scattering at an angle slightly less than 17°. The scattered beam is collected by two 4 inch aperture quadrupole magnets placed at 104 inches and 132 inches from the carbon target (measured along the orbit to the center of the magnets) and focused into the experimental area 134 inches from the second magnet.

Although the use of the regenerated beam to produce the polarized proton beam reduces the intensity of the polarized beam, a number of advantages outweigh this. The monoenergizing action of the regenerator results in a narrow energy width of the polarized beam. Its use also allows the positioning of the scatterer at a radius considerably outside the $n = 0.2$ point, and this permits the rapid extraction of the beam without the use of a magnetic channel. Besides the advantage of simplicity, the absence of a channel minimizes distortion of the effective source of the focusing magnets and helps in separating a lower energy component of the beam originating from a second traversal of the target.

Two focusing arrangements have been tried. The first, designed to give a small radial image, focuses the beam into a line 0.25 inches wide by 4 inches high (this height is determined by the vacuum pipe dimensions). Another much weaker and somewhat broader line appears 0.75 inches away from the main line. This weak second line is due to protons scattered from the internal target during a second traversal and has an energy 11 MeV less than that of the main beam. This lower energy component is easily removed by a slit. Under these conditons the intensity of the main beam is 3×10^6 protons per second with an internal beam of about 2×10^{12} protons per second. It has a vertical divergence of 0.8° and a horizontal divergence of 1.8°. The energy width obtained by range measurements is 3.5 MeV. Using the method suggested in section 2.2. and discussed more fully in section 4.5., the energy spread can be reduced to less than 1.5 MeV with a 65 percent loss of intensity. These values were obtained by unfolding the straggling function from the range data. It may be noted that the energy spread of the total polarized proton beam (3.5 MeV) is less than the energy spread of the total unpolarized proton beam (5 MeV). This may be due to energy analysis by the cyclotron fringing field.

The alternate focusing arrangement which reversing the currents in the quadrupole magnets is designed to give a beam with a minimum radial divergence and higher intensity. The image in the experimental area is 0.75 inches wide and 3 inches high. The lower energy component appears 2.5 inches away from the main image. Again this can be removed by a slit. The horizontal divergence of the beam is about 1°, the vertical divergence is 1.1° and the intensity is 2×10^7 protons per second.

[12]) Dickson, Rose and Salter, Proc. Phys. Soc. **68** (1955) 361.

4.5. INTERNAL ENERGY SELECTION

Since only partial monochromatization of the regenerated beam has been achieved, a method for selecting those particles with a definite energy is desirable. Such a selection is always possible by magnetic analysis of the external proton beams. However, large magnets and defining slits are required with resulting space and background problems and no such method exists for neutron beams. It is better to limit the energy of the protons inside the cyclotron tank before they enter the channel or strike a target. It has been shown in section 2.2. that such a method exists.

The application of this method is illustrated first for the use with internal targets, and secondly, for protons entering the magnetic channel. Fig. 9 (not to scale) illustrates the

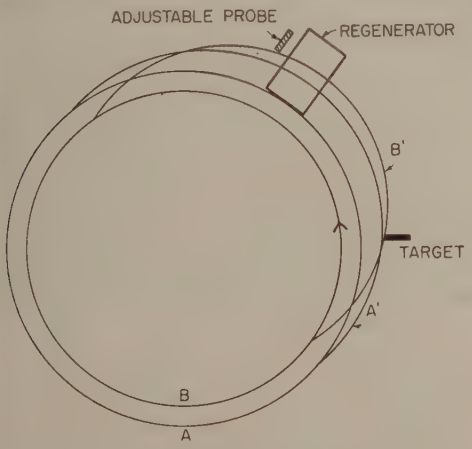

Fig. 9. An illustrative drawing, not to scale, showing the principle of energy selection for particles striking an internal target.

first case. Assume for simplicity that the regenerated beam has only two energy components whose equilibrium orbits are A and B respectively. A′ and B′ are regenerated orbits of the full and low energy components such that the particles just miss the edge of the target. If an adjustable probe is moved into the cyclotron at the position shown, it is clear that the low energy orbit B′ may be intercepted without affecting the high energy orbit A′ which strikes the target on the next revolution. Fig. 10 shows

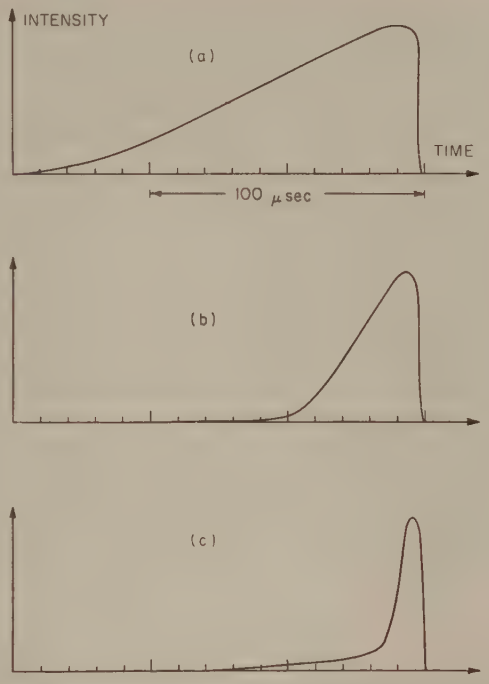

Fig. 10. Time distributions of the beam hitting an internal target after regeneration. (a) All the beam. (b) and (c) Beam reduced by the method of fig. 9.

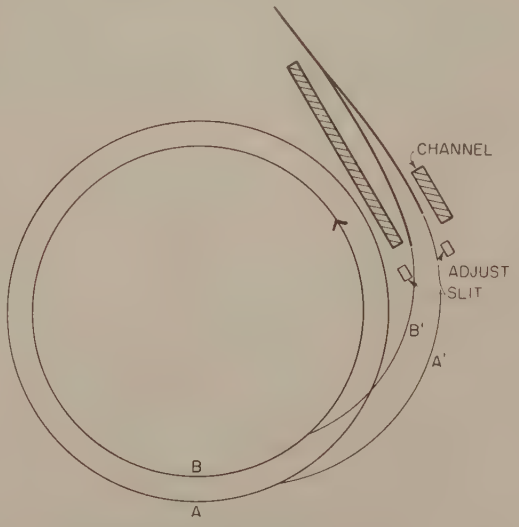

Fig. 11. The method of energy selection with the magnetic channel.

the time distribution of the neutron beam from the internal target for various probe positions. The time distribution may be made as small as

15 microseconds which is the time corresponding to the spread of the phase oscillations. The energy spread of the protons striking the target (neglecting multiple traversals) is then about 1 MeV. It is of interest, also, that the distance the probe has to be moved is in complete agreement with the orbit calculations of section 2.2. which further validates the method of calculation of particle orbits.

Fig. 11 illustrates the method used for particles entering the magnetic channel. Again A and B are the equilibrium orbits, and A′ and B′ are the regenerated orbits. A slit in front of the channel can select a narrow band of energies. This is illustrated by the time distributions in fig. 12. The pattern without reducing the beam, fig. 12a is not similar to that of fig. 10a. Presumably this is due to some energy selection in the channel.

All the members of the laboratory have helped this project in some way or another and their fine cooperation was responsible for its success. In particular M. Wanagel was responsible for the mechanical design features. We are very grateful to Professor K. J. LeCouteur for advice, to Dr. A Crewe and Dr. U. E. Kruse for information and discussion of the Chicago results before publication and to Dr. E. M. Hafner for informing us of his progress in beam extraction at Rochester.

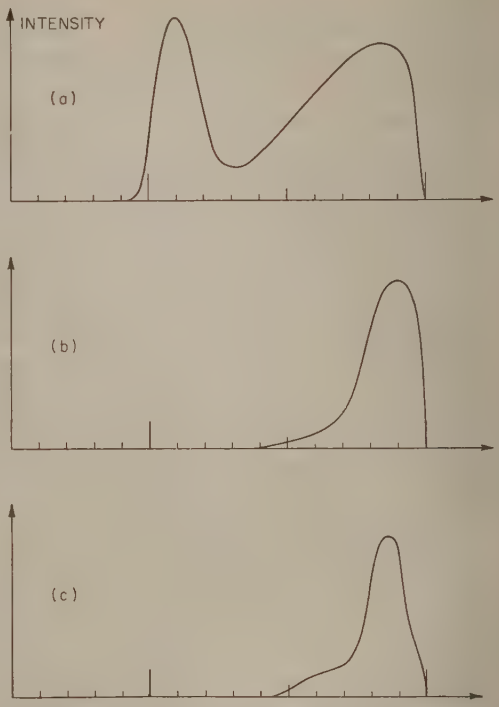

Fig. 12. Time distributions of the beam after passing through the channel and bending magnet. (a) All the beam. (b) and (c) Beam reduced by the method of fig. 10.

NUCLEAR INSTRUMENTS 1 (1957) 183–185; NORTH-HOLLAND PUBLISHING CO. – AMSTERDAM

A MILLIMICROSECOND PULSE-SHAPING CIRCUIT

P. R. ORMAN and F. H. WELLS

Atomic Energy Research Establishment, Harwell, Berks.

Received 28 March 1957

A pulse-shaping circuit is described which sharpens the output pulses from a secondary emission pulse generator, to produce negative pulses of one millimicrosecond rise-time and of seven volts amplitude at an output impedance of seventy ohms. The circuit is capable of being driven at a repetition frequency of 50 kc/s.

In the course of the development of fast electronic equipment such as distributed amplifiers and time spectrometers, the need has arisen for test pulses having a rise-time of one millimicrosecond. The relay pulse generator described by Garwin[1]) provides such pulses, but it appears that the maximum pulse repetition rate attainable from such devices is limited to about 100 per second, and this leads to difficulties with oscilloscope display. Whilst the extension of this method described by Dorn[2]) increases the possible repetition rate very considerably, the special mercury switch required appears to be costly and difficult to manufacture. The double pulse generator in common use[3]) in our laboratories and designed by one of us (F.H.W.) is a very much more flexible instrument than the relay devices but the rise-time of the output

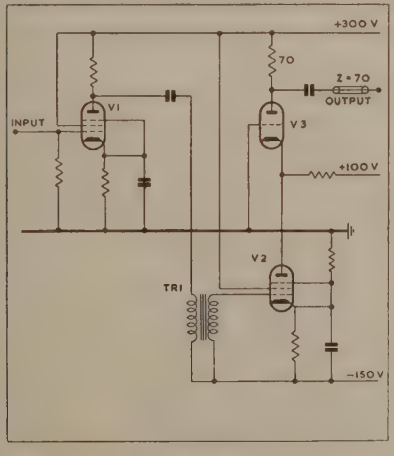

Fig. 1

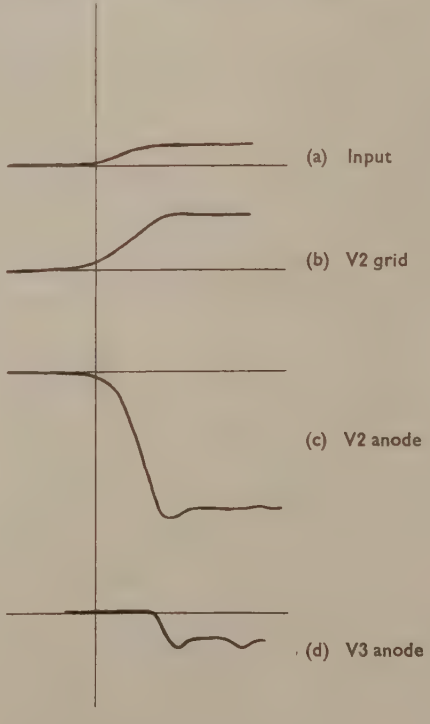

Fig. 2

[1]) A pulse generator for the millimicrosecond range. R. L. Garwin, Rev. Sci. Instr. **21** (1950) 11.

[2]) Fast-rise pulse generator with high pulse repetition frequency. C. G. Dorn, Rev. Sci. Instr. **27** (1956) 283.

[3]) Pulse generator type 1147. Specifications and Manuals Section, A.E.R.E., Harwell.

pulses, derived as they are from secondary emission pentode trigger circuits, is limited to about 8 mμsec. It was therefore felt that some means should be devised of decreasing the rise-time of these pulses using a separate pulse-shaping circuit. The resulting circuit will now be described.

The operation of the circuit may be understood from the simplified circuit diagram of fig. 1 and the waveform diagrams of fig. 2. The pentode V1 is normally conducting a small current (5mA) and is turned on further by the positive pulse applied at its grid. This pulse appears amplified and inverted at the anode, and is inverted again by the transformer TR1 before being applied at the grid of the pentode V2. In the quiescent state V2 is held cut off by the potential at its cathode to such an extent that it is the faster portion of the input pulse which turns the valve on. Nevertheless, as will be seen from fig. 2 (c), the current pulse in V2 rises quite slowly at first and is therefore unsuitable for use as an output. The high frequency triode V3 has its cathode held at 100 volts positive with respect to its earthed grid so that no current flows in this valve until its cathode potential has been reduced by almost 100 volts through the action of V2. By this time, however, the current in V2 is increasing very rapidly indeed and that in V3 rises in one millimicrosecond from zero to about 200 mA, this rate of rise being hardly affected by the small grid base of V3. The maximum duration of the output pulse is limited by the transformer TR1 to about 100 mμsec.

It should be noted that the waveforms given in fig. 2 are tracings from the face of a sampling oscilloscope which would be expected to introduce distortion at these high speeds. The rise-times shown at (c) and (d) particularly are slower than they should be, and it is also probable that the overshoots are produced by the oscilloscope. A more faithful reproduction of the output pulse has been obtained by using a developmental travelling-wave oscilloscope with a 70 ohm deflection system of very wide bandwidth. The rise time of the pulse is shown by this means to be 1 mμsec and the amplitude about 7 volts. Fig. 3 is a tracing from a photograph of

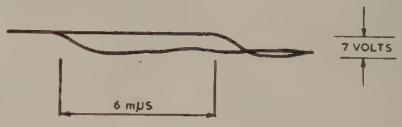

Fig. 3

the display on this oscilloscope representing the leading edges of two output pulses separated by 6 mμsec. It is at present uncertain whether the

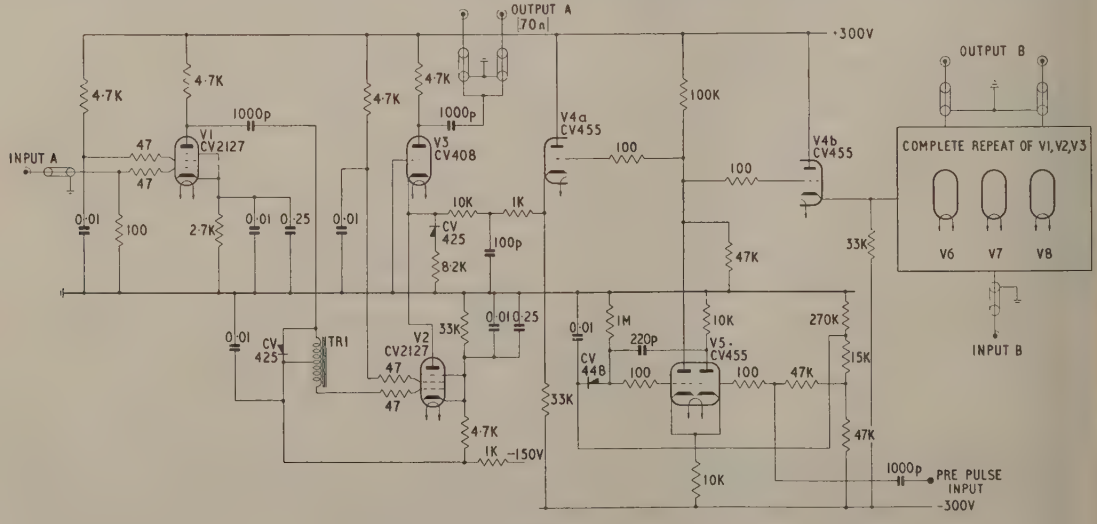

Fig. 4

shape of the top of the waveform is a faithful reproduction of the pulse shape, or whether this is again due to an imperfection in the oscilloscope. The latter is suspected.

In the simple circuit described above, the particular triode (V3) used has a very short life. The output pulse deteriorates both in amplitude and rate of rise after a few hours. Although valves rejected after failing in this way have not been thoroughly tested, it seems reasonable to suppose that the failure is due to the build-up of cathode interface resistance. In order to avoid this, the practical circuit takes the form of fig. 4. Here the triode V3 is arranged to conduct about 7mA in the quiescent state and is turned off a few microseconds before an output pulse is required. This is achieved by the action of the flip-flop circuit containing the valve V5. operated by a pre-pulse. Experience has shown that this method effectively prolongs the life of the triode V3, and no failures have been reported in over 100 hours running time. The crystal diode connecting the cathode of V3 to earth through an 8.2 kΩ resistor prevents damage to V3 when the negative 300 volts supply is switched on before the cathode has reached its operating temperature.

It will be seen from fig. 4 that two pulse-shaping circuits are provided. These are driven from the two output pulses of the double pulse generator mentioned previously. The pre-pulse is also obtained from this source. The flip-flop circuit in fig. 4 limits the maximum repetition frequency at which the pulse-shaper can be driven. Operation at 50 kc/s is however quite satisfactory and this is sufficient for most purposes.

NUCLEAR INSTRUMENTS 1 (1957) 186–196; NORTH-HOLLAND PUBLISHING CO. – AMSTERDAM

THE TIME-OF-FLIGHT TECHNIQUE APPLIED TO FAST NEUTRONS

K. G. MALMFORS, J. KJELLMAN and A. NILSSON

Nobel Institute of Physics, Stockholm

Received 9 April 1957

A system for the measurement of fast neutron velocities with the time-of-flight technique is described. The phase bunching of the extracted beam from a conventional cyclotron is used for the production of short bursts of neutrons. The integrated time-of-flight spectra are obtained by using a Tektronix 517 oscilloscope with a modified triggering device. The application of the system to a precision measurement of the mean energy of the accelerated protons is described.

1. Introduction

At the time when reactors were not yet available, cyclotrons were widely used as pulsed sources of slow neutrons. This was achieved by pulsing or modulating the ion source. The most commonly used method was to irradiate e.g. a thick Be-target with deuterons and moderate the neutrons in a block of paraffin. The duration of neutron pulses obtained in this way was given by the time taken to build up and quench the discharge in the ion source and also by the time for the slowing-down process. Since both effects take a time which is of the order of microseconds, the whole system was not capable of giving pulses of slow neutrons with a duration of less than a few microseconds. By applying the time-of-flight technique and by using a flight path of several meters, velocity analysis could be performed for slow neutrons. However, the method failed completely for neutron energies in the region above a few keV, since then the flight time became of the same order as the duration of the pulses. At that time the resolution of neutron detectors was also of the order of μ-seconds, so that even if sharper pulses had been available, the extension of the time-of-flight technique to higher energies would have been hindered by detection difficulties.

With present techniques, however, the above mentioned difficulties have been reduced and it is possible to extend the method into the region of fast neutrons (100 keV–10 MeV). The detector problem is no! onger a serious limitation. By the production of recoil protons within an organic scintillator, neutrons in the energy region above some hundred keV can be effectively counted with a time resolution of the order of millimicroseconds (mμs). Short bursts of fast neutrons are obtained from (p, n) or (d, n) reactions if the incoming ion beam is pulsed. With a Van de Graaff machine or a similar accelerator, such short bursts can be produced by sweeping the beam across a small slit[1]). Since the repetition time has to be long compared to the pulse length, the method suffers from the disadvantage that the effective beam is only a small fraction of the available current.

Cyclotrons seem to be a promising tool for providing short neutron pulses, since the ion beam from a cyclotron is pulsed as a consequence of the acceleration process[2]). Having such possibilities in mind the small cyclotron (7 MeV, deuterons) at the Nobel Institute in Stockholm has been reconstructed and moved so that it now offers good facilities for time-of-flight experiments to be made in an adjacent room which is well shielded from the cyclotron itself. A short description of the cyclotron, especially with respect to such details as are related to the problems discussed in this paper will be given in 4a.

During the last year some papers have been published which show that the same type of

[1]) L. Cranberg and J. S. Levin, Phys. Rev. **103** (1956) 343.

[2]) B. L. Cohen, Rev. Sci. Instr. **24** (1953) 589.

technique has been taken up also at other laboratories[3]).

The bunching mechanism in the cyclotron is discussed in 3. The experimental set up used at the Nobel Institute is described in 4 and a general discussion of the factors defining the energy resolution is found in 5. It is not to be expected that the time-of-flight technique applied to fast neutrons will yield a high energy resolution comparable with that of magnetic spectrometers for charged particles. The limitations of the method are discussed in 6, in connection with the determination of the mean proton velocity.

The method is suitable mainly for two different types of investigations.

1.1. THE DIRECT STUDY OF NUCLEAR REACTIONS INITIATED BY THE ACCELERATED IONS

In this field it is possible to identify different groups of neutrons and to measure the energy with an error of the order of a few percent. It is also possible to measure the angular distribution of each neutron group separately.

1.2. THE STUDY OF NEUTRON SCATTERING

By choosing a suitable reaction a pulsed source of monoenergetic neutrons is obtained. By exposing a scatterer to this neutron flux and observing the scattered neutrons only, it is possible to determine differential cross-sections for the eleastic scattering and for different groups of inelastic scattering. In the case of a heavy element as scatterer, the increasing number of nuclear levels can no longer be distinguished and the resulting spectrum is a continous distribution of inelastically scattered neutrons. Measurement of neutron scattering is of great interest in connection with current theoretical work on nuclear models.

2. The Time-of-Flight principle

There are four conditions which must be fulfilled for the determination of neutron velocities by the time-of-flight technique.

(1) The starting time of the neutrons must be well defined, i.e. the duration of a neutron burst must be short compared with the total flight time.

(2) The detection time must be equally well defined.

(3) A device must be available for the measurement of the time lag between these two events.

(4) The flight path must be known.

In most applications the flight path is a well defined quantity so that the uncertainty in the velocity determination is mainly due to errors in the time measurement.

The flight time, t (mμs), the flight path, L (cm) and the neutron energy E (MeV) are related in the following way:

$$E = 0.5220\,(L/t)^2\,[1 + 8.3\cdot 10^{-4}(L/t)^2] \quad .$$

With reasonable values ($L = 200$ cm, $E = 2$ MeV) the flight time is of the order 100 mμs. It follows that an energy resolution of about 10% (width at half max.) is obtained if the resolution of the flight time measurement is of the order of 5 mμs, which seems to be what is realizable with present techniques. The different contributions to this half width will be discussed in a later section.

The frequency of the cyclotron oscillator is 12.2 Mc/s so that the time interval between pulses is 82 mμs. Some ambiguity may seem to arise from this rather high repetition rate, since from one single measurement it is not possible to decide which ion bunch corresponds to a certain neutron group. As a rule this can be easily decided by changing the flight path. In the case of a continous neutron spectrum things are a little more complicated but, also in this case, it is possible to separate the contributions from different cyclotron periods by changing the flight path.

Since the neutron detector is sensitive to gamma radiation also, any γ-radiation from the target gives a "reference line" in the neutron velocity spectrum. The most convenient and reliable method of evaluating a spectrum is thus to measure the neutron flight time relative to the well known flight time of the γ-ray. In this way all constant delays in cables, amplifiers, photomultipliers and so on are eliminated.

[3]) G. F. Bogdlanov *et al.*, Soviet Physics JETP **3** (1956) 113. C. O. Muehlhause, S. D. Bloom, H. E. Wegner and G. N. Glasoe, Phys. Rev. **103** (1956) 720. R. Grismore and W. C. Parkinson, Rev. Sci. Instr. **28** (1957) 245.

3. On the Bunching Mechanism in the Cyclotron

During the last two years some papers have appeared concerning the phase bunching of cyclotron beams, but this special property of the cyclotron does not seem to have been utilized to any appreciable extent.

In order to see the mechanism of the bunching, let us first consider a cyclotron with a strictly homogeneous magnetic field. In this case the ions which are to be accelerated must move in such a phase that they pass the acceleration gap during the right half of the cycle and it goes without saying that those which pass the acceleration gap at maximum voltage are most effectively accelerated, since they have to go a smaller number of turns. Furthermore, if a deflected beam is considered, it is quite evident that ions which make a small radial increase per turn have a smaller chance of being accepted and passed through the deflector channel. This effect should be especially pronounced in the cyclotron described here due to the comparatively long and narrow deflector channel. Already from these purely geometrical considerations it follows that the beam from a cyclotron is pulsed.

In the real case the considerations are somewhat complicated by the fact that, for focussing purposes, the magnetic field decreases in the radial direction. Calculations show that this fact makes the "allowed" phase interval even smaller, since the ions change their phase during the acceleration. This effect is the more pronounced the larger the number of revolutions necessary to bring the ions to the final radius.

In addition to the type of pulsing indicated above, there is also a real bunching effect which has been treated numerically by Allwood[4]). The result of this effect is that ions which leave the ion source at different h.f. phase are confined, after one cycle, within a comparatively narrow phase interval.

The different contributions to the bunching may schematically be summed up in the following way. The condition that ions must be in the proper half of the cycle reduces the "allowed" angle to 180°. Due to small radial increase per turn, the "allowed" angle decreases to $\approx 90°$. By the phase change in the course of the acceleration the angle is reduced to $\approx 30°$ and due to the bunching near the ion source, the final angle can be estimated as being $\approx 15°$. This final angle corresponds to a pulse duration of ≈ 3 mμs, a value which is compatible with that observed in the experiments.

[4]) H. J. S. Allwood. Thesis, Birmingham University (1948).

4. Description of the System Used at the Nobel Institute

4.1. CYCLOTRON DATA

The 80-cm cyclotron at the Nobel Institute operates at 12.2 Mc/s and gives 7 MeV deuterons, or 3.5 MeV protons. The latter alternative —acceleration of hydrogen molecules—has been chosen for the work reported here mainly because background problems are in this case so much easier to overcome. Since the acceleration process is exactly the same in the two cases, it is to be expected that the discussions in this paper concerning resolution etc. will hold also if the neutrons are produced by a (d, n) reaction. The cyclotron is easily operated with some hundred μA internal current, and 5–10% of the internal current can be brought out through the deflector channel. The deflector operates at about —40 kV and is of the internal type. The beam is taken out in the conventional way by means of a thin (1 mm) molybdenum septum. At the entrance the deflector channel is 3 mm wide and the width gradually increases so that at the exit end it is about 12 mm. The deflector covers about 90°. The deflected beam is brought through a vacuum tube to a target about 8 meters from the cyclotron. The main focussing is done by two sector magnets. The first magnet which is placed just outside the cyclotron magnet, has a sector angle of 90° and a focal length of about 25 cm. This magnet focusses the beam in the horizontal direction and accordingly makes it divergent in the vertical direction. The second magnet, placed at a distance of about 1 meter, operates in the other way so that the combined system gives a fairly good focussing. In order to reduce the effect of the rather large magnification

of the system, a pair of quadrupole lenses is placed near the target end and, with the help of these two almost independent systems, it is possible to bring the total external beam to a focus of less than 1 cm^2. As the deflection angle in the sector magnets is rather small, there is practically no energy analysis of the ion beam. The mean energy of the protons has been determined by a time-of-flight method and is found to be 3.483 ± 0.004 MeV (cf. par. 6). From the experiments it is also possible to estimate the energy spread in the beam which is found to be less than $\pm$ 1%. The mean proton current has been kept at 5–10 μA.

4.2. TARGET

For scattering experiments there are several target materials that are suitable for neutron production. The most important reactions are listed below. In the second column the neutron energy region is given. The maximum and minimum values correspond to the forward and the backward direction respectively. (Proton energy 3.5 MeV, deuteron energy 7 MeV.)

$Li(p,n)^7Be$	1.9– 0.8 MeV
$T(p,n)^3He$	3.5– 0.5 MeV
$D(d,n)^3He$	8 – 1.8 MeV
$T(d,n)^4He$	20 –12 MeV.

All measurements reported in this paper have been made with a Li-target bombarded with protons. This reaction has one drawback, namely, the existence of a secondary ($\approx$ 10%) neutron group below the main group, corresponding to the excitation of the 435 keV state in Be^7. The target should be made so thin that its contribution to the broadening of a neutron group should not influence the resolution appreciably. If this condition is fulfilled, the width of a neutron group should be the same as that of a γ-group, since the latter is independent of target thickness. The target used for most of the measurements reported here had a thickness corresponding to about 30 keV. The target consisted of metallic Li evaporated onto a gold backing.

4.3. STARTING-TIME INDICATION

The starting time is defined by the incoming ion bunch. As it is easy to correct for constant time delays by using gamma ray counting as a "reference line", one would immediately think of the cyclotron oscillator itself as an indicator of starting time, since one would in the first instance imagine that all ion bunches enter the deflector channel in the same h.f. phase. Experiments have shown, however, that this method is not good, since the phase position of the ion bunch does depend on the adjustment of the cyclotron resonance so that the ions come out earlier if the magnetic field is on the upper part of the resonance curve. This can be eliminated, of course, by avoiding any changes in the cyclotron adjustment during one run which is, however, difficult in practice. Another way of indicating the starting time is to observe a fraction of the ion beam near the target, which should be the most direct and reliable method. For this purpose a thin-walled Al-tube, containing a liquid scintillator (terphenyl in xylene), is placed in the edge of the beam close to the second quadrupole lens. The light pulses are observed with an RCA 5819 photomultiplier. The reason for using a liquid scintillator is that it is not so quickly destroyed as a plastifluor.

4.4. DETECTOR

For the detection of the neutrons, a plastic scintillator (Plastiflour "B" from the Pilot Chemical Co.), diam. 2″, height 1″, has been used. It is covered with MgO for maximum light response. An RCA 6342 photomultiplier tube operated at about 1200 V has been used throughout the experiments. Pulses are amplified about 1000 times in distributed amplifiers and fed through a 140 Ω coaxial cable to the control room about 30 m away.

4.5. MEASUREMENT OF FLIGHT TIME

The information entering the time-measuring device is the amplified pulses from the neutron detector and a series of equidistant photomultiplier pulses indicating the starting time. In the choice between different possible methods it was decided that the method using a fast oscilloscope should be applied and, thanks to a

special grant from the Nobel Committé, it was possible to buy a Tektronix 517 oscilloscope, which has most of the properties needed for an experiment of the type discussed here. It has a vertical amplifier with sufficiently short rise-time (7 mμs), a high sweep speed of 10 mμs/cm at 24 kV acceleration voltage and a sensitive triggering device.

For some early experiments the oscilloscope was used in the following direct way. A pulse from the detector triggered the sweep and was also delayed and fed to the vertical plates so that the pulse was displayed on its own sweep. The starting pulses were continously fed to the same vertical plates and the oscilloscope screen was photographed continously with a camera with moving film. The developed picture was then projected onto a calibrated time scale. The cyclotron period (82 mμs) was devided into 50 intervals and the final result was represented by a histogram showing the number of events in each interval.

It was felt early, however, that an integrating method was extremely desirable. The principle of the system worked out for this purpose is the following: The pulses from the neutron detector are used to trigger the oscilloscope. The other set of pulses is continously fed to the vertical plates so that on each sweep there are two or three equidistant pulses. By using the latter pulses also for intensity modulation of the oscilloscope beam and by applying a suitable delay, it could be achieved that the whole sweep except for the rising part of the pulses was suppressed (cf. fig. 3a). Thus each event in the neutron detector is displayed on the oscilloscope screen as a steeply rising short line, the position of which depends on the neutron flight time.

By photographing the superposition of many such lines one obtains the time-of-flight spectrum, which is repeated periodically with the cyclotron frequency. For the quantitative evaluation, the film is analyzed with a photometer which gives the position, half width and relative height of the different "lines" in the spectrum.

Since, however, the conversion of photographic intensity to number of events in different groups may give poor accuracy, we are investigating the possibilities of converting time lengths to pulse heights, which could then be analyzed by an ordinary hundred channel analyzer. By using both of these systems simultaneously we retain the advantage of the photographic method for the energy measurements.

The first experiments with this technique gave rather bad resolution compared with the direct method described above which gave a

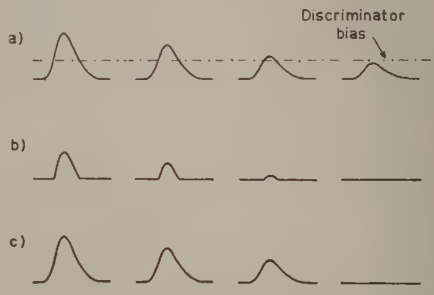

Fig. 1. a. Discriminator input pulses. b. Discriminator output pulses (original system). c. Discriminator output pulses (modified system).

half width in the histograms of about 5 mμs. Several modifications and improvements have been necessary to give an acceptable resolution with the integrating method. It was evident that the main source of error was associated with the triggering of the oscilloscope, due to the fact that the output pulses from the "trigger amplitude" discriminator were too small to give a perfect triggering of the sweep when the discriminator input pulses were just above threshold. (Cf. fig. 1a and b that shows some discriminator pulses of different input amplitudes.)

Fig. 2 shows the discriminator principle of the modified system. The input pulses go in two parallel branches to the two grids of the gate tube 6BN6. In one branch there is a fast multivibrator (6BN6 and EL 83) which is used as a discriminator by means of a variable negative bias on the input grid. The multivibrator pulse keeps the gate tube open for about 100 mμs. In the other branch there is a delay such that the pulse does not arrive at the limiter grid of the gate tube until its quadrature grid is fully opened.

The advantage of this system is that no small pulses will enter the sweep triggering device, since pulses go practically unchanged (except for sign) through the gate tube when it is opened, and since small pulses do not fire the multivibrator (cf. fig. 1c). The length of the multivibrator pulse and the delay in the second branch secure that a time "jitter" in the firing of the multivibrator will not affect the satisfactory operation of the circuit.

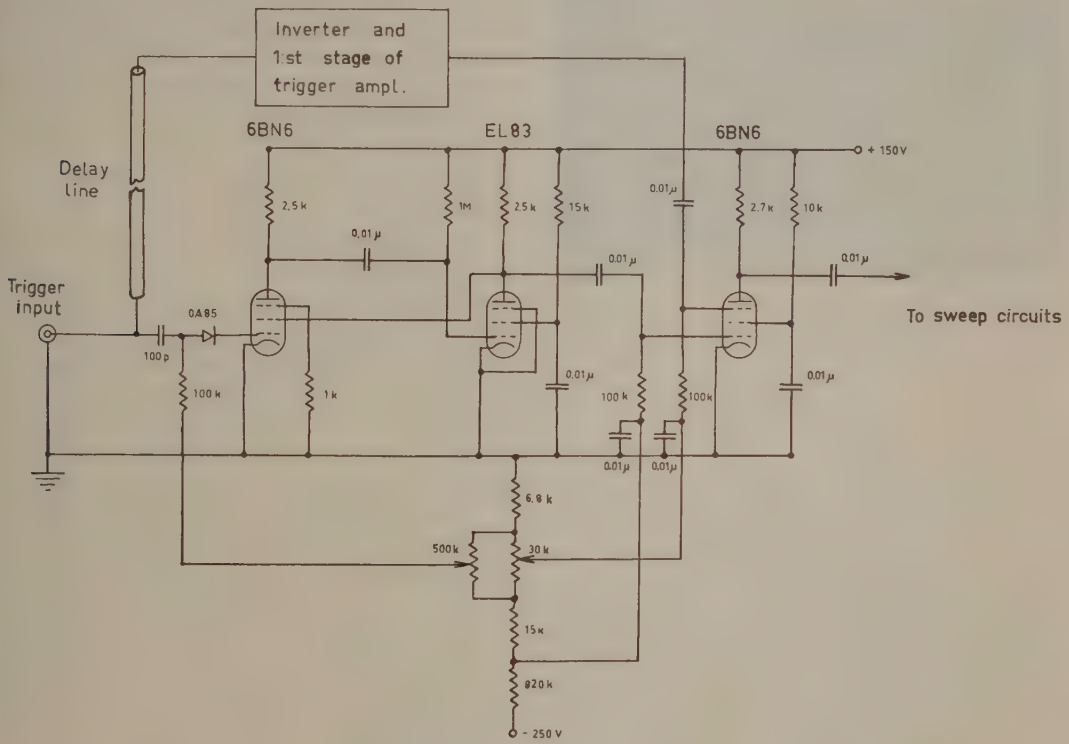

Fig. 2. Modified discriminator system.

As mentioned earlier, the pulses which indicate the starting time are taken to the input of the vertical amplifier of the oscilloscope. The output of the amplifier is a push-pull stage so that there is one positive and one negative output pulse available of about 70 volts. The negative one is used for the intensity modulation. It is coupled via a differentiating network (50 pF, 330Ω) to the cathode of the oscilloscope tube. The other pulse is delayed and goes to one of the deflector plates. Fig. 3 a shows schematically the appearance of a large and a small pulse. (Only the broad parts of the curves are visible on the screen due to the intensity modulation.) It could be expected that an intense ion bunch is recorded earlier than a small one, even if the width of the bunches is the same. In order to avoid this to some extent a shorted stub of

Fig. 3a

Fig. 3b

Fig. 3. Appearance of a large and a small pulse. a. Without stub. b. with stub.

about 1.5 meters in length is placed at the input to the oscilloscope, so that the pulse shape is the superposition of the primary pulse and the same pulse with opposite polarity and a delay of about 10 mμs. This new shape is indicated in fig. 3b. Since large and small pulses are conformal, all cross the zero level in the same point.

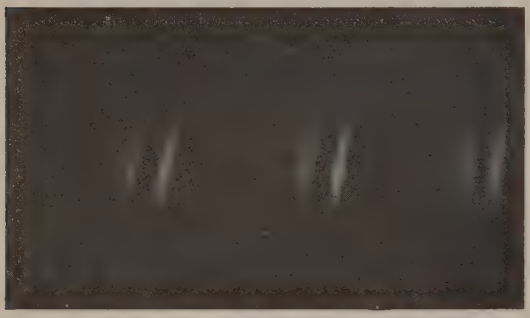

Fig. 4a. The main neutron group and the γ-group from the Li-target as seen on the oscilloscope screen. (10 000 sweeps recorded on 35 mm Ilford 5B52 recording film.)

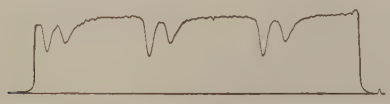

Fig. 4b. The corresponding photometer curve.

The intensity modulation is delayed so that maximum intensity occurs at this crossing point, where the spread can be expected to be a minimum. By this procedure the resolution was somewhat increased. Fig. 4a shows the appearance of a typical pattern on the oscilloscope screen and fig. 4b the corresponding photometer curve.

4.6. COLLIMATOR

For the measurement of scattered neutrons it is, of course, necessary to use some sort of a collimator, because the primary neutron flux from the target is several orders of magnitude more intense than that from the scatterer. The distance between target and scatterer must be kept rather small for intensity reasons. A reasonable distance is 10–15 cm. The arrangement used is shown in fig. 5. The diameter of the collimator channel is 5 cm and its total length is 100 cm. The detector is placed in the center of a 20 cm lead cube, which is surrounded on all sides with 20 cm of paraffin mixed with boric acid. The nose of the collimator is made of the same material. The collimator is placed on a carriage which can be rotated around the scatterer or alternatively around the target. The flight path can be varied from 1 m to about 4 m. Due to the fact that the distance from the target to the floor (1.5 m) to the ceiling (1.5 m) and to the walls ($\approx$ 5 m) is rather small, there is a considerable background of scattered neutrons and γ-radiation, so that a collimated detector is to be preferred also for the study of radiation directly from the target.

4.7. DISTURBANCES ASSOCIATED WITH THE CYCLOTRON

The background radiation from the cyclotron itself is effectively screened by a 90 cm concrete wall between the cyclotron and the target room. The h.f. disturbances from the cyclotron oscillator have been the cause of much trouble, which is quite natural as mV-pulses have to be observed in the close vicinity of the 30 kW oscillator. A good deal of h.f. power was transmitted along the metal tube leading from the cyclotron to the target. By inserting a 30 cm long quartz insulator in this vacuum tube the distortions were appreciably reduced, but still there was a large h.f. amplitude induced in the measuring system. The amplitude could be reduced to some extent by moving the coaxial cables leading to the control room into suitable relative positions. The h.f. disturbances are now reduced to the same level as the amplifier noise by means of an open quarter wave stub at the trigger input to the oscilloscope. There is also a stub adapted for the second harmonic. The detector pulses are, of course, also reflected in these stubs but, as the first pulse has triggered the sweep, the oscilloscope is insensitive to subsequent pulses arriving within this short time interval.

There has also been some trouble with disturbances from the oscillator for the heating of the ion source filament but, since the frequency in this case is only 1 Mc/s, conventional filter circuits could be applied.

4.8. COUNTING RATE

Some typical figures are given below in order to illustrate the relative magnitudes of counting rate and background effects (proton current ≈ 5 μA, Li-target 0.3. mg/cm^2, flight path 2 m).

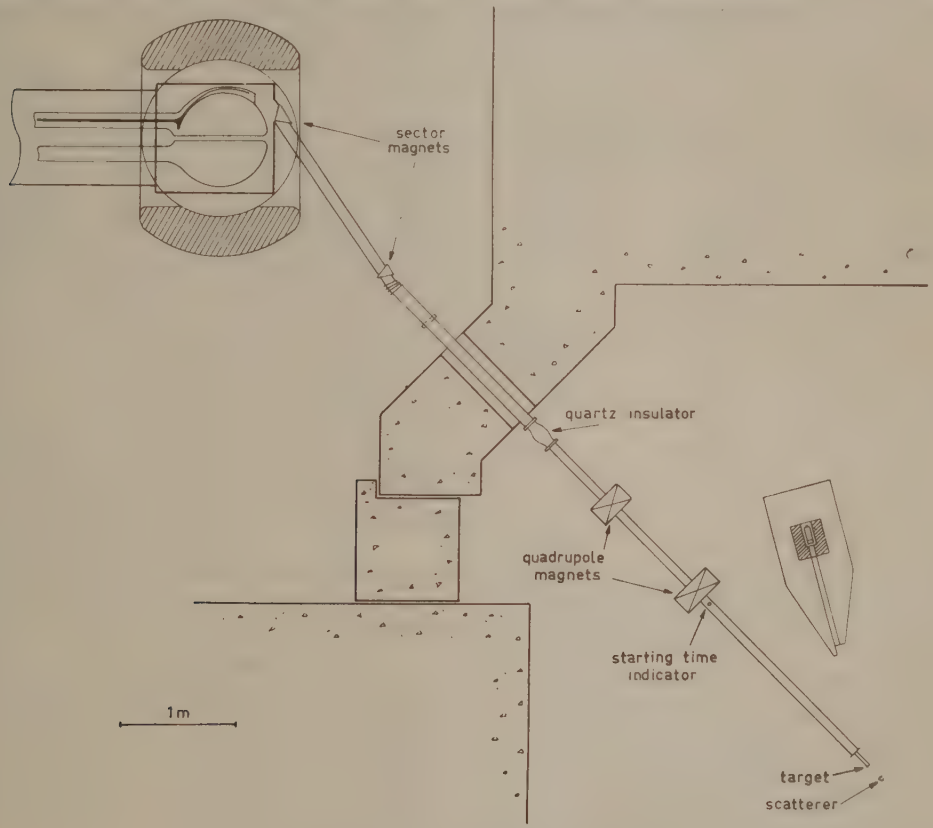

Fig. 5. General view of the experimental set-up.

Background (no external beam):	10 counts/s
Neutrons directly from the target (forward direction):	1000 counts/s
γ-radiation directly from the target (forward direction):	100 counts/s
Neutrons and γ-radiation from a scatterer (300 g of iron, 13 cm from the target, detector at 90°):	40 counts/s
Scatterer removed:	25 counts/s

As these figures show, there is a rather high counting rate also when the scatterer is removed, which is mainly due to γ-radiation arising from neutron capture in the collimator. It should be remembered, however, that this background is uniformly distributed in time, whereas the scattered radiation is confined to discrete energies so that the corresponding peak height is several times the background.

4.9. MONITORING

As the integrating method described here gives the whole time-of-flight spectrum simultaneously, a monitor is not needed for the evaluation of a single spectrum. However, when angular distributions are to be measured, it is necessary to use some sort of a monitor. A G.-M.-counter is placed at such a small distance from the target (20 cm near the backward direction) that the counting rate should not be influenced by the position of the collimator. The monitor counts mainly γ-radiation from the target and is shielded with lead so that it gives a reasonable counting rate.

4.10. CORRECTION FOR THE NON-LINEARITY OF THE SWEEP

The sweep speed on the oscilloscope screen is not strictly constant and a correction has to be applied. This was determined by photographing the trace of a high frequency ($\approx$ 150 Mc/s) oscillation. The sweep velocity varies smoothly. It goes through a maximum near the beginning of the sweep and then decreases by about 10%. The time scale of the oscilloscope is not used in the absolute sense since all measurements are made in relation to "reference lines" of γ-radiation. The sweep speed (20 mμs/cm) is such that two whole cyclotron periods are displayed on the sweep, which means that the position of a neutron peak can always be measured by interpolation between two γ-peaks the distance between which can be measured with a high precision. The maximum deviation from linearity within such an interval is about 1 mμs. By applying the correction this error is reduced to $\approx$ 0.1 mμs.

4.11. THE EFFICIENCY OF THE NEUTRON DETECTOR

The neutron counting efficiency of a plastic scintillator depends on the neutron energy. At high energies the efficiency decreases due to the decreasing cross-section for (n, p)-scattering. At low energies there is a cut-off defined by the discriminator setting. This level has to be chosen so that dark-current contribution from the photomultiplier tube is sufficiently low. As a rule this means that neutrons with energy below $\approx$ 0.3 MeV are below the discriminator treshold. Fig. 7 is reproduced from Cranbergs paper and shows the efficiency curve for a $1\frac{1}{2}''$ scintillator of the actual material.

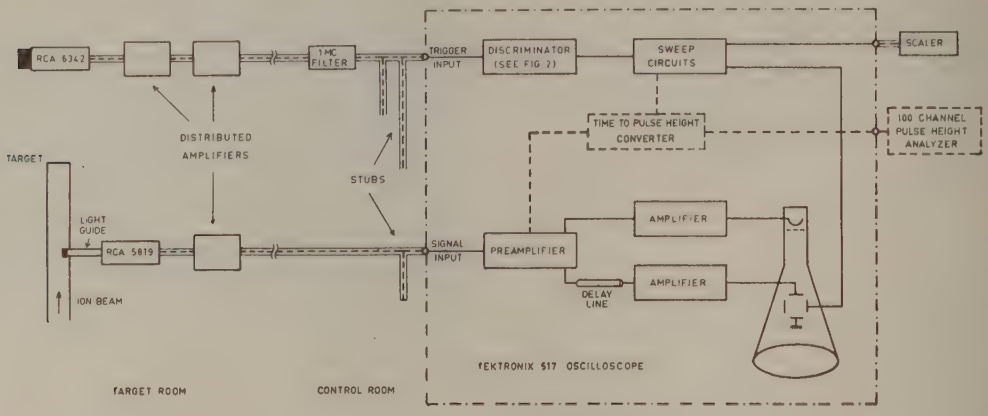

Fig. 6. Block diagram of the electronics.

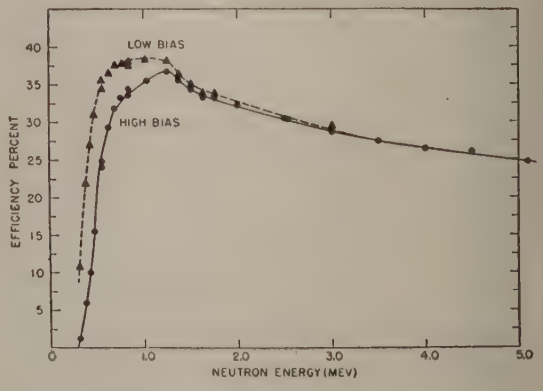

Fig. 7

5. Discussion of the Resolution

Due to the finite resolution of the experimental arrangement, a truly monoenergetic group of neutrons is revealed as a distribution defined by a certain half width. It is the purpose of this chapter to discuss in some detail the different contributions to this total half width, which in the following is expressed in units of mμs.

(1) The ion bunch has a certain initial width

Γ_1, when it leaves the cyclotron. Probably this width can be varied by changing the conditions in the cyclotron. It is to be expected, for instance, that the duration of the pulse increases with increasing D-voltage. It is difficult to measure this width separately since it cannot be distinguished from other sources of broadening but, considering that the overall resolution corresponds to a width of about 5 mμs, it seems reasonable that Γ_1 is ≤ 3 mμs.

(2) Since the target is situated about 8 meters from the cyclotron, any energy spread of the beam will give a broadening of the pulse. If the energy is defined by $E \pm \Delta E$, the corresponding pulse width, Γ_2, at the target is

$$\Gamma_2 = 310 \cdot \frac{\Delta E}{E} \cdot$$

At the target, the total ion pulse length is a combination of Γ_1 and Γ_2 defining the duration of the neutron pulse, since the target reaction takes place within such a short time that it can be neglected. Some indication regarding the relative magnitudes of Γ_1 and Γ_2 has been obtained in connection with a determination of the proton velocity, described in 6. The ions give rise to γ-radiation from two different targets simultaneously, the one placed about 2.5 m from the cyclotron and the other at the ordinary position about 8 m distance. This has the consequence that the broadening due to energy spread, Γ_2, should be different in the two γ-peaks, so that the width of the γ-peak from the first target, Γ_a, should be smaller than that from the second, Γ_b.

The half widths are related in the following way:

$$\Gamma_a^2 = \Gamma_1^2 + (\Gamma_2/3)^2 + \Gamma_3^2 + \Gamma_4^2 + \cdots$$
$$\Gamma_b^2 = \Gamma_1^2 + \Gamma_2^2 + \Gamma_3^2 + \Gamma_4^2 + \cdots$$

which gives approximately

$$\Gamma_2 \approx \sqrt{\Gamma_b^2 - \Gamma_a^2} \cdot$$

Experimental values of Γ_b and Γ_a indicate that ΔE is $< 1\%$. (This estimate holds only if Γ_1 and Γ_2 are independent and combine quadratically. There is, for instance, a remote possibility that the higher energy ions systematically come out later from the cyclotron and overtake the slower ones so that the combined width at the target is smaller than both Γ_1 and Γ_2.)

(3) The resolution of the time measuring device, Γ_3, can be determined separately by using a radioactive source. Pulses from the detector trigger the sweep of the oscilloscope in the usual way and the same pulses are delayed and displayed on their own sweep. Such measurements include the uncertainty in the triggering, the width due to the finite size of the focal spot on the oscilloscope screen and the width associated with the photographic and the photometric procedures. Measurements of this kind give values for the half width which are about 1 mμs.

(4) There is another cause of broadening, Γ_4, which is not included in the effects mentioned above, namely that associated with the spread in transit time in the photomultipliers.

(5) The finite size of the scatterer and the scintillator give a comparatively small contribution, Γ_5, to the broadening. It is sufficient to keep the linear dimensions below ≈ 3 cm, as the velocity of detectable neutrons is always > 1 cm/mμs.

6. Determination of the Mean Proton Energy

At first sight it is not to be expected that the technique described here is capable of giving particle velocities with high precision. The reason is on the one hand that the instrumental resolution is such that particle groups have a half width of ≈ 5 mμs, and on the other hand that there is an energy spread of the order of 1% in the proton beam.

By using a relative method with two targets, it seems possible, however, to measure differences in flight time with a fairly high degree of precision. This method has been used for the measurement of the mean proton velocity in the beam. The first target was placed about 5 meters in front of the second target which was at the ordinary position about 8 m from the cyclotron. The detector was placed in the forward direction. In the first target there was a hole so

large that the two targets gave the same contribution to the counting rate in the detector. The detector was shielded with paraffin so that only γ-radiation was counted. The measured spectrum then consists of two almost identical groups, corresponding to the γ-radiation from the two targets. The time lag between these two groups is the difference between the flight time of the protons and that of the γ-rays over the distance between the two targets. The advantage of this method is that one now has to measure the distance between two almost identical lines, which can be done with rather high precision even if the lines are relatively broad. The probable error in the measurement of this distance can be estimated to be about 0.2 mμs. The total flight time was 208.2 mμs, i.e. two whole cyclotron periods plus the time lag measured in the spectrum. The measurement of the cyclotron period and of the flight path could be made so accurately that these two sources of error are negligible in comparison with the time measurement mentioned above.

Flight path =	536.6 cm
Cyclotron frequency =	12.198 Mc/s
Flight time =	208.2 ± 0.2 mμs
Mean proton energy =	3.483 ± 0.007 MeV.

The same technique can probably be used also for measurements of neutron velocities, and the same order of accuracy is to be expected. The method is applicable only to very special reactions, however, having one dominating neutron group.

Our sincere thanks are due to Professor Manne Siegbahn for his interest and encouragement during the course of this work. Thanks are also due to Mr. T. Appelquist for valuable technical assistance.

NUCLEAR INSTRUMENTS 1 (1957) 197–199; NORTH-HOLLAND PUBLISHING CO. – AMSTERDAM

GLASS SCINTILLATORS FOR PROMPT DETECTION OF INTERMEDIATE ENERGY NEUTRONS

P. A. EGELSTAFF

A.E.R.E. Harwell, Didcot, Berks.

Received 16 April 1957

Borate and phosphate glasses have been made which dissolve organic scintillators. The use of such "glass scintillators" for the detection of neutrons has been investigated and the most promising type is a heavy element containing phosphate glass.

The prompt detection (i.e. within 0.1 μsec) of neutrons with energies between 100 eV and 10 keV at a high efficiency is very difficult. This is because the detection process must involve a nuclear reaction (the energies being too low for processes such as proton recoil to be detectable) and the reaction cross sections are small in this energy range. Prompt detection of particles is usually achieved by observing the scintillations produced in a suitable transparent material. In the case of neutrons the B(n, α) reaction is the most useful, and scintillation detectors have been made employing combinations of B_2O_3 with ZnS and methyl borate with organic phosphors (Bollinger (ref. [1])). The former combination can be used only in very thin layers due to light scattering by the ZnS, and the latter combination is very γ-sensitive and has a time delay > 0.1 μsec due to the moderation of

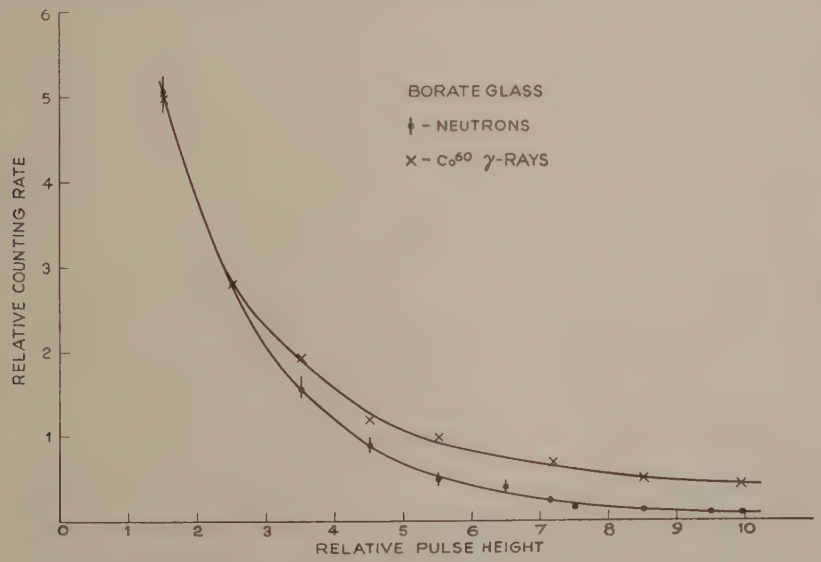

Fig. 1a

PULSE HEIGHT DISTRIBUTIONS FOR VARIOUS SCINTILLATING GLASSES

[1]) L. M. Bollinger, Proceedings of the International Conference on the Peaceful uses of Atomic Energy (United Nations, 1955) Vol. 4, paper 580.

the neutrons in the detector. A scintillator is required therefore which can be prepared in very thick layers so as to absorb all the neutrons, and which neither is very γ-sensitive nor involves a time delay in the detection process.

A preliminary investigation into the possibility of using a glass for this purpose has been completed. It was found that a series of borate and phosphate glasses could be prepared which tested and the greatest solubility was found for α-naphyl phenyl oxazole (α-N.P.O.). Fig. 1a shows the pulse height distribution for neutrons and Co^{60} γ-rays obtained with a glass containing 0.4% by weight of α-N.P.O. It can be seen that this combination is very γ-sensitive and therefore unsuitable for our purpose. However as compared to detectors based on methyl borate the boron content is much greater. This means

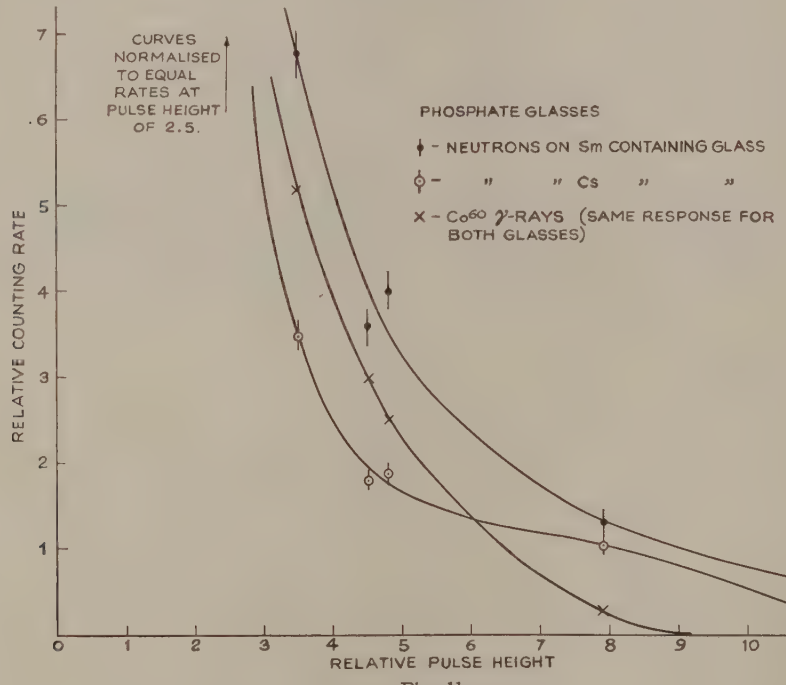

Fig. 1b

PULSE HEIGHT DISTRIBUTIONS FOR VARIOUS SCINTILLATING GLASSES

had melting points between room temperature and 400°C,—the actual melting point being determined by the water content of the glass. Further these glasses dissolve or are dissolved by organic materials including organic phosphors and in this way a scintillating glass can be prepared. All the water containing glasses made in this work were deliquescent.

In the case of borate glasses the most suitable one is prepared by heating boric acid to between 190 and 210°C when a glass of approximate composition $H_2B_4O_7$ is obtained. The solubility of various organic phosphors in this glass was

that the time delay will be small for this system.

In the case of phosphate glasses the (n, γ) reaction in various heavy elements was used as the detecting process. Here γ-discrimination in the detector would be achieved because the total γ-ray energy ($\approx$ 6 MeV) following neutron capture is much greater than the energy ($\approx$ 1 MeV) of the γ-rays constituting the background in many experiments. The elements, Cs, Nd, Sm, Gd and W were used in the phosphate glasses, the preparation of which involved only the reaction of excess orthophosphoric acid with the oxide. The amount of excess acid could

be reduced through the addition of alkali phosphates (e.g. Na).

Fig. 1b shows the pulse height distribution for neutrons and Co^{60} γ-rays obtained with both a samarium sodium phosphate glass and a caesium phosphate glass each containing 0.2% α-N.P.O. by weight. The thickness of glass used was about 1 gm/cm^2 so that only partial absorption of the neutron capture γ-rays was achieved. Nevertheless the pulse height due to neutrons is greater than that due to the 1.3 MeV Co γ-rays. This method therefore functions in the expected manner. Experiments carried out on thicker layers of glass indicate that some emitted light is reabsorbed.

In this work we have shown that it is possible to make glass scintillators for detection of γ-rays, and that the detection of neutrons through the (n, γ) process in the presence of a 1 MeV γ-ray background is possible. Further development is required to produce a slab of glass which has a satisfactory optical transmission, and is thick enough to absorb most of the capture γ-ray energy.

NUCLEAR INSTRUMENTS 1 (1957) 200; NORTH-HOLLAND PUBLISHING CO. – AMSTERDAM

THE OUTPUT DISTORSION OF A DIFFERENTIAL INTERVAL ANALYZER OF UNIVERSAL DESIGN

SAIT AKPINAR

Experimental Physics Department, University of Istanbul

Received 22 March 1957

The output distribution $N_d(t)$ of a differential interval analyzer which has the following characteristics is calculated for a constant input rate n.

(1) All events are to be counted which occur in time intervals of the size $\Delta t = \tau_3$ following zero point events with an interval $t = \tau_1 + \tau_2$. τ_1 is the effective resolving time of the detector preceding the analyzer. Compared with τ_2 and τ_3 it is sufficiently small and can be neglected. τ_2 is variable in a wide range.

(2) The recovery times of the circuit elements producing the time durations τ_2 and τ_3 are negligibly small.

(3) The circuit shall make no difference between the counted and uncounted events by zero point selection. This has always to be the first event which succeds the previous zero event by an interval greater than τ_2, in the case (a) of $\tau_2 > \tau_3$, or τ_3 in the case (b) of $\tau_3 > \tau_2$.

These characteristics, except 3b are fairly common and most easily realized by using nonparalyzable circuits as generating devices for τ_2 and τ_3 gates. It is therefore of general interest to know the distorsion which is introduced in the true input distributions to be determined by using analyzers of the stated characteristics.

The calculation is based on a Poisson input distribution

$$P_k = \frac{(n\tau_3)^k \cdot e^{-n\tau_3}}{k!}$$

and the following probability function

$$q_k = \frac{k}{\frac{\tau_3}{\tau_2} + k - 1} \quad ;$$

q_k is the probability for an event to be selected as a zero point event out of k events which coincide with a differential interval $\Delta t = \tau_3$.

The output distribution of the analyzer in third order approximation is

$$N_d = \frac{n^2\tau_3}{1 + n(\tau_2 + \tau_3)} \left\{1 + n\tau_\nu + \left(1 - \frac{\tau_3}{\tau_\nu + \tau_3}\right) n^2\tau_\nu^2\right\}$$

with

$$\nu = 2 \quad \text{for} \quad \tau_3 > \tau_2 \geqq 0$$
$$\nu = 3 \quad \text{for} \quad \tau_2 > \tau_3 \ .$$

In this formula high input rates n are considered which usually are not admitted in similar cases. Furthermore the range of t is extended by inclusion of the case $\Delta t > t$ in the direction of smaller values, until $t = \tau_2 \simeq 0$. Both these extensions are important if one is concerned with the experimental determination of interval distributions of weakly radioactive materials (a few hundred disintegrations per min) in reasonably short times.

An electronic single channel apparatus, based on highly unsymmetrical univibrator circuits was constructed and formula (1) was checked in the ranges $\tau_2 = 0 - 1000$ msec and $\tau_3 = 10 - 70$ msec. Interval distributions in the β-emission of Ra D, E, UX_2, Co^{60}, C^{14} and cosmic ray single events satisfied the formula until $n\tau_3 \simeq 0.2$. Radioactive fallout mixtures, which were the initial subject to this investigation, generally showed the same behavior, though in some cases a marked departure from the randomicity could be observed.

The details of this investigation, including the used circuit will appear in Rev. Fac. Sci. Univers. Istanbul, Serie C 22 (1957) 59.

NUCLEAR INSTRUMENTS 1 (1957) 201–212; NORTH-HOLLAND PUBLISHING CO. – AMSTERDAM

DÉMULTIPLICATEURS ÉLECTRONIQUES D'IMPULSIONS

2ème Partie

DÉMULTIPLICATEURS A HAUTE FRÉQUENCE

ROBERT L. FAVRE

Laboratoire De Recherches Nucleaires, Lausanne

Received 15 November 1956

The second part deals with high frequency scale, in which the secondary emission tube plays an important part. Aperiodic impulsion generators, frequency dividers impulsion counters and electronic chronograph benefit from the proposed base circuit. The frequency limit for these various applications reaches 30 Mc/sec, while the electronic chronograph recurence time can be lowered to 0.01 microsecond with a particular device.

1. Le Tube a Émission Secondaire Générateur d'Impulsions Cathodiques [7])

1.1. Le schéma de principe du tube à émission secondaire couplé en générateur d'impulsions cathodiques est donné par la fig. 11. L'anode, reliée directement à la haute tension, devient électrode "passive". L'impédance de dynode comprend dans la règle une self (L) de quelques μH, amortie par une faible résistance (R). La grille de commande, polarisée par une diode au germanium (d), est couplée à la dynode (D) par un condensateur (C) de haute qualité.

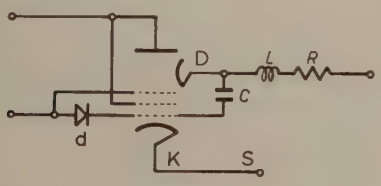

Fig. 11

Jusqu'ici la cathode (K) peut être considérée comme électrode "flottante", chargée par sa seule capacité propre. Si l'on abaisse, par un moyen extérieur, le potentiel de cathode jusqu'à l'apparition d'un courant anodique, il s'amorce une violente réaction qui trouve sa source dans le courant secondaire de la dynode dont le potentiel s'élève brusquement. Ce front positif est transmis à la cathode par l'intermédiaire de la grille de commande.

Les formes d'ondes sont reproduites par la fig. 12. L'impulsion cathodique affecte une allure

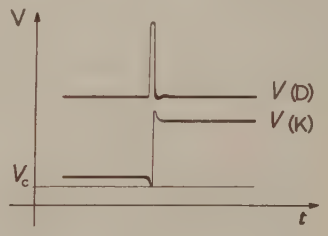

Fig. 12

qui rappelle la fonction d'Heaviside. Le temps de montée est de l'ordre de 20 mμsec pour une amplitude de 60 volts environ tandis que la largeur de l'impulsion de dynode n'excède pas 40 mμsec.

Les impulsions cathodiques sont délivrées sous une impédance particulièrement basse, résultant d'une pente élevée associée à la réaction de couplage.

De l'organe de charge cathodique dépend la plupart des applications. Un dispositif alliant la souplesse à la simplicité consiste à opérer par l'intermédiaire d'un tube électronique, singulièrement d'une pentode (fig. 13). Selon le régime de fonctionnement du tube de charge (T_1) on peut obtenir une grande variété de forme d'impulsions dont quelques-unes sont représentées à la fig. 14.

[7]) R. Favre, Le tube à émission secondaire générateur d'imp. cathodiques, Helv. Phys. Acta. **28** (1955) 167–171.

Les exemples peuvent être multipliés; on se bornera à signaler encore la possibilité de contrôler la grille de commande du tube de charge par une tension fonction quelconque du temps, de manière à générer sur la dynode des impulsions positives très brèves de caractère apériodique.

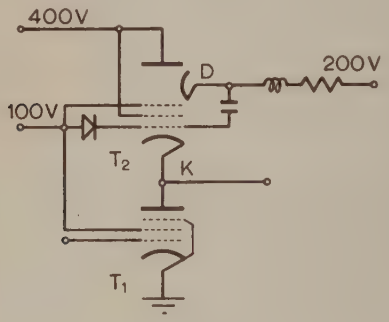

Fig. 13

Dans les conditions normales de fonctionnement l'amplitude des impulsions est voisine de 60 volts. Leur fréquence de répétition peut atteindre une valeur très élevée, en général limitée par la dissipation du tube à émission secondaire. Le tube EFP 60 permet le fonctionnement momentané à 10 MC/sec.

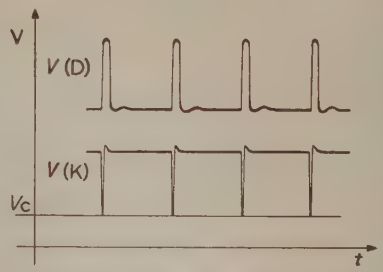

Fig. 14b

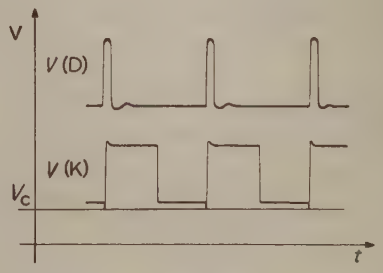

Fig. 14c

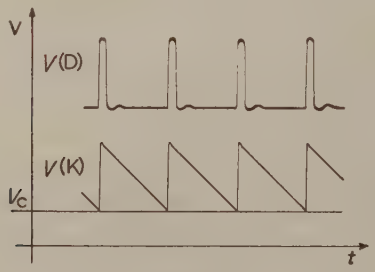

Fig. 14a

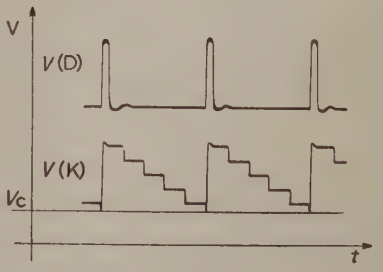

Fig. 14d

1.2. ÉTUDE DES RÉACTIONS

L'analyse mathématique rigoureuse des réactions se heurte aux difficultés, classiques en électronique, de non linéarité et dispersion des caractéristiques. Les inévitables perturbations introduites par l'invertigation expérimentale confèrent cependant un intérêt particulier à cette étude. Soient:

$_{d}$ = l' indice des grandeurs relatives à la dynode

V_d = la tension référée à sa valeur de repos

I_d = le courant interne

S_d = la pente du courant interne de dynode = $\dfrac{\Delta I_d}{\Delta(V_g - V_k)}$

C_d = la capacité

R = la résistance de charge de la dynode

L = la self de charge de la dynode

I_s = le courant dans le circuit de charge

$_g$ = l'indice des grandeurs relatives à la grille

V_g = la tension référée à sa valeur de repos

I_g = le courant interne

S_g = la pente du courant interne de grille = $\dfrac{\Delta I_g}{\Delta(V_g - V_k)}$

$_k$ = l'indice des grandeurs relatives à la cathode

V_k = la tension référée au "cut-off"

I_k = le courant interne

S_k = la pente du courant interne de cathode $\dfrac{\Delta I_k}{\Delta(V_g - V_k)}$

C_k = la capacité

I_c = le courant de charge cathodique

I_e = le courant d'écran.

L'état électrique de la dynode est déterminé par trois équations différentielles:

$$E \cdot C_k \cdot \frac{dI_k}{dt} = I_s + C_d \cdot \frac{dV_d}{dt} \tag{1}$$

$$C_k \cdot \frac{dI_k}{dt} = S_k \cdot (V_d - V_k) \tag{2}$$

$$V_d = L \cdot \frac{dI_s}{dt} + R \cdot I_s \cdot \tag{3}$$

En éliminant V_d et I_s de ces trois équations on obtient l'équation différentielle, linéaire, sans second membre, du troisième ordre suivante:

$$\frac{L \cdot C_k \cdot C_d}{S_k} \frac{d^3V_k}{dt^3} + \left(\frac{R \cdot C_k \cdot C_d}{S_k} + L(C_d - E \cdot C_k)\right) \frac{d^2V_k}{dt^2} + \left(\frac{C_k}{S_k} + R(C_d - E \cdot C_k)\right) \frac{dV_k}{dt} + V_k = 0 \cdot \tag{4}$$

X_1, X_2 et X_3 étant les trois solutions de l'équation caractéristique, on sait que la solution générale de l'équation différentielle est de la forme:

$$V_k = A \cdot e^{X_1 \cdot t} + B \cdot e^{X_2 \cdot t} + C \cdot e^{X_3 \cdot t} \quad \text{d'où} \tag{5}$$

$$V_d = \left(\frac{C_k \cdot X_1}{S_k} + 1\right) A \cdot e^{X_1 \cdot t} + \left(\frac{C_k \cdot X_2}{S_k} + 1\right) B \cdot e^{X_2 \cdot t} + \left(\frac{C_k \cdot X_3}{S_k} + 1\right) C \cdot e^{X_3 \cdot t} \tag{6}$$

$$\begin{aligned} I_s = {} & \left(E \cdot C_k - C_d - \frac{C_k \cdot C_d \cdot X_1}{S_k}\right) \cdot X_1 \cdot A e^{X_1 \cdot t} + \left(E \cdot C_k - C_d - \frac{C_k \cdot C_d \cdot X_2}{S_k}\right) \cdot X_2 \cdot B \cdot e^{X_2 \cdot t} \\ & + \left(E \cdot C_k - C_d - \frac{C_k \cdot C_d \cdot X_3}{S_k}\right) \cdot X_3 \cdot C \cdot e^{X_3 \cdot t} \cdot \end{aligned} \tag{7}$$

On écrira (6) et (7) sous la forme:

$$V_d = a_1 \cdot A \cdot e^{X_1 \cdot t} + b_1 \cdot B \cdot e^{X_2 \cdot t} + c_1 \cdot C \cdot e^{X_3 \cdot t} \tag{6'}$$

$$I_s = a_2 \cdot A \cdot e^{X_1 \cdot t} + b_2 \cdot B \cdot e^{X_2 \cdot t} + c_2 \cdot C \cdot e^{X_3 \cdot t} \cdot \tag{7'}$$

Dans le domaine d'utilisation pratique, l'équation caractéristique présente une solution négative et deux solutions positives ou complexes conjuguées.

Les conditions initiales suivantes sont particulièrement intéressantes:

$$\text{I)}\quad V_k(0) = h \qquad \text{II)}\quad V_d(0) = 0 \qquad \text{III)}\quad I_s(0) = 0 \cdot$$

Les constantes d'intégration sont obtenues en introduisant ces conditions initales dans les fonctions (5), (6) et (7).

Cas 1: Toutes les solutions de l'équation caractéristique sont réelles. On trouve:

$$A = \frac{[c_1(b_2 - c_2) + c_2(c_1 - b_1)]\, h}{(c_1 - a_1)(b_2 - c_2) + (b_1 - c_1)(a_2 - c_2)}$$

$$B = \frac{A(a_1 - c_1) + c_1 \cdot h}{c_1 - b_1} \qquad C = h - A - B \cdot$$

Que l'on peut écrire: $A = h \cdot K_1$, $B = h \cdot K_2$, $C = h \cdot K_3$. Expressions qui mettent en évidence l'importance de h.

Cas 2: Une seule solution est réelle, les deux autres étant complexes conjuguées.

Soient: X_1 réelle, X_2 et X_3 complexes. On peut écrire:

$$X_1 = X \qquad X_2 = R + iI \qquad X_3 = R - iI$$

$$V_k = A \cdot e^{X \cdot t} + B \cdot e^{(R+iI)t} + C \cdot e^{(R-iI)t} \cdot$$

La formule d'Euler donne alors:

$$V_k = A \cdot e^{X \cdot t} + D \cdot e^{R \cdot t} \sin(I \cdot t + \varphi)$$

A, D et φ sont les nouvelles constantes d'intégration.

$$V_d = A \cdot e^{X \cdot t}(1 + X \cdot C_k/S_k) + D \cdot e^{R \cdot t}\left[\sin(I \cdot t + \varphi) + (R \cdot \sin(I \cdot t + \varphi) + \frac{I \cdot C_k}{S_k} \cos(I \cdot t + \varphi)\right]$$

$$I_s = A \cdot X \cdot e^{X \cdot t}[(E \cdot C_k - C_d) - X \cdot C_k \cdot C_d/S_k] + D \cdot e^{R \cdot t}\{(E \cdot C_k - C_d) / [R \cdot \sin(I \cdot t + \varphi)$$

$$+ I \cdot \cos(I \cdot t + \varphi)] - [R^2 \cdot \sin(I \cdot t + \varphi) + 2R \cdot I \cdot \cos(I \cdot t + \varphi) - I^2 \cdot \sin(I \cdot t + \varphi)]\, C_k \cdot C_d/S_k\} \cdot$$

Relations que l'on écrira:

$$V_d = a_1 \cdot A \cdot e^{X \cdot t} + D \cdot f(\varphi, t) \cdot e^{R \cdot t}$$

$$I_s = a_2 \cdot A \cdot e^{X \cdot t} + D \cdot F(\varphi, t) \cdot e^{R \cdot t} \cdot$$

En introduisant les conditions initiales on obtient:

$$D = \frac{a_1 \cdot h}{a_1 \cdot \sin - f(\varphi, 0)} = \frac{a_2 \cdot h}{a_2 \cdot \sin - F(\varphi, 0)}$$

$$\operatorname{tg}\varphi = \frac{a_2 \cdot C_k \cdot I/S_k - a_1 \cdot I(E \cdot C_k - C_d) + 2R \cdot I \cdot C_k \cdot C_d \cdot a_1/S_k}{(E \cdot C_k - C_d)\, a_1 \cdot R + (I^2 - R^2)\, C_k \cdot C_d \cdot a_1/S_k - C_k \cdot R \cdot a_2/S_k - a_2} \cdot$$

Expressions d'où l'on tire dans l'ordre, φ, D et A.

On a représenté sur la fig. 15a la forme de l'impulsion cathodique V_k et sur la fig. 15b celle des impulsions de dynode V_d et V_r considérée sur la résistance d'amortissement, calculées dans les conditions suivantes:

$$L = 10^{-5}\text{H} \qquad R = 330\Omega \qquad C_k = 30, 40 \text{ et } 50 \text{ pF}$$

avec les caractéristiques du tube EFP 60

$$S_k = 10^{-2}\text{A/V} \qquad C_d = 30 \cdot 10^{-12}\text{F} \qquad E = 1.1 \cdot$$

Les conditions initiales sont supposées obtenues par injection, au début de la conduction, d'une charge de -10^{-10} Cb sur la cathode du tube à émission secondaire, valeur en parfaite harmonie avec les possibilités pratiques.

1.3. REMARQUES

L'expression mathématique que nous avons donnée au courant cathodique n'est pas restrictive quant au signe, d'où le facteur sinusoïdal

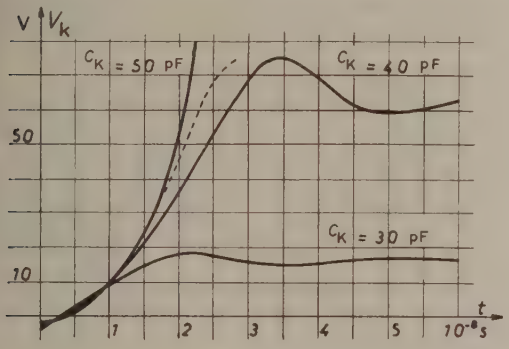

Fig. 15a

figurant dans la solution. En réalité, la tension V_k se maintient à sa valeur maximum, si ce n'est la légère ondulation amortie due au couplage parasite de la cathode avec la grille de commande et la dynode (fig. 15a).

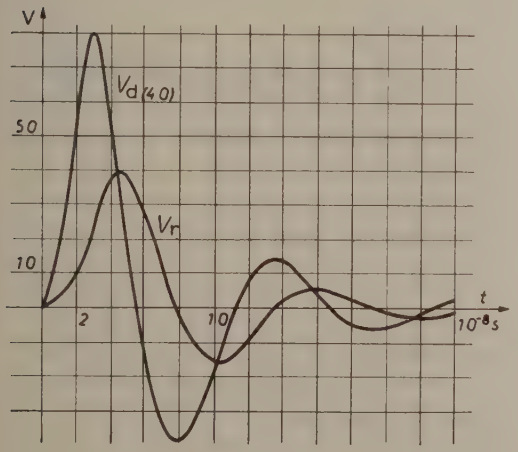

Fig. 15b

La tension cathodique à un instant quelconque de la réaction est proportionnelle à sa valeur initiale h et ceci jusqu'à une valeur de h très élevée. Il y a donc intérêt à choisir un tube de charge apte à délivrer des impulsions de très grande amplitude.

1.4. DISCUSSION DES RÉSULTATS

Les caractéristiques principales des impulsions de tension relatives à une capacité cathodique C_k de 40 pF sont rassemblées dans la table ci-dessous:

Impulsion	Amplitude A	Temps de mont. 10%–90% A	Temps de desc. 90%–10% A
V_k	60 V	$2.1 \cdot 10^{-8}$ sec	—
V_d	80 V	$1.8 \cdot 10^{-8}$ sec	$1.7 \cdot 10^{-8}$ sec
V_r	39 V	$2.5 \cdot 10^{-8}$ sec	$2.5 \cdot 10^{-8}$ sec

Dans la plupart des applications, les impulsions de dynode doivent être prélevées sur la résistance de charge et non directement sur l'électrode dont la capacité parasite joue un rôle extrêmement néfaste sur la vitesse de réaction. Il n'est donc pas toujours possible de bénéficier directement de l'extrême finesse des impulsions de dynode.

Pour obtenir des conditions initiales bien déterminées, il est nécessaire de maintenir un intervalle minimum, ou temps de recouvrement, entre chaque réaction. On peut l'estimer à 3 constantes de temps d'amortissement, soit ici, $18 \cdot 10^{-8}$ sec, valeur qui serait réduite par une résistance élevée dans le circuit de dynode ou une self L plus faible.

Il n'y a pas toujours intérêt à réduire le temps de recouvrement, l'oscillation libre de dynode pouvant être appliquée au déclanchement plus rapide des réactions. Deux cas sont à considérer dans cet ordre d'idées. Le premier est relatif à la génération d'impulsions apériodiques, à fréquence variable, ou distribuées par groupes délimités avec une grande précision. Le second comprend les impulsions périodiques à fréquence fixe.

Dans le premier cas un amortissement important assure une meilleure reproductibilité des impulsions très resserrées. Dans le second cas il est souhaitable d'amorcer les réactions durant la phase croissante de la tension de dynode, au voisinage du passage par zéro.

La fréquence maximum correspondant au

dispositif développé dans les lignes qui précèdent est d'environ 10 MC/sec, valeur remarquable si l'on considère que l'oscillation y conserve son caractère d'impulsions successives. A titre de comparaison, les impulsions d'un oscillateur bloqué à transformateur n'atteingnent que difficilement 1 MC/sec. Cette supériorité du tube à émission secondaire est particulièrement appréciée dans les applications à la démultiplication de fréquence qui vont suivre.

2. Diviseurs de Fréquence[8])

2.1. Les diviseurs de fréquence constituent une classe particulière de démultiplicateurs électroniques, spécialement destinée à réduire la fréquence de tensions sinusoïdales ou d'impulsions périodiques, sans assurer de dénombrement.

Le dispositif décrit au chapitre précédent se prête remarquablement à l'application envisagée. Pour la commodité de l'exposé on traitera le sujet en deux groupes comportant respectivement les diviseurs à haute puis à basse fréquence.

2.2. DIVISEUR À HAUTE FRÉQUENCE

Le circuit de la fig. 13 est directement applicable à la réduction des hautes fréquences, le régime de fonctionnement correspondant à celui de la fig. 14d). La fréquence primaire est appliquée à la grille de commande du tube de charge (T_1) sur l'anode duquel elle donne lieu à une succession d'impulsions de courant périodique, d'amplitude ajustée par la tension d'écran.

La capacité cathodique du tube à émission secondaire (T_2) est adaptée aux résultats de l'étude mathématique du chapitre précédent, résultats qui conservent intégralement leur valeur.

L'intervalle minimum entre impulsions de charge, compatible avec le temps de réaction, est tiré de la fig. 15b. On trouve, pour le circuit adopté dans ce cas particulier, environ $3.6 \cdot 10^{-8}$ sec, soit une fréquence voisine de 28 Mc/sec. En modifiant les conditions de fonctionnement on peut atteindre 30 Mc/sec.

Il est prudent de limiter le nombre d'impulsions à 5 par cycle, valeur correspondant à une tolérance générale de $\pm$ 10%.

Les impulsions de sortie captées sur la cathode du tube à émission secondaire ou sur la résistance d'amortissement R peuvent être appliquées sans autre à l'attaque de l'étage suivant.

2.3. DIVISEUR BASSE FRÉQUENCE

En raison d'inévitables fuites de courant, notamment entre la cathode et l'organe de chauffage, le dispositif de la fig. 13 n'est applicable à la division de fréquences primaires inférieures à 1 Mc/sec qu'en augmentant la capacité cathodique du tube à émission secondaire. En d'autres termes, le courant utile doit rester élevé par rapport à celui de fuite. Cette condition est convenablement satisfaite par un courant de charge de 100 à 200 μA.

La capacité cathodique supplémentaire ou "condensateur d'accumulation" est placée en série avec une impédance réduite en général à une résistance pure de 3 à 4 kΩ. Il faut utiliser ici un système de charge continue, les réactions étant synchronisées par les impulsions de fréquence primaire.

Le retour de la dynode à sa tension de polarisation peut s'effectuer dans un délai beaucoup plus long que précédemment ce qui autorise une impédance de rappel élevée d'où une amplitude accrue des impulsions.

La durée de la réaction ne se limite pas à celle du front positif mais se prolonge jusqu'à la décharge complète du condensateur d'accumulation à travers l'impédance additionnelle. Des précautions particulières doivent être prises pour éviter un "glissement" exagéré de la tension de grille par rapport à celle de dynode au cours de cette réaction prolongée.

Dans le dispositif schématisé par la fig. 16, la polarisation des électrodes est assurée sous une impédance élevée par une chaîne potentiométrique d'un débit inférieur à 1 mA. Cette manière d'opérer introduit un couplage continu entre la dynode et la grille de commande, couplage qui évite le "glissement" excessif des tensions relatives dont il est fait mention plus haut.

[8]) R. Favre, Diviseur de fréquence à large bande, Helv. Phys. Acta. **28** (1955) 172–178.

La réaction élève la tension de dynode à une valeur voisine de celle de l'anode aussi longtemps qu'il y a compensation entre le courant secondaire et celui de rappel. Ce dernier n'excèdant pas une fraction de mA, la décharge ne se termine pratiquement qu'avec la disparition du

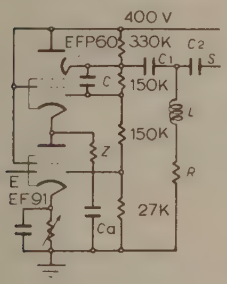

Fig. 16

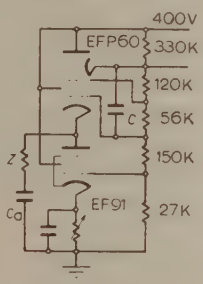

Fig. 17

courant cathodique. Durant cette opération, la tension de rappel de la grille de commande s'élève également, grâce au couplage continu, ce qui permet de maintenir, pour les fréquences les plus basses (1 c/sec), un condensateur de couplage C de petite dimension et faible capacité parasite, facteur important pour une réaction très rapide.

La charge continue du condensateur d'accumulation est assumée par une pentode permettant un courant constant, un réglage aisé et la superposition d'impulsions de synchronisation. Ces dernières, de signe positif, sont appliquées à la grille de commande et se manifestent sur l'anode du tube de charge par de brèves impulsions négatives.

L'amplitude élevée des réactions du diviseur basse fréquence permet un grand nombre d'impulsions par cycle. On réalise notamment des décades de stabilité parfaitement acceptable. Le taux de division est ajusté par la résistance variable insérée dans le circuit cathodique du tube de charge. Ce procédé permet une compensation très simple de modifications éventuelles à la suite du vieillissement des éléments ou tout autre cause.

Le système de polarisation du tube de charge à partir de la chaîne potentiomètrique, introduit un léger couplage continu entre le courant de charge et la tension d'alimentation, permettant à cette dernière d'importantes variations sans perturber le fonctionnement ($\pm$ 20% pour une décade).

La synchronisation des étages ne peut en général se faire à partir des impulsions cathodiques en raison d'un couplage inopportun provenant lui-même des impulsions de synchronisation. Il y a lieu d'opérer dans ce cas à partir de la dynode par l'intermédiaire du filtre C_1—L—C_2 qui confère une grande finesse aux impulsions de synchronisation.

La consommation de courant d'un étage comprend environ 600 μA pour la chaîne potentiomètrique, auxquels s'ajoutent 100 à 200 μA de courant cathodique soit au total moins de 1 mA, compte tenu du courant secondaire.

Sur la base des caractéristiques et des données du constructeur, il est rationnel d'adopter pour le tube à émission secondaire EFP 60, une tension anodique et d'écran de 300 volts par rapport à la tension cathodique considérée au début de la réaction. La tension totale est ainsi d'environ 400 volts.

Pour le diviseur haute fréquence, l'expérience montre directement que la tension de polarisation de dynode trouve sa valeur optima à 100 volts environ au-dessus de celle de la grille de commande.

Le problème est plus complexe pour le diviseur basse fréquence qui, à cet égard, donne lieu à un compromis. Il est en effet particulièrement avantageux pour la stabilité du dispositif de travailler avec une amplitude maximum, condition qui est remplie au mieux lorsque la tension de dynode est très basse. Malheureusement le déclanchement de la réaction est moins rapide dans ces conditions qu'avec une tension de dynode plus élevée. Pour conserver toute la rapidité de la réaction il faut se borner à une amplitude de 80 volts tandis que celle-ci peut atteindre 160 volts lorsque des conditions favorables lui sont réservées. On peut éviter ce compromis en remarquant que la grille suppresseuse du tube à émission secondaire EFP 60 est elle-même douée d'un pouvoir d'émission secondaire élevé et durable. La fig. 17 donne le schéma du dispositif qui fait appel à la suppresseuse comme dynode

auxiliaire, polarisée en vue d'une amplitude maximum tandis que la dynode régulière remplit les conditions de rapidité optima de la réaction.

2.4. ANALYSE DU DIVISEUR BASSE FRÉQUENCE

Du point de vue mathématique, le diviseur basse fréquence se distingue essentiellement par la suppression de la self anodique, simplification qui se traduit par l'abaissement de l'ordre de l'équation différentielle régissant la réaction. Les notations du chapitre précédent sont conservées avec l'adjonction de la résistance cathodique Z et du condensateur d'accumulation C_a (fig. 17). La tension de ce dernier peut être admise constante durant la partie aiguë de la réaction qui seule intéresse ce développement.

Les trois équations d'état de la dynode s'écrivent:

$$E(C_k \cdot dV_k/dt + V_k/Z) - I_s - C_d \cdot dV_d/dt = 0 \quad (1)$$

$$C_k \cdot dV_k/dt + V_k/Z = S_k(V_d - V_k) \quad (2)$$

$$I_s = V_d(1/R + S_g) \cdot \quad (3)$$

Puis, par élimination:

$$\frac{C_k \cdot C_d}{S_k} d^2V_k/dt^2 + [(1/R + S_g)\, C_k/S_k + C_d/Z \cdot S_k + C_d - E \cdot C_k]\, dV_k/dt + [1/R + S_g)\,(1 + 1/Z \cdot S_k) - E/Z] \cdot V_k = 0 \cdot \quad (4)$$

S_g est la pente du courant de grille qui n'apparaît que lorsque la grille devient positive par rapport à la cathode. On ne commet toutefois pas une grave erreur en l'introduisant dès le début de la réaction. Sa valeur est constante dans toute la région utile des caractéristiques.

Les grandeurs connues de cette équation sont:

$$E = 1.1 \quad S_k = 10^{-2}\text{A/V} \quad Z = 3.3\ \text{k}\Omega \quad R = 10^5\Omega$$

$$S_g = 4 \cdot 10^{-4}\ \text{A/V} \qquad C_d = 40 \cdot 10^{-12}\ \text{F}$$

(cette valeur C_d relativement élevée comprend le condensateur de couplage à l'étage suivant).

L'introduction des valeurs numériques permet d'alléger l'écriture en supprimant les termes négligeables.

$$4 \cdot 10^{-9} \cdot C_k \cdot \frac{d^2V_k}{dt^2} + (4 \cdot 10^{-11} - 1.1 \cdot C_k) \cdot \frac{dV_k}{dt} + 66 \cdot 10^{-6} \cdot V_k = 0 \cdot \quad (4)$$

Le discriminant D de l'équation caractéristique est:

$$D = (4 \cdot 10^{-11} - 1.1 \cdot C_k)^2 - 1056 \cdot 10^{-15} \cdot C_k \cdot$$

Un facteur sinusoïdal étant incompatible avec l'application envisagée, le discriminant doit satisfaire à la condition: $D > 0$ avec $4 \cdot 10^{-11} - 1.1 \cdot C_k < 0$ d'où l'on tire: $C_k > 4.25 \cdot 10^{-11}$ F. Lorsque C_k ne remplit pas cette condition, la réaction avorte avant la charge complète du condensateur d'accumulation C_a.

Sans entrer dans le détail, nous donnons sur la fig. 18 les impulsions de dynode V_d, respectivement le courant I_k en fonction du temps et du paramètre C_k. Les lignes pointillées indiquent la variation réelle, compte tenu du dépassement de la région linéaire des caractéristiques. On a d'autre part admis, comme précédemment, que la charge de l'impulsion de synchronisation est de -10^{-10} Cb et sa durée négligeable.

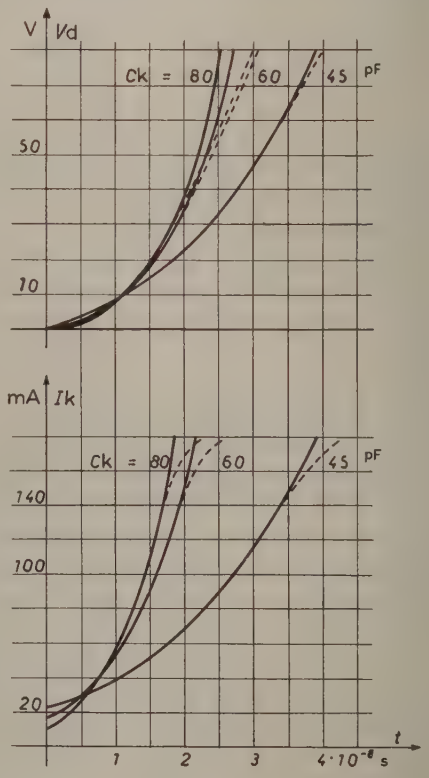

Fig. 18

2.5. PERFORMANCES DU DISPOSITIF

Trois caractéristiques essentielles émanent de l'exposé qui précède:

(1) La gamme de fréquences utiles s'étalant pratiquement de 1 c/sec à 25 Mc/sec.

(2) La précision des impulsions de synchronisation dont le temps de montée n'excède pas 20 mμsec.

(3) La faible consommation de courant, voisine de 1 mA par décade jusqu'à 1 Mc/sec, et proportionnelle à la fréquence au-delà de cette valeur.

On pourrait mentionner encore la simplicité du dispositif composé de deux tubes électroniques seulement et d'un circuit réduit.

dispositif d'accumulation, un circuit pilote d'interpolation et un démultiplicateur électronique de capacité d'enregistrement égale ou supérieure au nombre maximum d'impulsions résiduelles.

Au repos, la tension V_c est maintenue, par la résistance de rappel R et le courant de grille du tube T_3, au potentiel cathodique de ce dernier, choisi égal à la tension de crête des réactions. La self placée dans le circuit cathodique de T_3 évite l'apparition d'un intense courant de grille lorsque la réaction atteint le "niveau" de la cathode.

Lorsque la mesure est stoppée, la tension V_c gagne quasi linéairement sa valeur de repos en un temps proportionnel au nombre de charges unité accumulées sur le circuit cathodique du

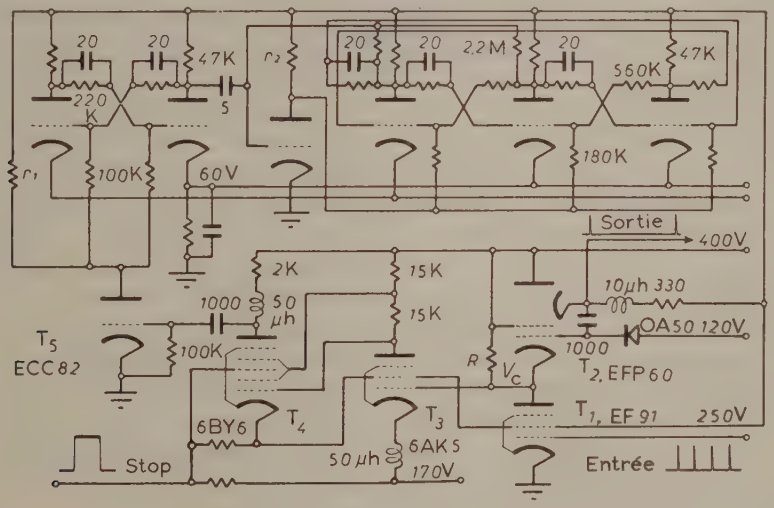

Fig. 19

3. Compteur d'Impulsions à Haute Fréquence[9])

3.1. Ce dispositif s'inspire du diviseur haute fréquence auquel est associé un circuit d'interpolation des impulsions résiduelles, c'est-à-dire celles qui ont pû charger partiellement le condensateur d'accumulation lorsque la mesure est arrêtée.

Le schéma de principe (fig. 19) comprend: le tube à émission secondaire. La méthode de dénombrement dérivée du dispositif exposé au chapitre 4/(1ère partie) conduit à faire osciller le premier étage du démultiplicateur électronique durant l'évacuation de la charge résiduelle. En déterminant convenablement la valeur des éléments du circuit, cette oscillation comportera autant d'alternances qu'il s'était accumulé d'impulsions sous forme de charges unité.

Le circuit pilote d'interpolation comprend, en principe, un tube de coïncidences (T_4) dont la

[9]) R. Favre, Compteur d'impulsions à haute fréquence, Helv. Phys. Acta. **28** (1955) 179–184.

première grille de commande est assujettie à la tension V_c par l'intermédiaire de T_3. La seconde grille de contrôle, normalement au-dessous du cut-off, reçoit une impulsion de déblocage de quelques microsecondes à la fin de chaque mesure. Les conditions de coïncidences sont déterminées de manière à ne rendre le tube T_4 conducteur que pendant la décharge finale du circuit cathodique d'accumulation. Le blocage de T_5 permet alors l'oscillation de l'étage d'entrée du démultiplicateur électronique d'où l'enregistrement du nombre de charges résiduelles.

Les impulsions d'entrée doivent être suffisamment rapprochées pour éviter une décharge intermédiaire appréciable de la capacité cathodique. Cette condition limite à environ 1 Mc/sec la fréquence de sortie minimum d'un étage à accumulation dépourvu de capacité auxiliaire. Il est dès lors possible de faire appel à l'un des nombreux types conventionnels de démultiplicateurs électroniques (Cf. première partie).

La durée du temps de décharge, pour un nombre d'impulsions déterminé, est subordonnée à la charge individuelle des impulsions et à la résistance R. C'est en opérant sur cette dernière que l'on obtiendra le réglage le plus simple.

3.2. PERFORMANCES ET APPLICATIONS

Par analogie de forme, les performances de ce compteur d'impulsions sont les mêmes que celles du diviseur haute fréquence traité au chapitre précédent. La fréquence maximum atteint donc 30 Mc/sec.

Le fonctionnement à 25 Mc/sec présente un intérêt particulier en ce qu'il permet d'une part la réduction à 1 Mc/sec au moyen de deux étages quinaires et d'autre part la multiplication facile à 100 Mc/sec, possibilité dont il sera fait usage dans une application décrite ultérieurement.

Réservé au dénombrement d'impulsions très resserrées (0.2 μsec d'intervalle au maximum) et par conséquent le plus souvent périodiques, ce type de compteur s'impose d'emblée à la chronographie électronique et aux mesures de fréquences.

Sous réserve de la stabilité de l'étalon de fréquence, la précision de mesure du temps est de l'ordre d'une alternance de la fréquence d'entrée, soit $\pm 4 \cdot 10^{-8}$ sec à 25 Mc/sec. Un développement de la méthode permet de faire mieux, comme on le montrera au paragraphe suivant.

3.3. APPLICATION À UN CHRONOGRAPHE ÉLECTRONIQUE

Le dispositif que nous donnons comme exemple de réalisation des différents organes fondamentaux d'un compteur d'impulsions est intéressant au point de vue de ses performances et en ce qu'il fait appel à l'ensemble des résultats obtenus tant dans la première que dans la seconde partie de ce travail.

Il se compose en principe d'un étalon de fréquence dont on sait que les variations relatives peuvent être limitées à 10^{-9}, et d'un compteur d'impulsions chargé de dénombrer les alternances. Le compteur travaille aisément à 25 Mc/sec d'où une précision absolue limitée à $4 \cdot 10^{-8}$ sec. Il nous est paru possible d'améliorer cette performance en associant au premier étage d'une chaîne chronométrique classique, plusieurs compteurs en parallèle. La chaîne, ou "compteur fondamental", comprend autant d'étages qu'il est nécessaire pour satisfaire à la capacité de mesure désirée, quitte à aboutir sur un numérateur mécanique, tandis que les "circuits associés" se limitent à un seul étage complet, avec dispositif de lecture. Le compteur fondamental et les circuits associés sont attaqués par la même fréquence pilote mais avec une phase différente pour chacun d'eux et également répartie sur un cycle.

La fig. 20 donne un exemple schématique de réalisation d'un chronographe à 4 canaux, chacun d'eux comprenant un compteur du type décrit dans ce chapitre avec T_1 à T_4 comme tubes de charge. Les dispositifs d'interpolation correspondant à chacune des sorties I_1 à I_4 ne figurent pas sur le schéma, mais sont identiques à celui de la fig. 19. Le compteur fondamental porterait par exemple l'indice $_1$ et serait seul suivi d'une chaîne de démultiplication.

La tension pilote (25 Mc) est appliquée à un transformateur doubleur de phase prolongé de

part et d'autre par une ligne de retard à constantes distribuées, de façon à réaliser un système d'attaque quadriphasé, appliqué aux grilles de commande des tubes de charge T_1 à T_4. Ces dernières sont polarisées au moyen d'une résistance découplée par une diode de manière à fixer le niveau de crête de la tension d'entrée.

Enfin la tension ajustable des suppresseuses est utilisée pour assurer l'équipartition des charges entre les différents canaux.

L'intervalle de récurrence, compté sur la somme des impulsions reçues par les canaux en parallèle, est, d'une façon générale, T/N, T étant la période et N le nombre de canaux associés. Dans notre cas $T/N = 0.01$ μsec. Il est à peine nécessaire de spécifier que la tolérance absolue peut être, en principe, réduite à la valeur de ce nouvel intervalle de récurrence. La commutation des impulsions, en un temps compatible avec l'intervalle de récurrence, compte parmi les questions les plus délicates. C'est avant tout par l'heureuse solution qu'il apporte à ce problème que le dispositif d'attaque polyphasé suggéré se justifie dans le cadre de cette étude.

Les cathodes de deux tubes de commutation (T_5 et T_6) sont à cet effet reliées en commun avec celles des tubes de charge (T_1–T_4) et à l'impédance cathodique Z. Ces tubes de commutation sont asservis d'autre part aux flip-flop bistables F_1 et F_2 dont l'état initial est imprimé par une pression sur les interrupteurs de remise à zéro R_e (dispositif armé). Le tube T_6 est alors conducteur tandis que T_5 et les quatre tubes de charge sont bloqués, ces derniers avec une très faible marge au-dessous du cut-off.

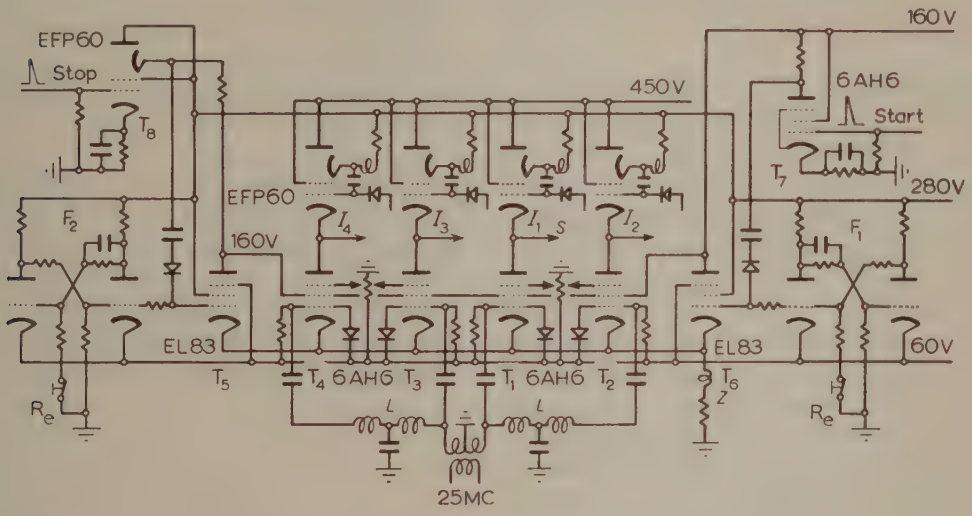

Fig. 20

L'application d'une impulsion positive "start" sur le tube T_7, entraîne le blocage quasi instantané de T_6 tandis qu'en basculant, le flip-flop F_1, maintient cet état de chose. Le second tube de commutation (T_5) est resté bloqué (très faiblement au-dessous du cut-off) ce qui assure aux tubes de charge la totalité du courant d'impédance cathodique dont l'équipartition peut être réalisée par les potentiomètres de polarisation des grilles suppresseuses.

L'impulsion "stop", appliquée au tube à émission secondaire T_8, est amplifiée sans déphasage sur la dynode puis transmise à la grille du tube de commutation T_5 qui se trouve quasi instantanément débloqué, état perpétué par le bascul du flip-flop F_2. Les tubes de charge cessent aussitôt leur activité, la totalité du courant cathodique étant absorbée par T_5. La transition du flip-flop bistable F_2 est simultanément utilisée à la production du signal de

déblocage d'où la mise en service du dispositif d'interpolation qui enregistre le résultat dans les quelques μsec suivantes. On montre que le délai de commutation n'excède pas, dans de bonnes conditions, 0.01 μsec.

Cet exemple, auquel nous limiterons notre exposé, concrétise l'intérêt d'un compteur d'impulsions à haute fréquence qui trouverait d'autre part de nombreuses applications non moins intéressantes.

4. Conclusions

Le bilan des résultats de la première partie se résume par une légère simplification des circuits décimaux tandis qu'à consommation égale, le pouvoir de résolution et la stabilité dynamique sont sensiblement doublés. Le pourvoir de résolution relatif à la numération d'impulsions de nature statistique est d'autre part décuplé par la simple adjonction de 1 ou 2 tubes électroniques.

Les applications de ce genre de circuit sont aussi nombreuses que variées. Nous citerons pour mémoire leur utilisation en physique nucléaire, chronométrie, mesures de fréquences, dans les calculateurs électroniques et dans l'industrie. La "transistorisation" des circuits démultiplicateurs offre des perspectives riches en promesses, grâce notamment à leur consommation insignifiante et à leur endurance, facteurs éminemment précieux pour certaines applications.

Le tube à émission secondaire, utilisé comme générateur d'impulsions cathodiques, se prête à une grande variété de possibilités. L'impédance de sortie accuse une valeur très réduite pour des impulsions d'amplitude plus élevée que par d'autres procédés de couplage. Du type "oscillateur bloqué", il présente sur les dispositifs classiques à transformateur, les avantages que lui confèrent une souplesse plus grande et des temps de montée et de recouvrement des impulsions inférieurs. Le caractère parfaitement apériodique et la grande finesse des impulsions obtenues par ce procédé, permettent d'envisager leur emploi en physique nucléaire, pour l'étude de coïncidences de haute précision, aussi bien qu'en télécommunication multiplexe à impulsions codées.

Directement dérivée du dispositif précédent, le diviseur de fréquence et le compteur d'impulsions proposés en ont hérité les qualités fondamentales.

Il nous reste l'agréable devoir d'exprimer nos sentiments de gratitude à la Commission Suisse de l'Energie Atomique et au Fonds National Suisse de la Recherche Scientifique pour leur appui financier et plus particulièrement à Monsieur le Professeur Ch. Haenny qui a manifesté à notre égard une constante sollicitude.

Bibliographie

A. Dauphin, Les compteurs arithmétiques d'impulsions, L'onde électrique (1952) 459–463.

P. Naslin et A. Peutman, Les compteurs électroniques d'impulsions, L'onde électrique (1949) 241–254.

J. P. Oehmichen, Circuits électroniques, Société des éditions Radio, Paris (1954).

N. F. Moody, G. J. R. Maclusky and M. O. Deighton, Millimicrosecond Pulse Techniques, Electronic Engng. **24** (1952) 214–219.

F. H. Wells, Fast pulse circuit techniques for scintillation counters, Nucleonics **10** (1952) 28–33.

Lewis and Wells, Millimicrosecond Pulse Techniques (Pergamon, London, 1954).

F. H. Wells, A fast amplitude discriminator and scale-of-ten counting unit for Nuclear Work, J. Sci. Instr. **29** (1952) 111–115.

E. Baldinger und M. Nicolet, Ein Impulsgenerator mit Sekundäremissionsröhren, Z.A.M.P. **5** (1954) 508–511.

NUCLEAR INSTRUMENTS 1 (1957) 213–226; NORTH-HOLLAND PUBLISHING CO. – AMSTERDAM

SURVEY ARTICLE

ON DIFFUSION CLOUD CHAMBERS

HILDING SLÄTIS

Nobel Institute of Physics, Stockholm

Received 9 April 1957

A short survey is given on the development of the diffusion cloud chamber. Langdorf's theory is briefly reproduced, and some important improvements in the theory made by Shutt and other investigators are mentioned. Different diffusion cloud chambers are described, and photographs of tracks demonstrate the use of these chambers.

1. Introduction

In spite of the important results obtained with the wellknown Wilson-chamber the equipment has the great disadvantage of being able to record tracks of charged nuclear particles only in a time interval which is short (at the best 10 percent) compared with the time necessary for making the chamber ready for a new record. This disadvantage was partly removed, in any case for cosmic rays, when it was possible to let the particles themselves release the operations necessary for a photographic record of the events, which had occurred in the chamber[1,2,3,4]). Later, the high energy accelerators were able to produce such a large yield of mesons that the need for a cloud chamber sensitive at any instant was obvious. However, the desire to make such an apparatus was of current interest long before the cosmotrons appeared.

In order to make a continuously working cloud chamber, one has either to find a new principle for the recording of tracks of charged particles, or still to use supersaturated vapours, but these should be produced continuously instead of being created in adiabatic expansions.

The first way was tried by Regener[5]), who used a cloud of small slowly-falling oil droplets. An ionizing particle going through this cloud made the oil droplets along the path of the particle electrically charged. A moment later the cloud passed through an electric field between two condenser plates. In this field the charged oil droplets were separated from the uncharged droplets. By use of an illumination equiment it was then possible to observe and to take photographs of the charged droplets, which formed the tracks to be studied. The quality of the tracks was, however, not good.

On the other hand the second method, the continuous production of supersaturated vapours, has given extraordinarily good results. The first experiment was made by Hoxton[6]), who let air pass over hot water and then through an observation channel at room temperature. However, Hoxton got condensation phenomena only by means of electric discharges. Paths of particles were not obtained.

Vollrath[7]) used vapours of HCl and water, which diffused through each other. The vapour mixture was then supersaturated with respect to both components. Paths of charged particles were observed in the supersaturated region. A disturbing effect was turbulences in the neighbourhood of the tracks. These whirls were caused by heat liberated in the condensation process. The cloud chamber principle of Vollrath was therefore not able to compete with that of

[1]) D. Skobelzyn, Z. Phys. **54** (1929) 686.

[2]) L. M. Mott-Smith and G. L. Locher, Phys. Rev. **38** (1931) 1399.

[3]) Th. H. Johnson, W. Fleisher, Jr. and J. C. Street, Phys. Rev. **40** (1932) 1048.

[4]) P. M. S. Blackett and G. Occhialini, Nature **130** (1932) 363.

[5]) E. Regener, Festschrift der Technischen Hochschule Stuttgart (1829–1929) p. 331.

[6]) L. G. Hoxton, Proc. Virginia Acad. Sci., Abst. **9** (1933–34) 23.

[7]) R. E. Vollrath, Rev. Sci. Inst. **7** (1936) 409.

Langsdorf[8]). Langsdorf's principle has been the basis for all later constructions of continuously working cloud chambers. A more detailed account of the contribution by Langsdorf might therefore be justified.

2. The Diffusion Cloud Chamber by Langsdorf

Langsdorf[8]) made his diffusion cloud chamber at M.I.F. already 20 years ago. A vapour, usually methanol, diffuses vertically downward through a permanent gas (carbon dioxide or air) from the upper, heated part of the cloud chamber to the bottom plate, which is effectively cooled by means of, for instance, carbonic acid ice. The vapour is condensed on the bottom. plate. In an intermediate region supersaturation will occur to such an extent, that tracks of ionizing particles appear.

The construction of the cloud chamber is shown schematically in fig. 1. Methyl alcohol

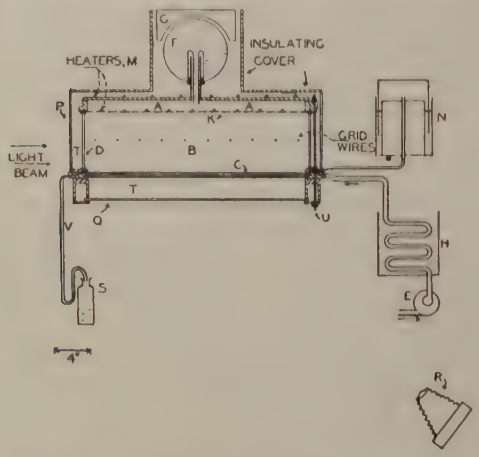

Fig. 1. Schematic drawing of Langsdorf's diffusion cloud chamber (Rev. Sci. Inst. **10** (1938) 91).

is heated in the boiler F by means of the radiant heater G. The vapour developed is distributed in the space A and flows through the holes K into the cloud chamber B. K is heated by means of the electric heaters M. The floor of the cloud chamber is made of two glass sheets C, between which a cooling liquid is pumped by a pump E. The liquid is cooled in the coil H by carbonic acide ice (the return tube is not shown). The tracks of ionizing particles are photographed from below by means of the camera R. The gas pressure in the chamber is kept near 1 atm by the gas float reservoir N. The sensitive region was about one inch deep near the chamber floor. Later it was possible to increase this region to 3–4-inches. When the sensitive layer is thick, however, the tracks are not as sharp as for thinner sensitive regions. An electric field (100 V/cm) is applied either between different parts of a system of grid wires or between the plate K and the bottom of the chamber. In this way most of the ions formed in the upper, insensitive region of the chamber are removed. Otherwise these ions, when entering the sensitive region, would cause a disturbing condensation.

[8]) A. Langsdorf, Jr., Phys. Rev. **49** (1936) 422; **51** (1937) 1026; Rev. Sci. Inst. **10** (1938) 91.

3. Langsdorf's Theory for the Diffusion Cloud Chamber

Langsdorf made some calculations under simplified assumptions. Thus, the influence of the walls of the cloud chamber is neglected in order to get one-dimensional equations for the diffusion and heat transfer. The formation of droplets is also neglected, and the vapour is treated as a perfect gas even when supersaturated. The vapour and heat fluxes are considered stationary.

3.1. TEMPERATURE DISTRIBUTION IN THE DIFFUSION CLOUD CHAMBER

If the height over the bottom plate be x, the energy flux f through the chamber in cal·cm^{-2}·sec^{-1} is

$$f = c_1 C_p t - K_0(1 + bt)\frac{\mathrm{d}t}{\mathrm{d}x} \,. \qquad (1)$$

The first term on the right hand side of (1) is the heat transported by the mass flux c_1, the second term represents the heat conduction. The symbols in (1) are defined by

c_1 = flux of vapour in g·cm^{-2}·sec^{-1}
C_p = specific heat of vapour in cal/g/degree
t = temperature T at x minus temperature T_0 of the bottom plate
K_0 = heat conductivity of mixture at T_0
b = temperature coefficient of heat conductivity $K = K_0(1 + bt)$.

Introducing the parameter r, defined by

$$f = c_1 C_p t_1 r \tag{2}$$

into (1), integrating and using the boundary conditions $x = 0$, $t = 0$ and $x = h$, $t = t_1$, where h is the height of the chamber, one gets

$$x = \frac{K_0}{c_1 C_p}\left[bt + (1 + brt_1)\log\left(1 - \frac{t}{rt_1}\right)\right] \tag{3}$$

and hence

$$h = \frac{K_0}{c_1 C_p}\left[bt + (1 + brt_1)\log\left(1 - \frac{1}{r}\right)\right] . \tag{4}$$

These relations give the temperature distribution in the cloud chamber. Fig. 2 shows some of the distributions computed by Langsdorf for three different values of the vapour flux c_1.

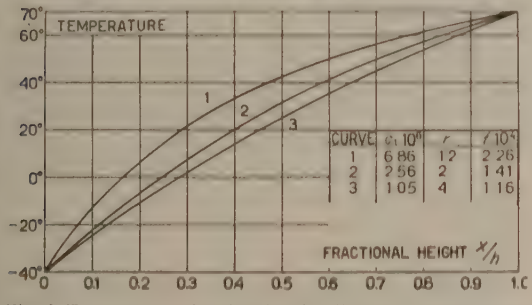

Fig. 2. Temperature distribution for different vapour fluxes according to Langsdorf (Rev. Sci. Inst. **10** (1938) 91).

3.2. DISTRIBUTION OF VAPOUR PRESSURE IN THE DIFFUSION CLOUD CHAMBER

The next step in Langsdorf's theory comprises the calculation of the vapour pressure as a function of x/h. For one-dimensional isothermal diffusion Salin[9]) gives the equations

$$\begin{cases} C_1 = wD_1 - k\dfrac{\partial D_1}{\partial x} \\ C_2 = wD_2 - k\dfrac{\partial D_2}{\partial x} \\ w = c_1 v_1 - C_2 v_2 \end{cases} \tag{5}$$

We have

C_1 = flux of vapour in $g \cdot cm^{-2} \cdot sec^{-1}$
C_2 = flux of gas, in this case = 0
D_1 = concentration of vapor $= M_1 p_1 / RT$
D_2 = concentration of gas $= M_2 p_2 / RT$
M_1 = molecular weight of vapour
M_2 = molecular weight of gas
p_1 = pressure of vapour
p_2 = pressure of gas
w = convective flux associated with diffusion
k = diffusion constant $= (K_0/P_0)/(T/T_0)^{1+\alpha}$
α = temperature coefficient
P_0 = total pressure in chamber in atm
T_0 = 233°K = temperature of surface bottom layer.

Considering $c_2 = 0$ and the expressions for D_1, D_2 and k the equations (5) give

$$\frac{dp_2}{p_2} = \frac{c_1 R T_0 dx}{M_1 k_0 \left(1 + \dfrac{t}{T_0}\right)^{\alpha}} . \tag{6}$$

For methanol and carbon dioxide $\alpha \approx 1$. If dx is expressed in terms of dt by means of (1) and $\alpha = 1$, integration of (6) gives

$$\frac{\log p_2(t)}{\log p_2(0)} = \frac{T_0}{T_0 + rt_1} \cdot \frac{RT_0 K_0}{M_1 k_0 C_p}\left[(1 + brt_1)\log\left(1 - \frac{t}{rt_1}\right) - (1 - bT_0)\log\left(1 + \frac{t}{T_0}\right)\right] . \tag{7}$$

This equation gives the relation between the pressure of the gas (and hence also immediately that of the vapour) and the temperature. In connection with (3),(4) or fig. 2, we then get the connection between p_1, p_2 and x/h. Fig. 3 shows the pressures which correspond to the curves in fig. 2.

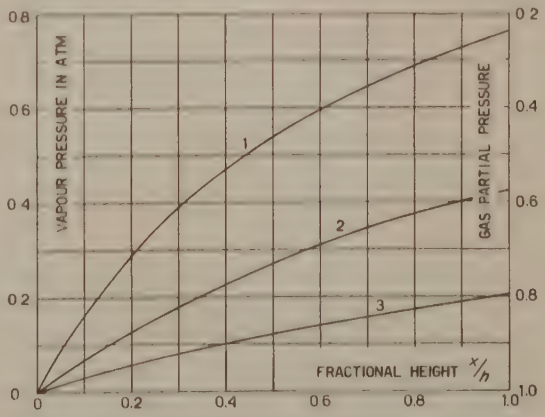

Fig. 3. Vapour pressure distribution for the vapour fluxes given in fig. 2, according to Langsdorf (Rev. Sci. Inst. **10** (1938) 91).

[9]) J. Kuusinen (now Salin), Ann. d. Physik **24** (1935) 445, 447.

3.3. CALCULATION OF THE SUPERSATURATION

Using (6), the supersaturation S may be determined by

$$S = p_1/p_{1S} = (P_0 - p_2)/p_{1S}$$
$$= [P_0 - p_2/p_2(0)\ (P_0 - p_1(0))]/p_{1S}$$
$$\approx P_0\,(1 - p_2(t)/p_2(0))/p_{1S}\ . \qquad (8)$$

Consequently, the supersaturation will be nearly proportional to the total pressure.

Because x does not appear in (7) and only as x/h in (3):(4) it is seen that if r is kept constant, also the form of the supersaturation curve is unaltered. However, c_1 decreases when h increases (see 4)), and the lower vapour flux might be unsufficient for a satisfactory operation of the diffusion chamber, because the higher the chamber, the more vapour is spent to form droplets by condensation. Therefore, the diffusion cloud chamber should not be made too high.

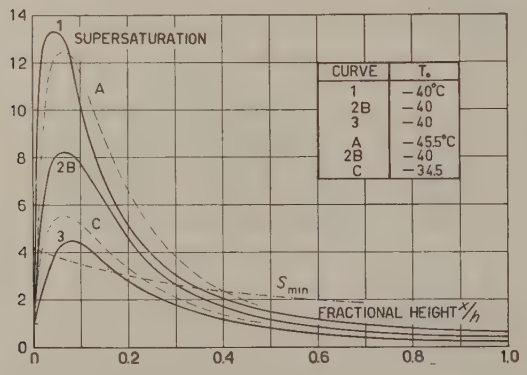

Fig. 4. Supersaturation distribution (the curves 1, 2B, 3) for the three vapour fluxes given in fig. 2, and supersaturation distribution (the curves A, 2B, C) for different bottom temperatures according to Langsdorf (Rev. Sci. Inst. 10 (1938) 91).

The curves 1, 2B, 3 in fig. 4 show the distribution of the supersaturation for the three vapour flux values 1, 2, 3 given in fig. 2. For these three curves $T_0 = -40°\,\mathrm{C}$. The dot-dashed curve $S_{\min}$ shows a rough estimate of the minimum saturation, which is necessary for condensation upon ions,

$$\log S_{\min} = A \cdot \frac{M}{d} \cdot \frac{\sigma^{4/3}}{T}\ , \qquad (9)$$

which corresponds to calculations made by Powell[10]). A is a constant, M, d, and σ are the molecular weight, density and surface tension, respectively, of methanol, and T the absolute temperature. That part of the fractional height x/h, which is defined by the points of intersection between $S_{\min}$ and some of the supersaturation curves, corresponds to the sensitive region of the cloud chamber. The curves 1, 2B, 3 show that the sensitive region becomes higher when the vapour flux increases. The curves A, 2B and C belong to the same flux $c_1 = 2.56 \times 10^{-4}\,\mathrm{g/cm^2}$ sec and show the influence of T_0 on the supersaturation. Thus a lower T_0 increases the height of the sensitive region.

4. Further Contributions to the Diffusion Cloud Chamber Theory

Shutt[11]) at Brookhaven National Laboratory has made a more strict analysis of the conditions in the diffusion cloud chamber by taking into account the following circumstances:

(1) A one-dimensional diffusion equation shall relate the downward flux of vapour to the vapour density at all points except near liquid drops.

(2) Spherically symmetrical vapour and heat diffusion equations determine the growth of the drops.

(3) Stoke's equations determines the rate of fall of the drops through the regions at varying temperatures.

(4) A relation is set up between the gradient of the vapour flux and the rate at which vapour is removed by condensation of drops on ions.

(5) An energy equation shall make it possible to calculate the convection in the gas necessary to establish proper heat exchange with the walls.

Shutt found that the temperature gradient as a function of x depends with good approximation only on the single parameter β:

$$\beta_a = \mu_0 P^{5/3}(n_0 \tau Z)^{4/3} k_0^{-\frac{1}{3}} \quad \text{if} \quad T < 260°\,\mathrm{K} \qquad (10a)$$

$$\beta_b = \mu_0 P^2 (n_0 \tau Z)^{4/3} k_0^{1/3} \quad \text{if} \quad T > 260°\,\mathrm{K}\ . \qquad (10b)$$

The notations, meanings and values of the quantities in the expressions for β are given in table 1.

[10]) C. F. Powell, Proc. Roy. Soc. **119** (1928) 553.

[11]) R. P. Shutt, Rev. Sci. Inst. **22** (1951) 730.

TABLE 1
DATA FOR CALCULATION OF THE PARAMETERS β FOR AIR (SHUTT[11])

Symbol	Explanation	Value
Z	Atomic number for the gas	7.2
τ	Number of atoms in gas molecule	2
k_0	Diffusion constant at N.T.P.	0.133
K_0	Heat conductivity at N.T.P.	5.3×10^{-5}
μ_0	Viscosity of gas-vapour mixture at N.T.P.	1.71×10^{-4}
P	Total pressure in atm	1
n_0	Number of ions per cm³ per sec at N.T.P., liberated by the radiation considered. For cosmic radiation $n_0 =$	2

For air at N.T.P. $\beta_a = 0.77 \times 10^{-2}$, $\beta_b = 1.47 \times 10^{-4}$. Fig. 5 shows some temperature distributions calculated by Shutt for different parameters, temperatures and temperature gradients at the bottom of the diffusion cloud

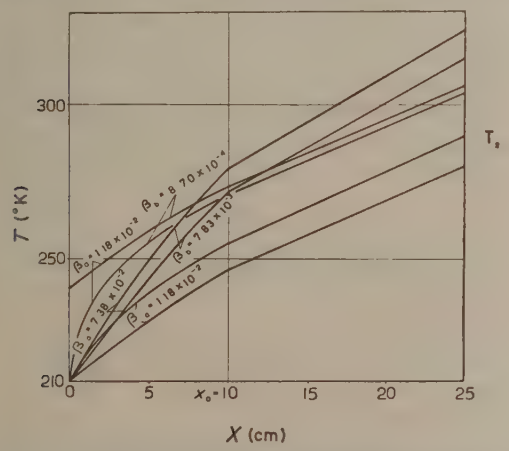

Fig. 5. Temperature distributions for different parameters, and for different temperatures and temperature gradients at the bottom of a diffusion chamber, according to Shutt (Rev. Sci. Inst. 22 (1951) 730).

chamber. The distributions have a form different from those calculated by Langsdorf (fig. 2). Fig. 6 shows the experimentally found temperature distribution in a diffusion cloud chamber made by the author (similar temperature distributions have been published by Morrison and Plain[12]). It is obvious that this type of temperature distribution is in closer agreement with the form given by Shutt than by Langsdorf.

The parameters[10]) are of great interest. One finds, for instance, that different gases might give identical temperature distributions, if the pressures are chosen in a suitable way. Thus, table 2 shows the relative pressures computed

TABLE 2
P/P_{air} = PRESSURES OF SEVERAL GASES, RELATIVE TO AIR, REQUIRING IDENTICAL TEMPERATURE DISTRIBUTIONS (SHUTT[11])

Formula	H_2	D_2	He	A
10 a	9.7	7.7	5.6	0.70
10 b	6.1	4.5	3.7	0.75

from[10]) for a number of gases under the conditions that the temperature distributions be the same as for air.

The formulas (10) show further, that an increase of the ionization density by a certain

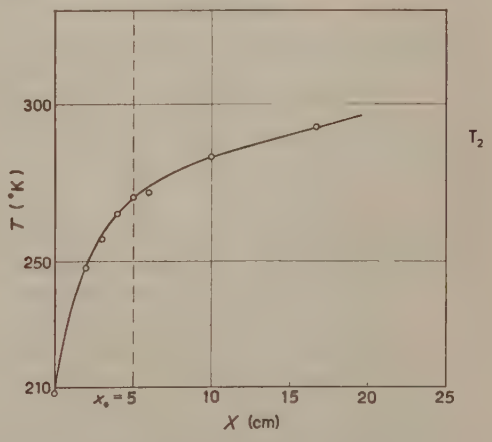

Fig. 6. Experimental temperature distribution in an 1 atm air-methanol diffusion cloud chamber. Depth of sensitive layer 2 in. (Slätis[36,37]).

factor has the same effect as if P is increased by the same factor raised to the $^4/_5$ power (10a) or to the $^2/_3$ (10b). Hence, if n_0 becomes so large that the diffusion cloud chamber stops functioning a reduction of the pressure might possible bring the apparatus to operate again.

[12]) H. L. Morrison and G. J. Plain, Rev. Sci. Inst. 23 (1952) 607.

Succi and Tagliaferri[13]) in Milano have considered the influence of ionization in a simpler way than Shutt did. The radii of the droplets are supposed to grow as the square root of the time, and the droplets are assumed to fall with constant velocity. The effect of release of heat of condensation is considered. Advice concerning the choice of chamber gas and vapour is given.

Bevan[14]) (Harwell) applied Shutt's strict theory studying the optimum conditions for diffusion chambers[15]). The theory was completed by taking account of the formation of neutral condensation nuclei and thus the parameter β_a (10) was a little modified, and called B_a. Bevan gives in diagrams the connection between B_a and minimum temperature gradient, position and temperature of the alcohol trough in order to get tracks at —20°C, as well as that trough temperature, above which distrubances in the normal operation of the diffusion cloud chamber appear.

5. Examples of some Diffusion Cloud Chambers

The Langsdorf[8]) diffusion cloud chamber, already described, was not very simple, and the charged particle tracks published were not of the same quality as tracks obtained in the Wilson-chamber. This explains the long time-lag before the diffusion cloud chamber aroused more intense interest. Not until Needels and Nielsen[16]), and—may be still more—Cowan[17]) had shown how it was possible—using very simple constructions—to get tracks as good or still better than those obtained in the Wilsonchamber, did the construction of diffusion cloud chambers start. Cloud chambers were made for demonstration purposes as well as for recording nuclear particles created in experiments with high energy accelerators.

Needels and Nielsen[16, 18]) (Ohio State University) simply put a glass beaker on a block of dry ice and covered it with a sheet of cardboard moistened with alcohol. Ion tracks of excellent quality and sharp tracks of both electrons and protons were observed in a shallow layer near the cold bottom of the beaker. The best working conditions were obtained when a clearing field was placed across the sensitive region. In order to have better vision from above, a hole was cut in the cardboard and covered with a glass plate, and a piece of black velvet cloth moistened with alcohol was put in the bottom of the beaker. The height of the sensitive region could be increased by use of mixtures of different alcohols and water.

Choyke and Nielsen[19]) made a low pressure (75–15 cm Hg) diffusion chamber filled with helium and ethanol. The bottom plate was cooled to approximately —130°C by inserting an aluminium cylinder connected to the bottom plate into a Dewar flask filled with liquid nitrogen. The maximum permissible top temperature for a helium filled chamber was calculated to be and kept at —20°C.

Cowan's[17]) diffusion cloud chambers are similar to those of Needels and Nielsen. Fig. 7 shows one of the cloud chambers schematically.

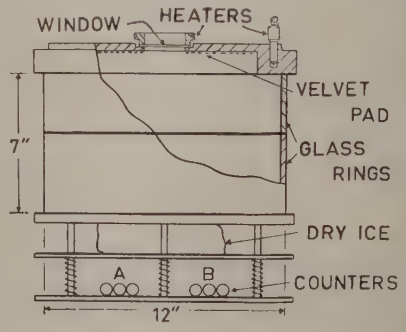

Fig. 7. Schematic drawing of Cowan's diffusion cloud chamber (Rev. Sci. Inst. **21** (1950) 991).

This type can be considered as a pattern for all later diffusion cloud chambers. The floor of the chamber is made of aluminium blackened by an anodizing process or of black bakelite. This bottom is cooled by direct contact with a block

[13]) C. Succi and G. Tagliaferri, Nuovo Cimento **9** (1952) 1092.

[14]) A. R. Bevan, A.E.R.E. GP/R (1953) 1215.

[15]) M. Snowden and A. R. Bevan, J. Sci. Inst. **30** (1953) 3.

[16]) T. S. Needels and C. E. Nielsen, Rev. Sci. Inst. **21** (1950) 976.

[17]) E. W. Cowan, Rev. Sci. Inst. **21** (1950) 991.

[18]) C. E. Nielsen, T. S. Needels and O. H. Weddle, Rev. Sci. Inst. **22** (1951) 673.

[19]) W. J. Choyke and C. E. Nielsen, Rev. Sci. Inst. **23** (1952) 307.

of dry ice. The cylindrical glass wall is made of two glass rings, separated by a conducting rubber gasker which is one of the sweep-field electrodes. The other electrode is the top and bottom of the chamber. This arrangement removes the ions from the upper part of the chamber without pulling them down into the sensitive layer. The top plate of aluminium is heated electrically and carries a velvet pad sewn to a perforated aluminium sheet. A glass window in the centre of the top makes it possible to take photographs of the tracks in the chamber. The exposure may be released by the G.M.-counters below the bottom of the chamber, for instance, in the case of cosmic rays by mesons.

The height of the sensitive layer is about 3 inches at a top temperature of 44°C, if the chamber is filled with air and methanol. With a liquid mixture of about equal parts of methyl alcohol, ethyl alcohol, and water, it is possible to obtain a sensitive layer five or six inches deep after passing a pulse of sweep voltage.

When photographed, the tracks are illuminated by means of a flash lamp (General Electric Type FT-422), connected to 250 μF charged to a voltage of 2000 volts. When operated with counter control, a sweep voltage pulse of 1.5 sec duration and 600 volts amplitude is applied every 45 seconds.

The first high pressure diffusion cloud chamber was constructed by Miller, Fowler, and Shutt[21]). Experiments were made with methanol and hydrogen (12–16.5 atm), helium (3.1–8.9 atm) and air (1–3.1 atm). With H_2 or He, violent conversion occurs up to a pressure at which the density gradient from top to bottom becomes positive. At 12 atm the hydrogen-filled cloud chamber records continuously ionizing radiation having an intensity 2–3 times that of cosmic rays at sea level. On the other hand, there is no limit to the chamber's ability to record bursts of radiation if an electric sweeping field is applied during the intervals. A novelty was the temperature distribution control along the stainless steel walls by means of heating wires soldered to them.

Immediately after this Shutt, Fowler, Miller, Thorndike, and Fowler[22]) made a new high pressure diffusion cloud chamber for 21 atm working with hydrogen and methanol vapour filling. The bottom temperature was —65°C and the top temperature +20°C. The chamber was used for a study of the scattering of the 60 MeV π^--mesons from the Columbia University Nevis cyclotron. After some changes, the construction[23]) of the cloud chamber was that shown schematically in fig. 8. To the left a vertical

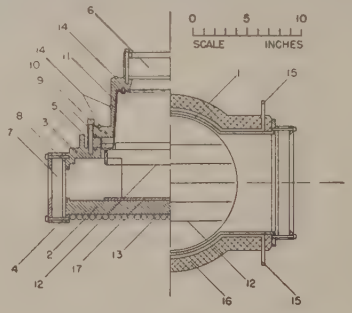

Fig. 8. Diagram of diffusion chloud chamber designed for operation at 20 atm according to Fowler, Fowler, Shutt, Thorndike, and Whittemore (Phys. Rev. **91** (1953) 135).

projection, to the right a horisontal projection of the chamber is seen. It consists of welded steel bottom and top cylinders separated by a bakelite insulating ring (5). The bottom can has a $^1/_4$-inch stainless steel cylinder wall (1) and a 1.25-in. bottom plate (2), and top flange (3). The top is made in a hat shape so that the top window (6) can be close to the camera and hence be small in size. The copper through (9) is in good thermal contact with the base plate (10) of the top. Cooling coils (13) at the bottom and heating wires at the top (14) and the side (15) provide temperature control of the chamber, which is temperature insulated (16) from the surrounding air. The tracks are illuminated through windows

[20]) M. M. Block, W. W. Brown and G. G. Slaughter, Phys. Rev. **86** (1952) 583.

[21]) D. H. Miller, E. C. Fowler and R. P. Shutt, Rev. Sci. Inst. **22** (1951) 280.

[22]) R. P. Shutt, E. C. Fowler, D. H. Miller, A. M. Thorndike and W. B. Fowler, Phys. Rev. **84** (1951) 1247.

[23]) E. C. Fowler, W. B. Fowler, R. P. Shutt, A. M. Thorndike and W. L. Whittemore, Phys. Rev. **91** (1953) 135.

(7) by light from flash tubes. A sweeping field is obtained by a suitable voltage on the wires (12).

The good results obtained with this diffusion cloud chamber gave rise to the construction of still larger chambers for the Cosmotron at Brookhaven National Laboratory. Thus a larger chamber[24]) of a type similar to that already described was built, having a diameter of 16 inches and operating in a field of 10 500 oersted. wires through copper tubes (11) soldered to the sides of the chamber and to the alcohol tray. In order to get an optical background, black dye is added to the alcohol layer on the bottom. The chamber is illuminated by flash tubes near the ends of the top window and the light is reflected by mirrors (13) at 45° into the sensitive layer.

In order to reduce the time spent in scanning to find the events, a special projector was

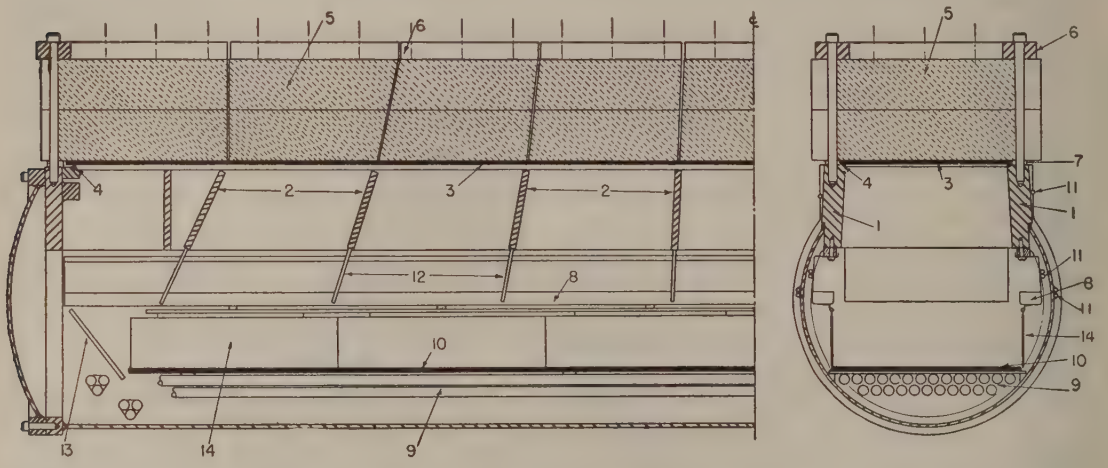

Fig. 9. Schematic drawing of the 6 foot diffusion cloud chamber at Brookhaven. The chamber operates with H_2 or He at pressures up to 21 atm and is used in connexion with the Cosmotron. At the right a transverse section through the centre is shown. At the left, one half of a lengthwise section is given, the other half being symmetrical. Fowler, Shutt, Thorndike, and Whittemore (Rev. Sci. Inst. **25** (1954) 996).

In order to be able to record more events, a long cloud chamber with an effective length of 6 ft, width of 11 in., and no magnetic field was built. Fig. 9 shows this chamber schematically. It has a horizontal cylindrical shape, but with the top of the cylinder modified to provide a window, consisting of a single Allite sheet $^1/_4$ in. thick (3) and heavy Lucite blocks (5). The window is mounted on heavy longitudinal bars (1) with transverse tie bars (2). The bottom is cooled by a set of cooling coils, through which trichloroethylene is pumped at the temperature of dry ice. Vapour is supplied to the chamber from methyl alcohol in trays (8) thermally insulated from and mounted on the side bars. The temperature distribution is controlled by heating devised in which the image of the length of the sixfoot cloud chamber is compressed to a length of about 18 in. in the projected image, while perpendicular distances remain full size. In addition to saving up to 75 percent scanning time, this method has several other advantages, for instance, small angular deflections of longitudinal tracks are magnified 4 to 5 times so that deflections as low as 1° can be detected easily.

In U.S.A. other high pressure diffusion cloud chambers have been made at Berkeley and Chicago, in each case in connection with high energy accelerators. Thus Elliott, Maenchen, Moulthrop, Oswald, Powell, and Wright[25]) describe a 36 atm diffusion cloud chamber for use

[24]) W. B. Fowler, R. P. Shutt, A. M. Thorndike and W. L. Whittemore, Rev. Sci. Inst. **25** (1954) 996.

[25]) J. B. Elliott, G. Maenchen, P. H. Moulthrop, L. O. Oswald, W. M. Powell and R. W. Wright, Rev. Sci. Inst. **26** (1955) 696.

with the 184 in. cyclotron and the bevatron in Berkeley. The diffusion cloud chamber is built into a magnet giving a field of 21 000 oersted every 11th second, with a duration of the field of about 0.2 sec. The outside diameter of the chamber is 19.23 in. and the useful diameter of the sensitive region is 10 in. with a height of 2 to 2.5 in.

At the University of Chicago Schluter[26]) studied the $n + p \rightarrow d + \pi^0$ reaction with a similar diffusion cloud chamber connected to the 170 in. cyclotron. The field strength was 10 500 oersted. As all the semagnetic field

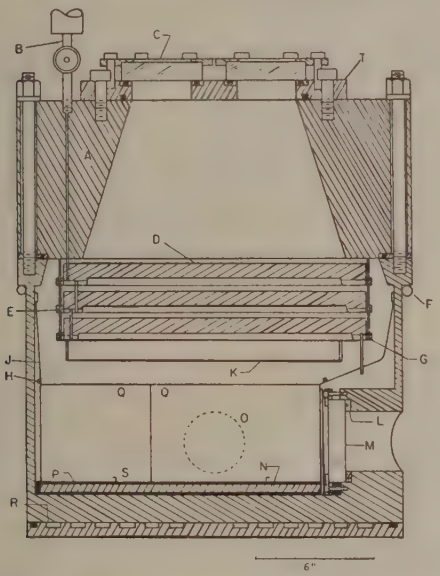

Fig. 10. Vertical section of the high-pressure diffusion cloud chamber in Chicago. A. Top pole, part of the iron yoke (fig. 11). B. Alcohol insertion. C. Camera window. D. Wick. E. Alcohol trays, F. Circultaion tubing. G. Tray heater. H. Thin wall heater. J. Thin wall. K. Clearing electrode. L. Soft copper ring. M. Tempered glass window. N. Copper plate. O. Beam entrance window. P. Dyed alcohol pool. Q. Mirrors. R. Grooves for acetone circulation. S. Fiducial markers. T. Top cover plate. Schluter and Wright (Rev. Sci. Inst. **26** (1955) 1053).

equipped chambers in Brookhaven, Berkeley, and Chicago are of a similar type, it might be sufficient here to describe the one in Chicago[27]). A vertical section of this 30 atm hydrogen filled chamber is shown in fig. 10, where the text to the figure might be sufficient to make the construction clear. Fig. 11 shows the position of the cloud chamber in the iron yoke and fig. 12

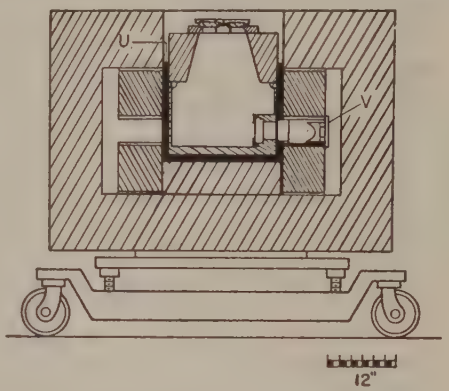

Fig. 11. Magnetic yoke of the Chicago diffusion cloud chamber. Schluter and Wright (Rev. Sci. Inst. **26** (1955) 1053).

shows schematically the temperature control of the system. The temperature of the bottom of the chamber is kept at —55° to —60°C by means of an acetone (or later methylene chloride) circulation system shown schematically in figs. 12–14. The liquid flows through a spiral passage (R in fig. 10, see also figs. 13 and 14) attached to the bottom of the cloud chamber and is cooled in a small heat exchanger by

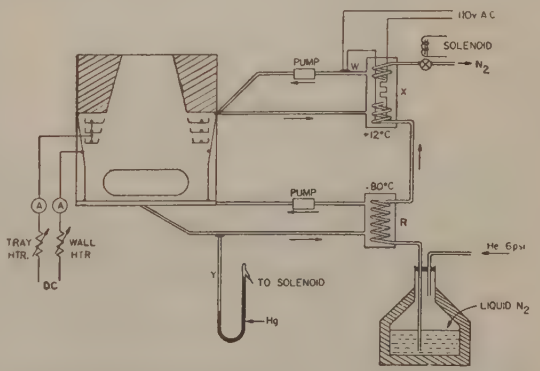

Fig. 12. Schematic diagram of the Chicago chamber thermal control system. Schluter and Wright (Rev. Sci. Inst. **26** (1955) 1053).

evaporating liquid nitrogen. With the circulating liquid at —75°C, the temperature of the pool of alcohol in the bottom of the chamber is about

[26]) R. A. Schluter, Phys. Rev. **96** (1954) 734.

[27]) R. A. Schluter and S. C. Wright, Rev. Sci. Inst. **26** (1955) 1053.

—55°C, that is, the temperature loss through the bottom is about 20°C†. The top temperature was kept at +12°C. The height of the sensitive layer was 2½ to 3 inches.

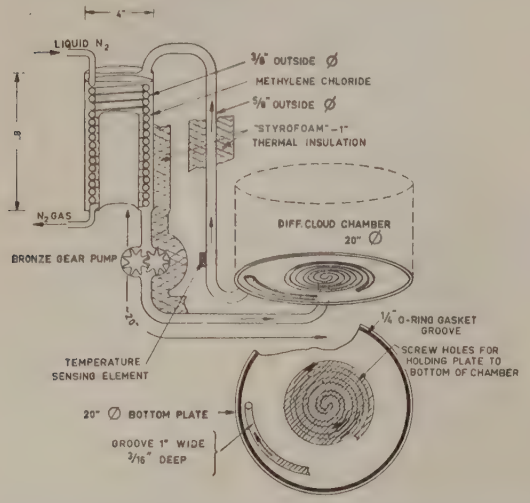

Fig. 13. Schematic detail of the Chicago chamber cooling system, according to a sketch obtained by the courtesy of Dr. R. A. Schluter.

In connexion with the high energy physics programme at Harwell Snowden and Bevan[28]) built a small 9 in. diameter diffusion cloud chamber to study the operating characteristics

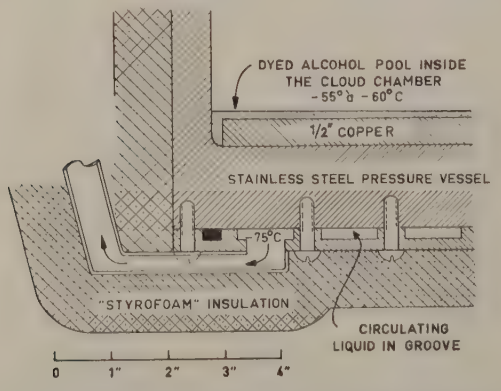

Fig. 14. Schematic detail of the Chicago chamber bottom plate, according to a sketch obtained by the courtesy of Dr. R. A. Schluter.

and to form the basis of a design for an 18 in. diameter chamber operating with hydrogen at 24 atm. Fig. 15 shows schematically the experimental cloud chamber. The details are explained in the text to the figure. With methanol and air at 1 atm, a sensitive layer of 1 in. in height was

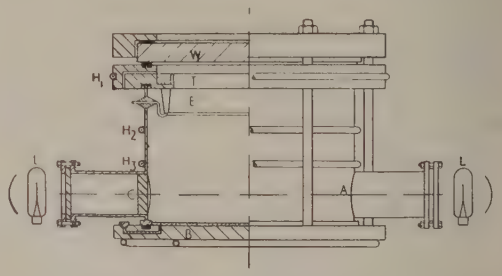

Fig. 15. Schematic drawing of Snowden's and Bevan's experimental 4 atm diffusion cloud chamber. T. Brass trough for alcohol. H_1. Heater for this trough, which is insulated from top and walls. W. Glass window. E. Ring electrode, supported by insulators from the bottom of the trough. H_2, H_3. Heaters for the temperature gradient control. L. 500 W projector lamps. C. Perspex lenses to diverge light into a 60° fan-shaped beam. B. ½ inch thick copper sheet cooled by methanol circulated from a heat exchanger cooled to —75 C° with solid carbon dioxide. The chamber wall made of $^1/_{16}$ inch mild steel (J. Sci. Inst. **30** (1953) 3).

easily obtained, but in order to increase this to 2–3 in., control of the temperature gradient by means of the heaters H_1, H_2, H_3 and the use of a clearing field were required. The best results (2½–3 in. sensitive height) were obtained with the wall heaters adjusted to give a gradient of 9°C/cm and a field potential of —1200 V. Both argon and nitrogen gave results similar to air. Successful operation at pressures up to 4 atm was achieved.

In Liverpool Crewe and Evans[29]) built a 30 atm diffusion cloud chamber for the 156 in. synchrocyclotron, and recently Margaret Alston, Crewe, Evans, and v. Gierke[30]) have made a quite new chamber, used to investigate the production of π^+-mesons in p-p collisions at 383 MeV. The 18 in. diffusion cloud chamber is shown schematically in fig. 16a and photographically in fig. 16b. The details might be clear from the text to the figures. The chamber is

† R. A. Schluter, personal communication.

[28]) M. Snowden and A. R. Bevan, J. Sci. Inst. **30** (1953) 3.
[29]) A. V. Crewe and W. H. Evans, Atomics **3** (1952) 221.
[30]) Margaret H. Alston, A. V. Crewe, W. H. Evans and G. von Gierke, Proc. Phys. Soc. A **69** (1956) 691.

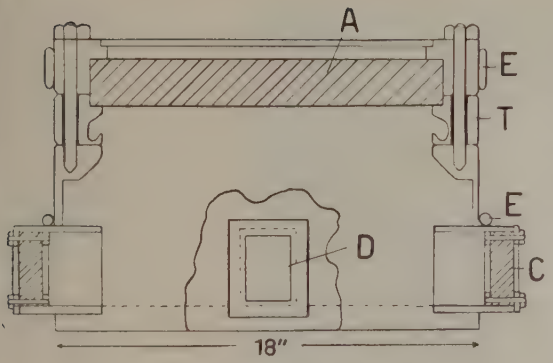

Fig. 16a. Schematic drawing.

filled with 28 atm of hydrogen and works in a magnetic field of 11 200 oersted. The base of the chamber is cooled to —60°C by passing cold acetone through copper pipes soft-soldered to the base. The temperature gradient in the sensitive region is 5°C/cm for hydrogen at 20–28 atm, and 7.5°C/cm for air at 1 atm. The sensitive depth is 2½–3 in.

In addition to these large diffusion cloud chambers numerous small chambers have been described[31–36]) and built in many places. Thus, fig. 17 shows a low pressure chamber[36]), made by the author and used for the study of the spontaneous fission of Cf^{252}. Figs. 18 and 19 show some fission tracks obtained in this chamber. The pressure of the airmethanol gas mixture was 0.2 atm and the depth of the sensitive layer about 1½ in. (without heaters). When photographed, the tracks were illuminated by means of a commercial xenon flash light tube, "Brown-Hobby" type BH 100. The xenon tube was then placed in front of a reflector in the cover F (fig. 17).

[31]) A. J. Barnard and J. R. Atkinson, Nature **169** (1952) 170.
[32]) A. L. Kuehner, J. Chem. Educ. **29** (1952) 511.
[33]) A. Voisin, J. Phys. et Rad. **14** (1953) 459.
[34]) T. Wilner, Elementa **36** (1953) 265.
[35]) A. B. Milojević, M. A. Cerineo, and B. J. Lalović Bull. Inst. Nucl. Sci. "Boris Kidrich" **3** (1953) 23.
[36]) H. Slätis, Arkiv f. Fysik **10** (1956) 479.

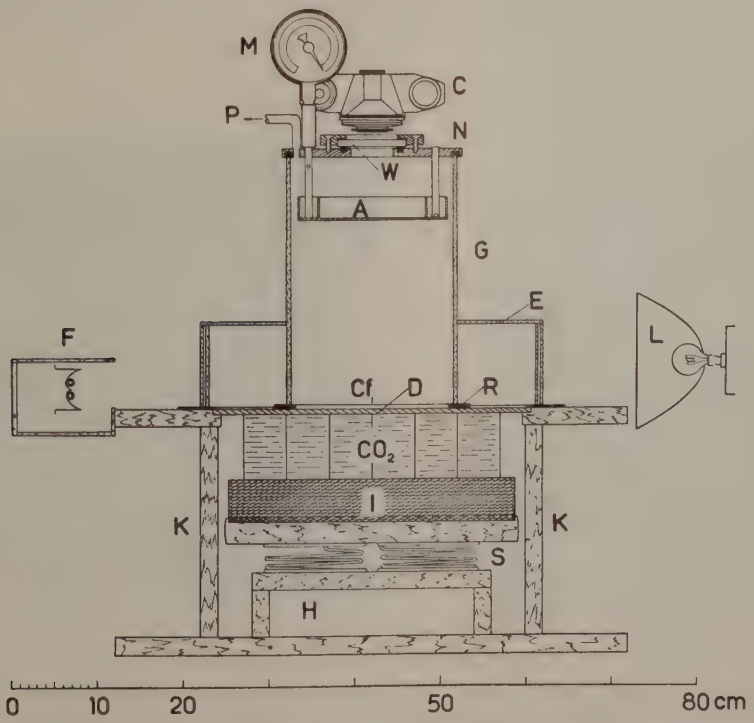

Fig. 17. Design of a low pressure diffusion cloud chamber used for the study of the spontaneous fission of Cf^{252}. A. Brass trough for alcohol. M. Pressure gauge. W. Window. C. Camera. N. Filling pipe. G. Glass cylinder. E. Heat insulating glass box (Slätis, Arkiv f. Fysik **10** (1956) 479).

6. Some Properties of the Diffusion Cloud Chamber

6.1. FORMATION OF "RAIN"

Already Langsdorf[8]) payed much attention to the formation of rain of condensation which was apparently not dependent on the presence of ions. Cosmic and gamma rays produce nearly as many ions in the upper part of the chamber as in the sensitive region. The ions in the upper part will diffuse downward until they are condensed upon to form a diffuse rain, unless they are removed by an electric sweep field. However, it does not seem to be possible to remove completely the rain by an electric field. Presumably also light induces some photochemical action which creates condensation nuclei. Rain condensation not dependent upon the presence of ions might be caused in connexion with the bubbling of boiling liquid, contact of boiling liquid and a metal surface etc.[8]). The formation of rain increases the alcohol consumption and decreases the supersaturation in the lower layers, thus decreasing the sensitivity of the chamber.

Cowan[17]) also treats the formation of rain. Streamers of droplets will sometimes be produced by leaks that permit contaminated air from the outside to enter the chamber, or by the formation of coronas from fine points when a high voltage is used.

Bevan[14]) finds that if the alcohol temperature in the trough is raised to its boiling point, fine streamers of descending rain are produced, probably due to the evolution of large numbers of neutral condensation nuclei from tiny bubbles.

Thus in order to avoid rain formation, care should be taken in the construction of the sweeping field, the trough temperature should not be too high, and the chamber should, of course, be airtight, even if the pressure is 1 atm.

6.2. THE HEIGHT OF THE SENSITIVE REGION

The use of metal walls with heaters for the control of the temperature gradient in the cloud chamber made it possible to increase the height of the sensitive layer. However, for layers higher than about 3 in., an increase of the height is counterbalanced by a decrease in the sharpness of the tracks. Also, the method of decreasing the bottom temperature cannot be extended below —70° C. A decrease from —70° to —90° C increases the height of the sensitive layer by about ¾ in., it is true, but the tracks in the bottom layer are very thin because of the low vapour pressure in this region[23,35]).

6.3. TRACK RECORD CAPACITY OF THE DIFFUSION CLOUD CHAMBER

Already Langsdorf[8]) pointed out that the diffusion cloud chamber during long periods can show tracks only for ionizations of the same order of magnitude as the normal background of ionization in an unshielded chamber. As mentioned before, this was confirmed by Miller, Fowler, and Shutt[21]). Hence, it is advantageous to shield the chamber from local gamma-radiation[8]). On the other hand, there is no limitation in the chamber's capacity to record bursts of radiation if an electric sweeping field is applied during the intervals[21]).

6.4. THE SAMPLE HOLDER

Rigid bodies in the sensitive region of the chamber will be condensed upon. This phenomenon is very disturbing, if one wants to investigate the radiation from a radioactive sample put into the chamber and especially for α-particles, as these will be absorbed by the condensed alcohol layer. The formation of this layer can be prevented by heating the sample holder, either electrically or by heat radiation. However, this will give rise to a small, disturbing convective current and hence a small insensitive region in the vicinity of the sample (see figs. 18 and 19).

7. Some Examples of the Use of the Diffusion Cloud Chamber

Shutt, Fowler, Miller, Thorndike, and Fowler[22]) at Brookhaven determined the cross section for the scattering of 60 MeV π^--mesons by protons using their high pressure diffusion cloud chamber (similar to that in fig. 8) in connexion with the Columbia University Nevis cyclotron. The

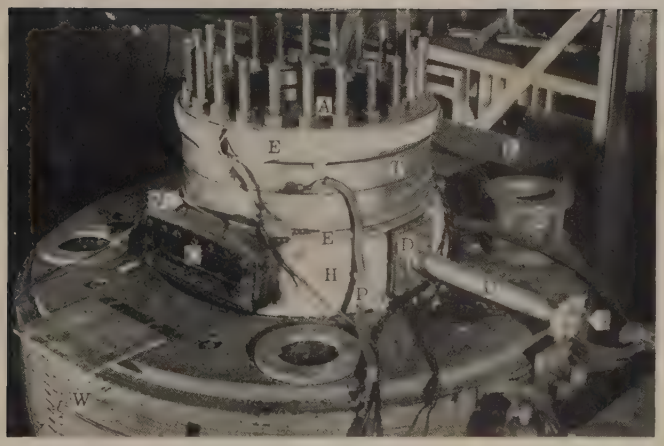

Fig. 16b. Photograph of the new Liverpool 18 inch diffusion cloud chamber (top coil removed). (Alston, Crewe, Evans and von Gierke, Proc. Phys. Soc. A **99** (1956) 691). A. Top window. T. Alcohol tray. C. Side window. D. Beam entry port. E_1 N. Heaters. H. Insulating glass wool jacket. P. Filling pipe. U. Extension tube. I. 0.006 inch duraluminium. S. Support for the (removed) top coil. W. Bottom field coil. The figures were obtained by the courtesy of Dr. Margaret H. Alston.

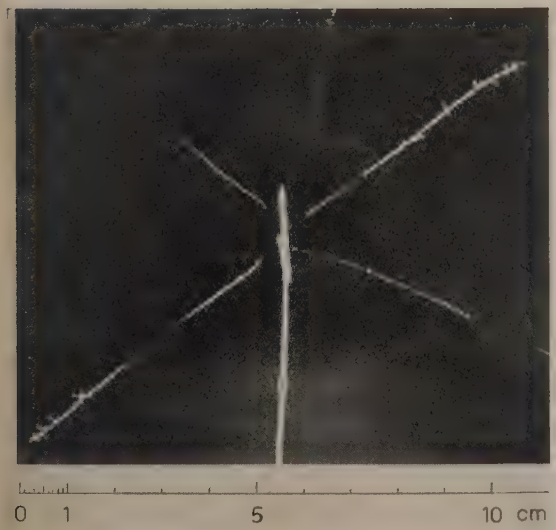

Fig. 18. Fission tracks (emitted in opposite directions) and two α-tracks from Cf^{252}. The α-track to the right is older than the others and is disappearing. The sample is held by a copper wire (the heavy vertical line). Pressure 0.2 atm Slätis[36]).

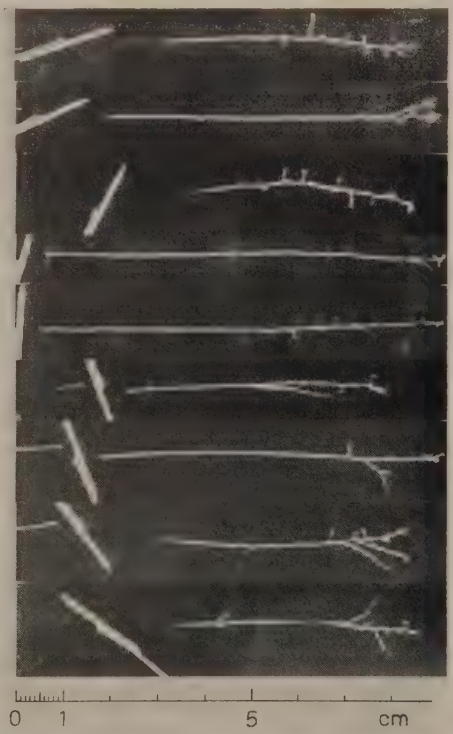

Fig. 19. A number of fission tracks from Cf^{252}. The heavy line to the left is the sample. The range of the fission track decreases, when the number of branches increases. Pressure 0.2 atm Slätis[36]).

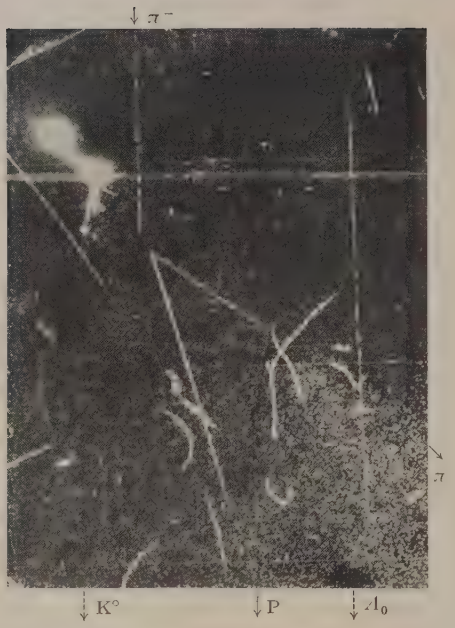

Fig. 21

Fig. 21. A neutral hyperon Λ_0 is produced in a collision between a 1.5 GeV from the Brookhaven Cosmotron and a proton in 20 atm of hydrogen in a diffusion cloud chamber. The Λ_0 particle is produced at the point where the π^- ceases to ionize, its electric charge being neutralized by that of a proton. This Λ_0 decays into a proton (p) and a π^- after living for 4×10^{-11} seconds. If only one single neutral particle

Fig. 22a.

Fig. 22b.

is assumed to conserve momentum and energy of incident π^-, its mass would have to be 1300 electron masses and its direction of flight as indicated by (K°). The picture was obtained by the courtesy of Dr. R. P. Shutt and earlier published. Fowler, Shutt, Thorndike, and Whittemore (Phys. Rev. **91** (1953) 1287).

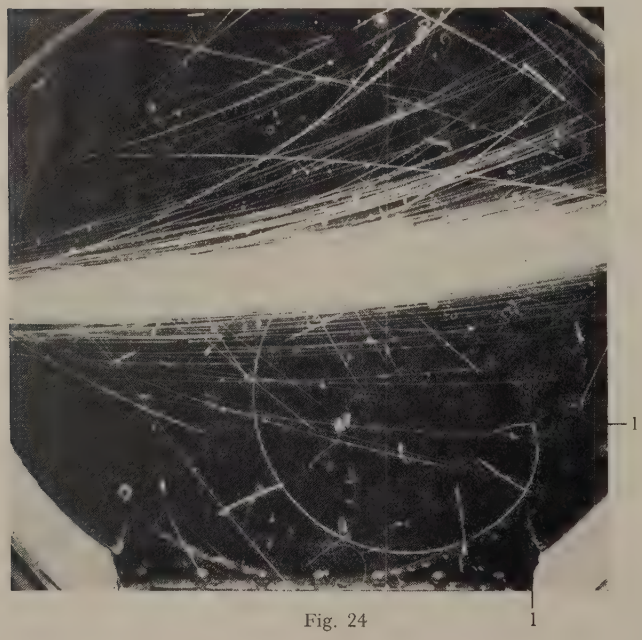

Fig. 24

Fig. 22. Simultaneous production of a Λ_0 and a ϑ^0 by a Cosmotron-produced 1.5 GeV π^- in a hydrogen-filled diffusion cloud chamber. The collision takes place where the incident π^- track disappears abruptly. The decay products of the ϑ^0 are visible a short distance away (π^-, π^+). Further down, the decay products of (he Λ_0, (p, π^-) can be seen. The pictures were obtained by the courtesy of Dr. R. P. Shutt and earlier published. Fowler, Shutt, Thorndike, and Whittemore (Phys. Rev. **93** (1954) 861).

Fig. 24. About 20 000 protons of 380 MeV energy enter the Liverpool diffusion cloud chamber. The G-shaped track is produced by a π^+-meson, which decays at the point (1.1) into a μ^+-meson. Field strength 11 200 oersted. The picture was obtained by the courtesy of Dr. Margaret H. Alston, and earlier published. Alston, Crewe, Evans, von Gierke (Proc. Phys. Soc. A **69** (1956) 691).

chamber was filled with 21 atm of hydrogen and methanol. The cyclotron ion source was pulsed every 4 to 6 sec, and the 5600 stereoscopic pictures taken during the first day's operation were examined. Each picture showed about 20 tracks. Three cases were observed, which could be considered to be π^--p scatterings. Fig. 20 shows one of these events. In a similar way the cross section was determined for the scattering of 50-MeV π^+-mesons by helium[38]).

Fig. 20. Stereoscopic view of a π^--p scattering event. A π^- (thin track) from below, a recoil proton (short track) and a scattered pion are seen in the middle of the right hand picture, a bit to the left on the left hand picture. Shutt, Fowler, Miller, Thorndike, Fowler (Phys. Rev. **84** (1951) 1247).

In the high pressure diffusion cloud chamber exposed to a neutron beam from the Cosmotron at Brookhaven Fowler, Shutt, Thorndike, and Whittemore[41]) observed two Λ_0 particles, which decay according to $\Lambda_0 \rightarrow \mathrm{p} + \pi^- + Q$. For Q the values 39 ± 16 and 37 ± 8 MeV, respectively, were found in both cases. The cloud chamber was filled with 18 atm of hydrogen and methanol. In addition, Fowler, Shutt, Thorndike and Whittemore[43]) found that 1.5 GeV π^--mesons from the Cosmotron produce Λ_0 particles in collisions with protons. Figs. 21 and 22 show such events.

The Berkeley Bevatron giving 6.2 GeV protons might be expected to produce more mesons than the Brookhaven Cosmotron. This is indeed the case. High energy neutrons were obtained by bombarding copper with protons. The erarlier mentioned high pressure cloud chamber was placed 75 feet from the target along a line tangent to the proton beam. The neutron energies extended from a few MeV up to 6.2 MeV. Among more than 500 events showing pion production in n-p collisions, there was one with seven outgoing prongs (fig. 23), 5 of them interpreted as pions, two as protons.

[37]) H. Slätis, Kosmos **34** (1956) 33.

[38]) A. M. Thorndike, E. C. Fowler, W. B. Fowler and R. P. Shutt, Phys. Rev. **85** (1952) 928.

[39]) E. C. Fowler, W. B. Fowler, R. P. Shutt, A. M. Thorndike and W. L. Whittemore, Phys. Rev. **86** (1952) 1053.

[40]) K. A. Brueckner, Phys. Rev. **86** (1952) 106.

[41]) W. B. Fowler, R. P. Shutt, A. M. Thorndike and W. L. Whittemore, Phys. Rev. **90** (1953) 1126.

[42]) W. B. Fowler, R. P. Shutt, A. M. Thorndike and W. L. Whittemore, Phys. Rev. **91** (1953) 758.

[43]) W. B. Fowler, R. P. Shutt, A. M. Thorndike and W. L. Whittemore, Phys. Rev. **91** (1953) 1287; **93** (1954) 861.

[44]) W. B. Fowler, R. M. Lea, W. D. Shephard, R. P. Shutt, A. M. Thorndike and W. L. Whittemore, Phys. Rev. **92** (1953) 832.

[45]) R. C. Cornelius, C. P. Sargent, M. C. Rinehart, L. M. Lederman and K. Rogers, Phys. Rev. **92** (1953) 1583.

[46]) C. P. Sargent, R. Cornelius, M. Rinehart, L. M. Lederman and K. Rogers, Phys. Rev. **98** (1955) 1349.

[47]) C. P. Sargent, M. Rinehart, L. M. Lederman and K. C. Rogers, Phys. Rev. **99** (1955) 885.

Fig. 24 shows a proton beam exposed in the above mentioned Liverpool diffusion cloud chamber (fig. 16a and b).

The author would like to thank the following institutions and persons for the permission to reproduce figures and information in quoted articles as well as publish data obtained by communication:

The American Physical Society (The Physical Review), The American Institute of Physics (The Review of Scientific Instruments), The Institute of Physics, London (The Journal of Scientific Instruments), United Kingdom Atomic Energy Authrority, Leonard Hill Limited, London (Atomics), Dr. Margaret H. Alson, Liverpool, Dr. Robert Schluter, M.I.T., Cambridge, U.S.A., Prof. R. P. Shutt, Brookhaven National Laboratory, Prof. M. Snowden, Harwell.

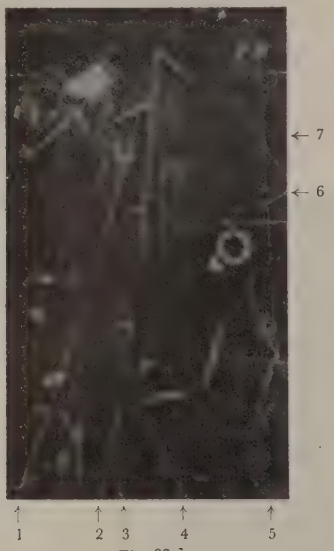

Fig. 23a

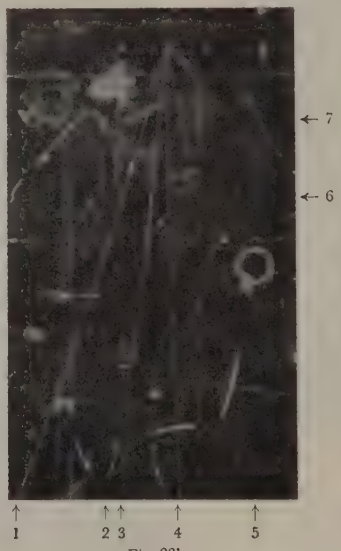

Fig. 23b

Fig. 23. π-meson production with neutrons from the Berkeley Bevatron. Tracks 1 and 5 are protons, tracks 2 and 6 are π^+-mesons, while tracks 3, 4 and 7 are π^--mesons. Fowler, Maenchen, Powell, Saphir, Wright, (Phys. Rev. **101** (1956) 911).

[48]) M. C. Rinehart, K. C. Rogers and L. M. Lederman, Phys. Rev. **100** (1955) 883.

[49]) R. A. Schluter, Phys. Rev. **96** (1954) 734.

[50]) W. B. Fowler, G. Maenchen, W. M. Powell, G. Saphis and R. W. Wright, Phys. Rev. **101** (1956) 911.

[51]) M. Snowden, The Diffusion Cloud Chamber, Progress in Nuclear Physics **3**, Editor O. R. Frisch (London, 1953) p. 1.

NUCLEAR INSTRUMENTS 1 (1957) 227–231; NORTH-HOLLAND PUBLISHING CO. – AMSTERDAM

AN APPLICATION OF MAGNETIC TAPE RECORDING TO NEUTRON TIME-OF-FLIGHT SPECTROSCOPY

E. R. RAE and F. W. K. FIRK

UKAEA, *Atomic Energy Research Estableshment, Harwell*

Received 21 February 1957

The technique of recording nuclear pulses on a twin-track magnetic tape has been applied to the examination of the prompt gamma rays following the capture of a slow neutron. The pulse-height spectrum produced by the gamma rays in a NaI crystal spectrometer is recorded on one track and a pulse denoting the time-of-flight of the neutron on the other. In this way the spectra of gamma rays due to capture of a neutron into a number of different resonances are recorded simultaneously and can be reproduced individually by selecting the gamma ray pulses corresponding to the appropriate group of timing pulses and playing them back into a multi-channel pulse-height analyser. The play-back time is a small fraction of the recording time so that the method, in addition to eliminating monitoring difficulties and providing a permanent record of the experiment, also leads to a considerable saving in time, both of the time-of-flight equipment and of the pulse-height analyser.

The gamma rays due to neutron capture in Hg^{199} have been examined with this equipment and the results are discussed.

Cavanagh and Boyce[1]) have shown that the amplitude recording of nuclear pulses on magnetic tape can lead to an increase in simplicity and reliability of many experiments in physics. In particular they have shown that by recording two sets of data on twin tracks, it is possible to analyse this data later and to select coincidences between different types of events on the two tracks. If the two sets of data are obtained from nuclear events caused by the beam from a machine, then clearly a great saving in machine-time is obtained since many different types of coincidence can be recorded simultaneously and analysed in sequence. In addition, since the tape may be played back at speeds many times greater than the recording speed, an overall saving in experimental time is achieved together with the advantages of a permanent record and an absence of monitoring difficulty.

One of the possible applications pointed out by Cavanagh was the simultaneous recording of the time-of-flight of a neutron, and the spectra of gamma rays caused by resonance capture in a target nucleus.

Unless several multi-channel analysers are available, any method of direct measurement of the gamma ray spectra is essentially one-dimensional: that is, either the pulse-height spectrum is obtained for one resonance at a time or else several resonances and the background are observed simultaneously, but for only one pulse-height. The advantage of recording the information on a twin-track magnetic tape is that this is a two-dimensional recorder and the pulse-height spectrum for several resonances, together with the background, can be recorded simultaneously. The playing back is also speeded up by a large factor, and can be repeated if desired, thus reducing the demands on the reliability of the multi-channel kicksorter used to analyse the spectra.

To record the time-of-flight of a neutron on the magnetic tape, it is necessary to produce a pulse whose amplitude is uniquely related to the flight time. This was done by constructing a circuit which, on being triggered by a signal pulse from the sodium-iodide crystal spectrometer (Rae and Bowey[2])), produces a pulse whose amplitude is proportional to the excess of the flight-time over some fixed, pre-set delay. The circuit

[1]) P. E. Cavanagh and D. A. Boyce, Rev. Sci. Instr. **27** (1956) 1028.

[2]) E. R. Rae and E. M. Bowey, Journal Nuc. Energy (in the Press).

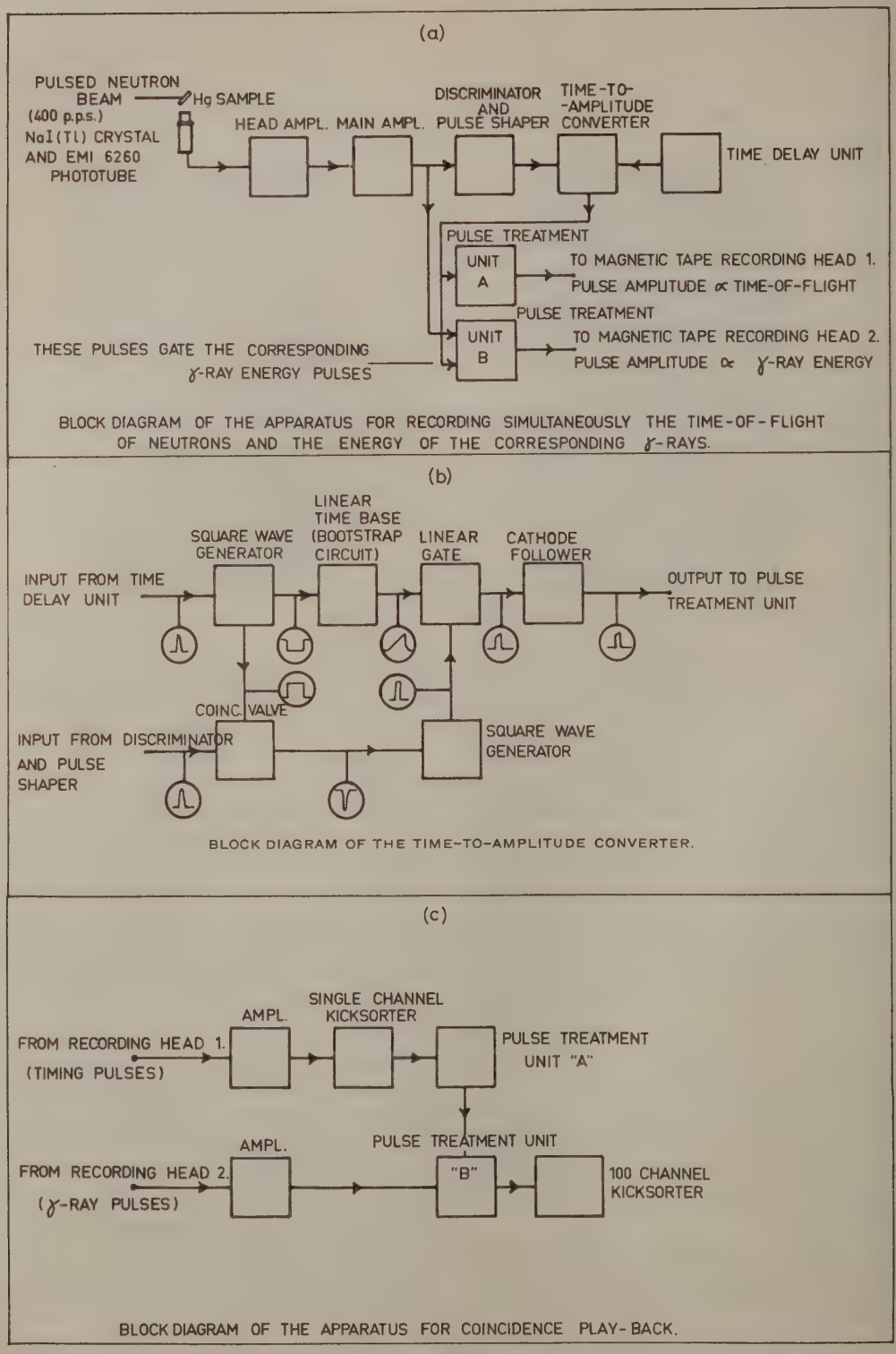
(a)
PULSED NEUTRON BEAM
(400 p.p.s.)
NaI(Tl) CRYSTAL AND EMI 6260 PHOTOTUBE
Hg SAMPLE
HEAD AMPL.
MAIN AMPL.
DISCRIMINATOR AND PULSE SHAPER
TIME-TO--AMPLITUDE CONVERTER
TIME DELAY UNIT
PULSE TREATMENT
UNIT A
TO MAGNETIC TAPE RECORDING HEAD 1.
PULSE AMPLITUDE ∝ TIME-OF-FLIGHT
PULSE TREATMENT
UNIT B
TO MAGNETIC TAPE RECORDING HEAD 2.
PULSE AMPLITUDE ∝ γ-RAY ENERGY
THESE PULSES GATE THE CORRESPONDING γ-RAY ENERGY PULSES
BLOCK DIAGRAM OF THE APPARATUS FOR RECORDING SIMULTANEOUSLY THE TIME-OF-FLIGHT OF NEUTRONS AND THE ENERGY OF THE CORRESPONDING γ-RAYS.
(b)
SQUARE WAVE GENERATOR
LINEAR TIME BASE (BOOTSTRAP CIRCUIT)
LINEAR GATE
CATHODE FOLLOWER
INPUT FROM TIME DELAY UNIT
OUTPUT TO PULSE TREATMENT UNIT
COINC. VALVE
INPUT FROM DISCRIMINATOR AND PULSE SHAPER
SQUARE WAVE GENERATOR
BLOCK DIAGRAM OF THE TIME-TO-AMPLITUDE CONVERTER.
(c)
AMPL.
SINGLE CHANNEL KICKSORTER
FROM RECORDING HEAD 1.
(TIMING PULSES)
PULSE TREATMENT UNIT "A"
PULSE TREATMENT UNIT
AMPL.
"B"
FROM RECORDING HEAD 2.
(γ-RAY PULSES)
100 CHANNEL KICKSORTER
BLOCK DIAGRAM OF THE APPARATUS FOR COINCIDENCE PLAY-BACK.

Fig. 1

is arranged to cover a period of about 100 μsec following the pre-set delay. Fig. 1(b) shows schematically the method of operation: after the pre-set delay, the saw-tooth generator starts a linear run-up which reaches a potential of 50 volts after 100 μsec and then falls rapidly to zero. The signal pulse from the crystal spectrometer, if sufficiently large, opens a linear gate which remains open for 4 μsec and "samples" the saw-tooth wave-form. The output of the gate is therefore a pulse whose amplitude is proportional to the difference in time between the signal pulse and the pre-set delay. The signal pulse itself is increased in duration, (stretched), and recorded on one channel of the tape, and the timing pulse stretched and recorded on the other. The signal pulses are gated by the timing pulses before recording on the tape so that only those pulses which occur during the 100 μsec when the timing circuit is sensitive, are recorded. The tape-speed used on recording was 0.6 in./sec and under these circumstances the duration of the stretched pulses was 5 msec (Cavanagh and Boyce[1]). A block schematic diagram of the recording arrangement is shown in fig. 1(a).

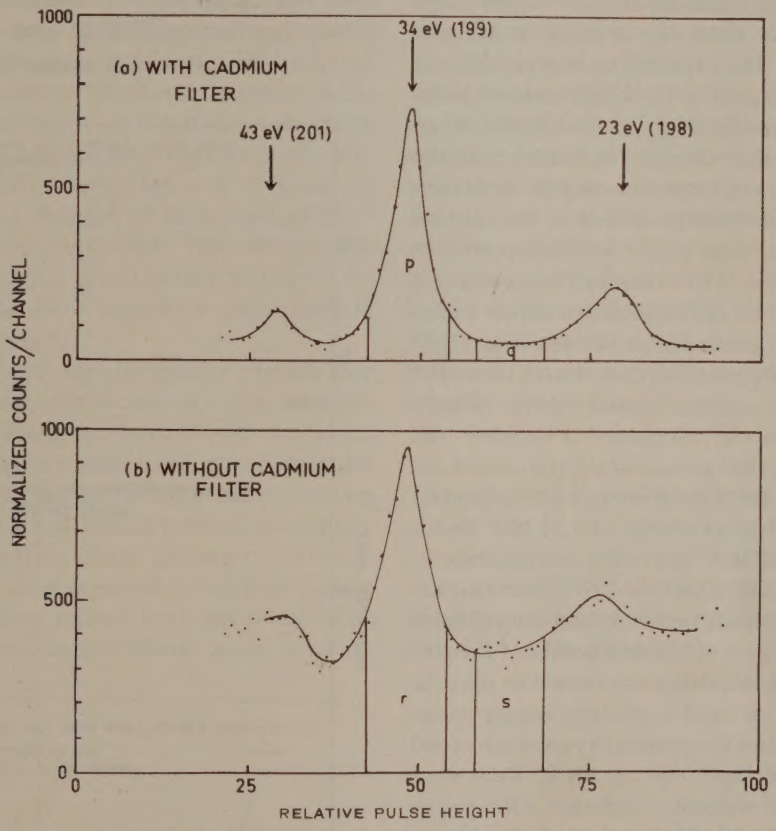

Fig. 2. Time spectrum of recorded pulses for neutrons incident on HgO sample. The arrows indicate positions of resonances: neutron energies and isotopes responsible are marked.

On play-back, the resonance, or other region of neutron time-of-flight is selected by means of a single-channel kicksorter, and the output of this kicksorter is used to gate the gamma ray pulses which are fed into a 100 channel kicksorter. The play-back arrangements are shown schematically in fig. 1(c). The play-back speed was 15 in./sec.

Gamma Rays from Neutron Capture in Mercury

The technique mentioned earlier of using a single-channel kicksorter together with a multi-channel time analyser has been used by Rae and Landon[3]) to compare the spectra of gamma rays from the capture by Hg^{199} of thermal neutrons and of resonance neutrons of 34 eV (Palmer and Bollinger[4])). In order to achieve reasonable counting-rates, the experiment was carried out with a wide channel in the single-channel kicksorter, and correspondingly bad resolution. Even so the information obtained indicated that the gamma rays due to resonance capture were considerably harder than those due to the capture of thermal neutrons, which was interpreted as meaning that the 34 eV resonance leads to a (1^-) state in Hg^{200} thus allowing electric dipole radiation to the (0^+) ground state of even-even Hg^{200} nucleus. The thermal capture leads to a (0^-) state below the neutron binding energy (Kinsey and Bartholomew[5])); (Adyasevich Groshev and Demidow[6])) so that ground-state transitions are forbidden and the highest energy strong gamma ray transition has an energy of 6.44 MeV and is to a level at 1.6 MeV above the ground state.

The tape recorder was used to repeat this experiment with much better resolution available for the comparison of the end points of the two spectra. The pre-set delay was chosen so that the timing circuit covered a neutron energy range of 20 to 45 eV, and the gamma rays were recorded for a sample of HgO, one cm thick. Runs were taken with and without a cadmium filter in the neutron beam and the spectra of the timing pulses obtained are shown in fig. 2. Since the run-up of the time to amplitude converter is 100 μsec and the pulse spectra are displayed on a 100 channel pulse analyser, the points are plotted at intervals of about 1 μsec. The three mercury resonances in the energy interval studied are very well defined and it is possible to select the areas p, q, r and s where the counts obtained are due to gamma rays from resonance capture (34 eV) + background, background alone, resonance + background + thermal capture, and background + thermal capture, respectively. The coincidence play-back system

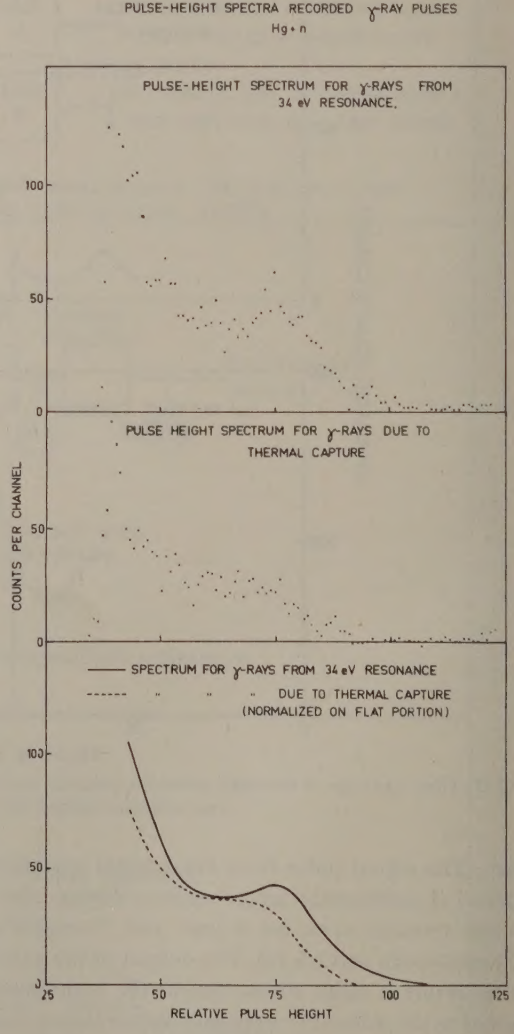
PULSE-HEIGHT SPECTRA RECORDED γ-RAY PULSES
Hg + n
PULSE-HEIGHT SPECTRUM FOR γ-RAYS FROM 34 eV RESONANCE.
PULSE HEIGHT SPECTRUM FOR γ-RAYS DUE TO THERMAL CAPTURE
COUNTS PER CHANNEL
SPECTRUM FOR γ-RAYS FROM 34 eV RESONANCE
" " " DUE TO THERMAL CAPTURE
(NORMALIZED ON FLAT PORTION)
RELATIVE PULSE HEIGHT

Fig. 3

was used to obtain the pulse-height spectra corresponding to those areas, the resonance spectra being given by p — q and r — s, and the thermal spectrum by s — q. Satisfactory

[3]) E. R. Rae and H. H. Landon, Bull A. P. S. Ser. II **1** (1956) 347.

[4]) R. R. Palmer and L. M. Bollinger, Phys. Rev. **102** (1956) 228.

[5]) B. B. Kinsey and G. A. Bartholomew, Canadian J. Phys. **31** (1953) 1051.

[6]) B. P. Adyasevich, B. D. Groshev and A. M. Demidov, Conf. Acad. Sci. USSR on Peaceful use of Atomic Energy, Phys. Math. Sci. (July 1955) p. 220 Translation; Consultants Bureau New York, p. 195.

agreement was obtained between the spectra corresponding to p — q and r — s though the statistical errors in the latter were large owing to the large effective background which was subtracted. The spectra corresponding to p — q and s — q are shown in fig. 3 both separately and superposed. Calibration of the crystal spectrometer with the 4.47 MeV gamma ray from C^{12} following the reaction Be^{9} (α, n) C^{12*} indicated that the end point of the thermal capture radiation was in the region of 6.4 MeV as expected. The resonance capture spectrum is clearly considerably harder, indicating the presence of radiation of E1 strength of an energy which is certainly greater than 7 MeV. This confirms the result of the earlier investigation and again indicates that the 34 eV resonance corresponds to a (1^-) level in Hg^{200}.

This analysis of the high energy gamma rays from neutron capture in mercury illustrates the type of work which can be done with a neutron time-of-flight spectrometer and a tape-recorder using only a simple time to amplitude converting circuit. Such a circuit makes possible the simultaneous examination of the gamma rays from a small number of resonances or neutron energy groups. For more refined work involving large numbers of resonances where more accurate timing of the neutron pulses is desirable, some form of coding of the time-of-flight information would be necessary. Various methods of doing this have been suggested using multi-tracked tapes, including simple binary coding on a relatively large number of tracks (scale of 2 per track), and decimal coding of the amplitude on a small number of tracks (scale of 10 per track). In each case the time-of-flight of a neutron would be measured by counting timing impulses derived from a crystal controlled or other stable oscillator, the number of impulses counted being printed on the tape in binary or decimal form. Consideration of the resolution available in printing amplitude information on the tape (Gaussian distribution with full width at half height $\approx 3\%$) suggests that the intrinsic simplicity and reliability of the binary system would outweigh its disadvantage of requiring a large number of recording channels.

We should like to acknowledge our indebtedness to Dr. P. E. Cavanagh for suggesting the use of magnetic tape recording in time-of-flight work, and to Mr. D. A. Boyce for his assistance in setting up the recording equipment which was loaned to us for this study.

CONFERENCES

EXTRA-ATMOSPHERIC COSMIC RADIATION RESEARCH

On March 29, 1957 a conference of a group of cosmic ray physicists interested in the application of emulsion techniques and a number of engineers and government scientists interested in the scientific application of rockets was held in Baltimore under RIAS sponsorship. The main business of the conference was the consideration of the possibility of studying by the use of nuclear emulsions cosmic ray primaries outside the atmosphere, and in particular, of detecting the presence of any hitherto unobserved component of a low penetrating power.

Mr. R. Patterson and Mr. W. J. Benckert, engineers of the Advanced Design Department of the Martin Company of Baltimore, presented a preliminary design of a vehicle which would allow an oriented stack of 50 pounds of emulsions to be exposed for 40 minutes with a total shielding of less than 0.1 gm/cm^2 while outside the atmosphere. This vehicle, which is to be launched in a vertical shot, would be capable of preserving the emulsion during re-entry into the earth's atmosphere and the eventual fall to earth. During the subsequent discussion, it became evident that such a vehicle could also be used to great advantage for a number of other experiments without interfering with the emulsion studies.

In view of the great scientific potentialities of such a cosmic ray experiment, the physicists formed a committee to consider it in more detail and to arrange a program of cooperative research of all interested scientists at such time as the vehicle is launched. The membership of the committee is: G. Groetzinger (chairman), M. F. Kaplon, S. A. Korff, E. P. Ney, W. J. Otting, A. Pevsner, M. Pomerantz, B. Rossi, M. Schein, M. M. Shapiro, S. Silverman, and H. Yagoda. In a subsequent meeting the committee chose to designate itself as "National Committee for Extra-Atmospheric Cosmic Ray Research" and to consider also the possibility of other new extra-atmospheric cosmic ray experiments. At this meeting, J. A. Simpson joined the committee and W. A. Benckert was designated a consultant.

MESONS AND RECENTLY DISCOVERED PARTICLES

From September 22:nd to 28th 1957 a Conference will be held at the University of Padova and the Foundazione Cini in Venice on "Mesons and Recently Discovered Particles". Both theoretical and experimental work will be presented. The Conference will be sponsored by the International Union of Pure and Applied Physics and the Societa Italiana di Fisica, in co-operation with the Consiglio Nazionale delle Ricerche.

A tentative list of the chief topics to be discussed during the Conference is as follows:

A. Pions
   (1) Experimental
   (2) Theoretical

B. Strange Particles, K-mesons and Hyperons
   (1) Properties and Production
   (2) Interactions
   (3) Models and Theories of Nuclear Interactions

C. Properties and Interactions of Antinucleons